8-2017

Geochemical and Particle Size Analysis of East Antarctic Shelf Sediments Through the Eocene Oligocene Transition

Jennifer Joanne Light
Montclair State University

ABSTRACT

The Eocene Oligocene Transition (EOT) at ~34 million years ago (Ma), marked the global change from greenhouse to icehouse, and the establishment of the East Antarctic Ice Sheet (EAIS). The timing involved with initiation of the EAIS and ice growth during the EOT is still poorly understood due to poor core recovery. The purpose of this study was to expand upon existing knowledge of EAIS dynamics by applying updated age models to geochemical and sedimentological records from three marginal shelf sites that contain Eocene and or Oligocene sediments.

This study used inductively coupled plasma optical emission spectrometry and mass spectrometry (ICP-OES/ICP-MS) to determine the bulk chemical composition of samples from marginal east Antarctic shelf sites: ODP Site 1166A [O'Brien et al., 2001] and IODP Site U1360 [Expedition 318 Scientists, 2010]. Particle size analysis was conducted on sediments from west Antarctic ODP Site 696 [Barker et al., 1988], and the distributions were compared to particle size data from Ciarletta [2014] for Sites 1166 and U1360. Overall, Site 696 shows a fining upward sequence indicative of a marine transgression, that could have been caused by depression of continental crust as the EAIS grew or tectonic deepening during the formation of the Powell basin.

Major element data was used to calculate various paleoclimate proxies including the Chemical Index of Alteration (CIA), mean annual temperatures, and mean annual precipitation. The paleoclimate of a region can affect the advance and retreat of ice and is therefore important in the study of glaciation in Antarctica. Results show a dominant warm humid environment for the Late Eocene (Site 1166); in contrast, the Lower Oligocene (Site U1360) shows a cooler more arid environment. The provenance of sediments was constrained by calculating Al_2O_3/TiO_2 ratios. Al and Ti are conservative elements and are

representative of their source material; therefore, the ratios can be a good indicator of changes in provenance. It was determined that a slight provenance change occurred at Site 1166 and may indicate a glacial advance and retreat. At Site U1360 the source remained relatively the same. Changes in the Al/Ti ratios at Site U1360 are likely due to changes in particle size.

MONTCLAIR STATE UNIVERSITY

Geochemical and Particle Size Analysis of East Antarctic Shelf Sediments Through the Eocene Oligocene Transition

by

Jennifer Light

A Master's Thesis Submitted to the Faculty of

Montclair State University

In Partial Fulfillment of the Requirements

For the Degree of

Master of Science

August 2017

College/School: College of Science and Mathematics

Department: Earth and Environmental Studies

Thesis Committee:

[redacted]

Sandra Passchier
Thesis Sponsor

[redacted]

Stefanie Brachfeld

[redacted]

Michael Kruge
Committee Member

GEOCHEMICAL AND PARTICLE SIZE ANALYSIS OF EAST ANTARCTIC SHELF SEDIMENTS THROUGH THE EOCENE OLIGOCENE TRANSITION

A THESIS

Submitted in partial fulfillment of the requirements

for the degree of Master of Science

By

JENNIFER JOANNE LIGHT

Montclair State University

Montclair, NJ

2017

Acknowledgements

I would first like to thank my wonderful mentor, Dr. Sandra Passchier for giving me the opportunity to cultivate a passion for Antarctica through this project. Thank you for your ceaseless patience and encouragement, and for reminding me to take a step back when I was caught up in the details. This project was made possible through a grant from the National Science Foundation (ANT1245283).

I would also like to thank my committee members Dr. Stefanie Brachfeld, and Dr. Michael Kruge, for walking me through some difficult concepts and always making the time to answer even the silliest of questions. I would also like to extend a special thank you to Dr. Xiaona Li for her help and guidance in the lab.

I would like to acknowledge my family; I would not be where I am without their constant support. A big thank you to all of the wonderful graduate students at Montclair State who made the East Coast feel like home. Thank you for helping me settle in, and forcing me to get out of the office. I extend a special thank you to the ladies who kept me sane through it all, Melissa Hansen, Pricila Iranah, April Kelly, Ashley Cirone, and Alie Lepp. I am forever grateful.

TABLE OF CONTENTS

LIST OF FIGURES

LIST OF TABLES

1. INTRODUCTION

1.1 OVERVIEW

The Antarctic continent today is geographically located at southern high latitudes. Roughly 98% of the continent is covered by ice that is 1-4 km thick [Anderson, 1999]. The ice is subdivided into two main ice sheets, the West Antarctic Ice Sheet (WAIS) and the East Antarctic Ice Sheet (EAIS). Due to ice coverage, what is currently known about the geology of the Antarctic continent comes from exposed outcrops and proxy data from marine sediment cores. Antarctica was not always ice covered; paleo-reconstructions show that the continental conditions were much warmer during the Eocene Epoch [Pross et al., 2012].

The Eocene Epoch (~56 – 34 Ma) marked a time of great change in Antarctica from the early Eocene thermal maximum [Zachos et al., 2003], to the arrival of polar glaciation in the late Eocene and into the Oligocene. The transition from Eocene greenhouse conditions to Oligocene cooling conditions is documented by a distinct increase in benthic foraminifera $\delta^{18}O$ values (Figure 1). These values become more strongly positive as ice takes up and stores lighter ^{16}O isotopes, and heavier ^{18}O concentrations increase in marine environments [Zachos et. al., 2001]. The changes are documented as two distinct steps, the EOT-1 (34.4 Ma), and the Oi-1 (Oligocene isotope event-1, 33.7 Ma); the first is attributed to cooling and the later to significant ice growth of the EAIS [Zachos et al., 2001]. The Eocene Oligocene Transition (EOT) has been widely studied and modeled to better understand the initiation, and advancement of glaciation in Antarctica.

The initiation of the EAIS during the EOT is believed to have also been a step-wise transition coinciding with oxygen isotope excursions and beginning with smaller mountain glaciers, transitioning to ephemeral ice sheets, and eventually a large continental scale ice sheet [Ladant et al., 2014]. However, the timing of ice sheet advancement through the EOT is still poorly understood due to a previous lack of detailed age models and poor recovery for cores from marginal shelf sites. The purpose of this study is to expand upon existing knowledge of EAIS dynamics spanning

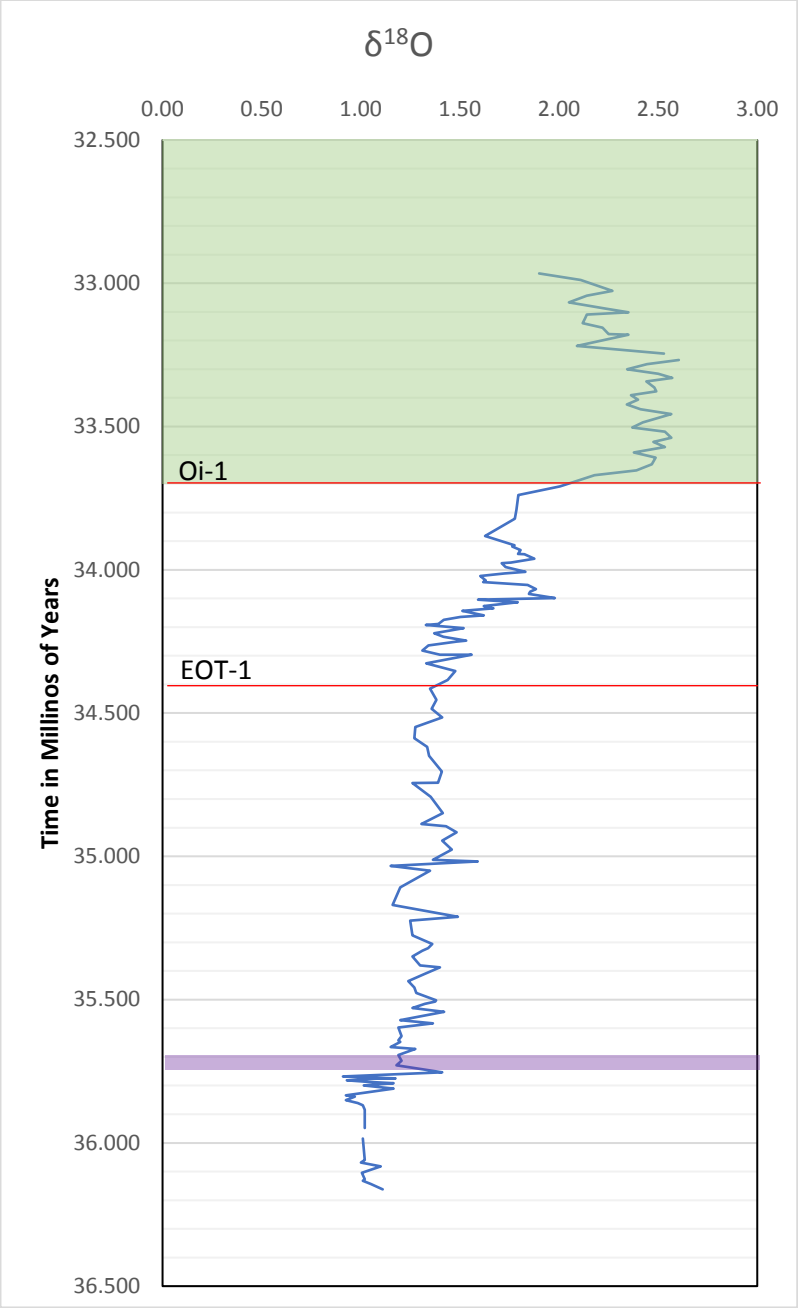

Figure 1: Compiled Oxygen 18 curve from Bohaty et al. [2013] for ODP site 689, using data from Diester-Haass & Zahn [1996], Vonhof et al. [2000], Bohaty et al. [2013]. Colored sections show time periods of Site 1166 (purple) and U1360 (green).

the EOT by creating a detailed geochemical and sedimentological record of shelf sediments around the Antarctic Margin, using cores from three continental shelf sites (Figure 2). Updated detailed age models have been recently created for each of the three sites and have been found to contain Eocene to Oligocene aged sediment [Florindo et al, 2003, Houben et al, 2013, Passchier et al.,

2017]. By applying new age models to higher resolution continental margin geochemical and sedimentological records, paleoclimatic conditions and ice growth through the EOT can be better understood.

1.2 REVIEW OF DRILL SITES

1.2.1 **Study Sites**

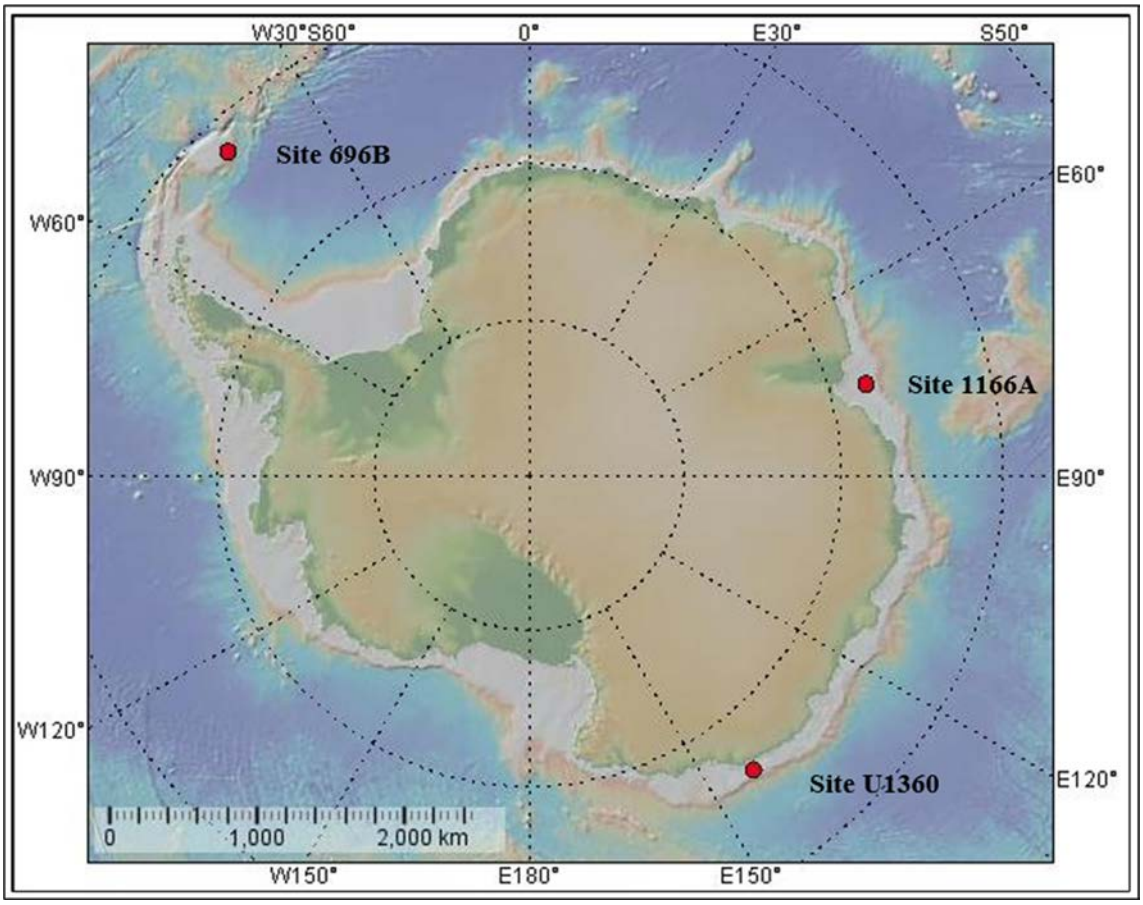

Figure 2: GeoMapApp rendered map of Antarctica with the locations of drill sites being used in this study (Ryan et al., 2009).

South Orkney Islands (Site 696B)

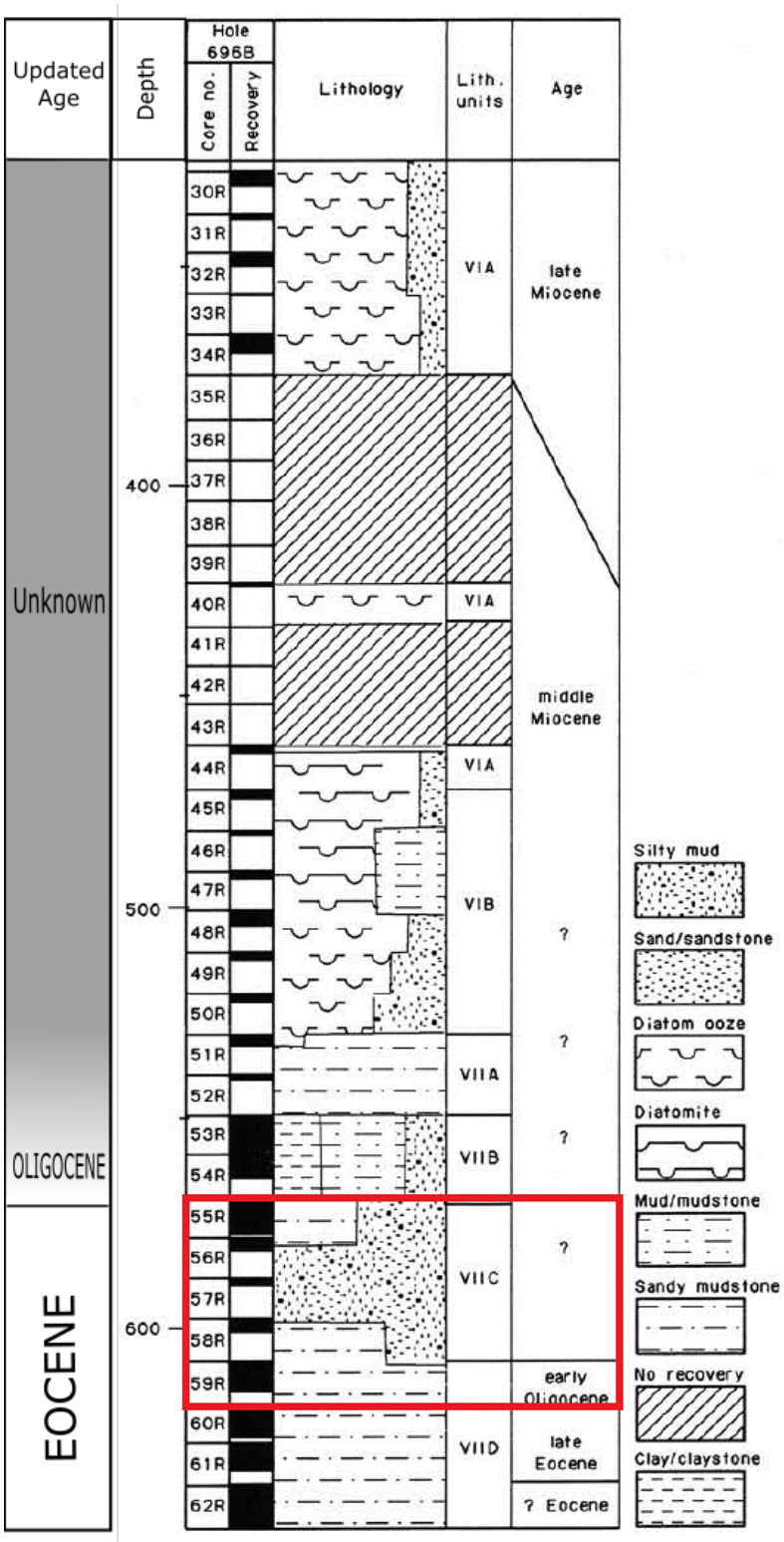

Figure 3: Lithology of the lower half of Site 696B [Barker et al., 1988]. Red box indicates the Cores used in this study from Unit VII. Updated ages are from Houben et al. [2013] where Oligocene ages are seen in cores 53R and 54R. It is unknown where Oligocene ages end up-core, therefore a gradient is used.

Hole B was one of two drilled at Site 696 during Ocean Drilling Program (ODP) Leg 113 [Barker et al., 1988]. Hole B was drilled in 650 m of water depth off the southeastern coast of the South Orkney Microcontinent, between Feb. 24th and March 2nd, 1987; the hole was drilled to a depth of 645.6 meters below sea floor (mbsf) [Barker et al., 1988]. The site has been subdivided into seven units by shipboard scientists based on lithology. This study will use samples from Unit VII (figure 3), specifically sub-units B, C and D, based on ages from Houben et al. [2013]. Subunit B consists of olive gray to black mudstones, similarly, subunit C contains olive grey to black mudstones with a greater percentage of sand and up to 45% glauconite in certain samples [Barker et al., 1988]. Subunit D contains a similar overall lithology to subunit B and C, but instead of abundant glauconite it contains abundant shell fragments [Barker et al., 1988]. The overall purpose of this expedition leg was to try to establish the timing of the formation of the Antarctic ice sheets, Antarctic bottom waters, and environmental changes [Barker et al., 1988].

Prydz Bay (Site 1166A)

Hole A was one of three holes drilled at site 1166 in Prydz Bay during ODP expedition 188 [O'Brien et al., 2001] between Feb 16th and Feb 21st, 2000; it was drilled in 475.4 m of water depth, and the hole was drilled to 381.3 mbsf [O'Brien et al., 2001]. This hole was divided into units based on lithology (Figure 4) [O'Brien et al., 2001]; our study will use samples from what has been classified as Unit II consisting of interbedded sands and mudstones. Site 1166 was cored in the hope of recovering Cenozoic sediments that would show the first occurrence of glaciers into Prydz Bay, and the environmental changes that led to the introduction of glaciers to the marine environment [O'Brien et al., 2001].

Wilkes Land/Terra Adélie Coast (Site U1360)

Hole A at site U1360 was drilled by the Integrated Ocean Drilling Program (IODP) on expedition 318 off the Adélie Coast in 495 m of water depth, between Feb 12th and Feb 14th, 2010; the hole was drilled to 70.8 msbf [Expedition 318 Scientists, 2010]. The percentage of recovered material was only 10%; as with the other sites, sediment from this hole was divided into separate

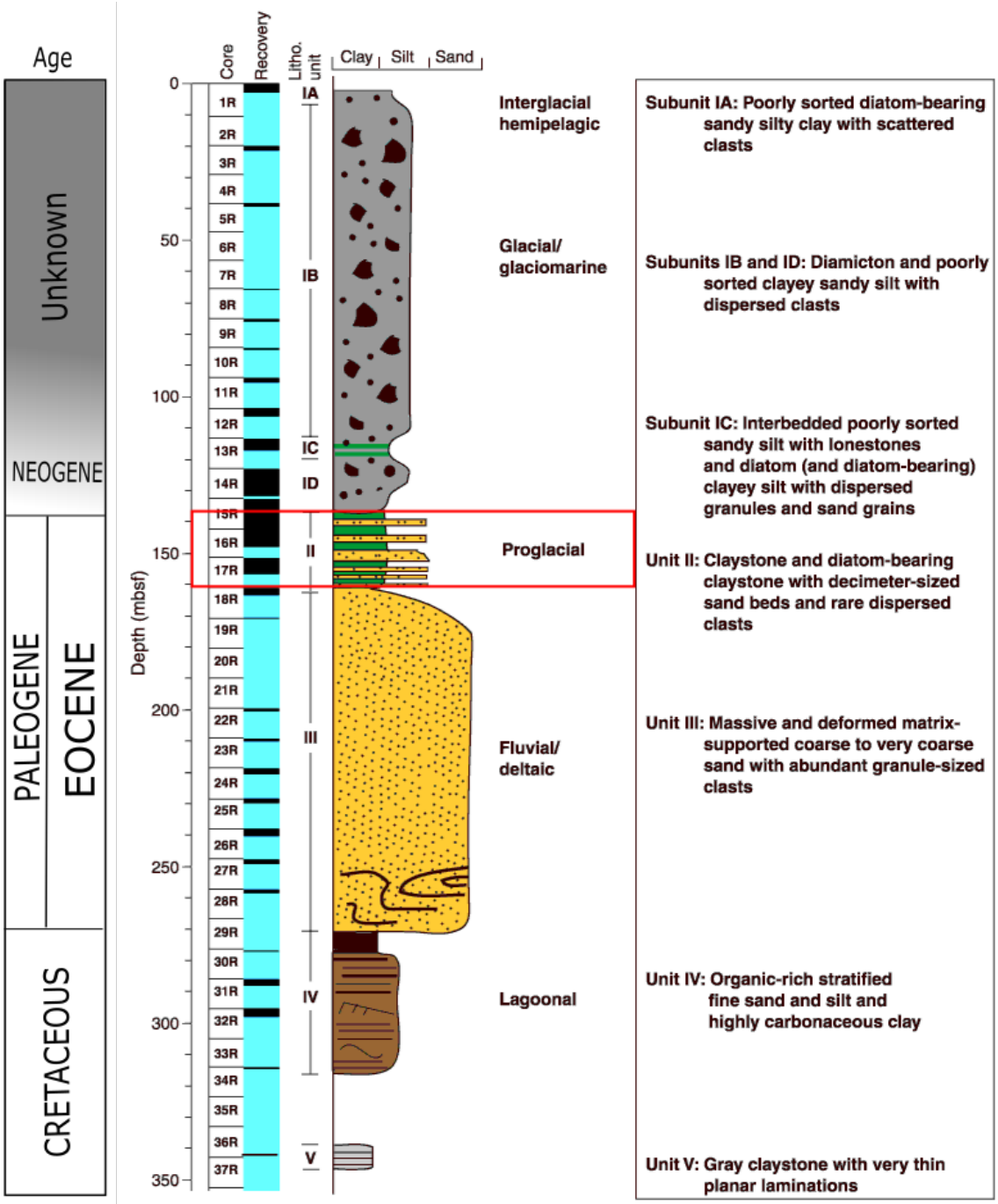

Figure 4: Lithology of Site 1166 showing where Unit II proglacial sediments lie from O'Brien et al. [2001]. Red box indicates the cores used in this study. Ages are taken from Florindo et al. [2003] and Passchier et al. [2017]. Ages for core 13R are known to be Neogene but it is uncertain where Neogene sediments end up-core and have been graded to unknown

units. For this study, we will be focusing on samples from Unit II (Figure 5), specifically cores 3R through 6R, that show a fining upward sequence. Site U1360 was drilled with the intention of

establishing the timing for the arrival of the ice sheet to the Wilkes Land Margin through a proximal sediment record [Expedition 318 Scientists, 2010].

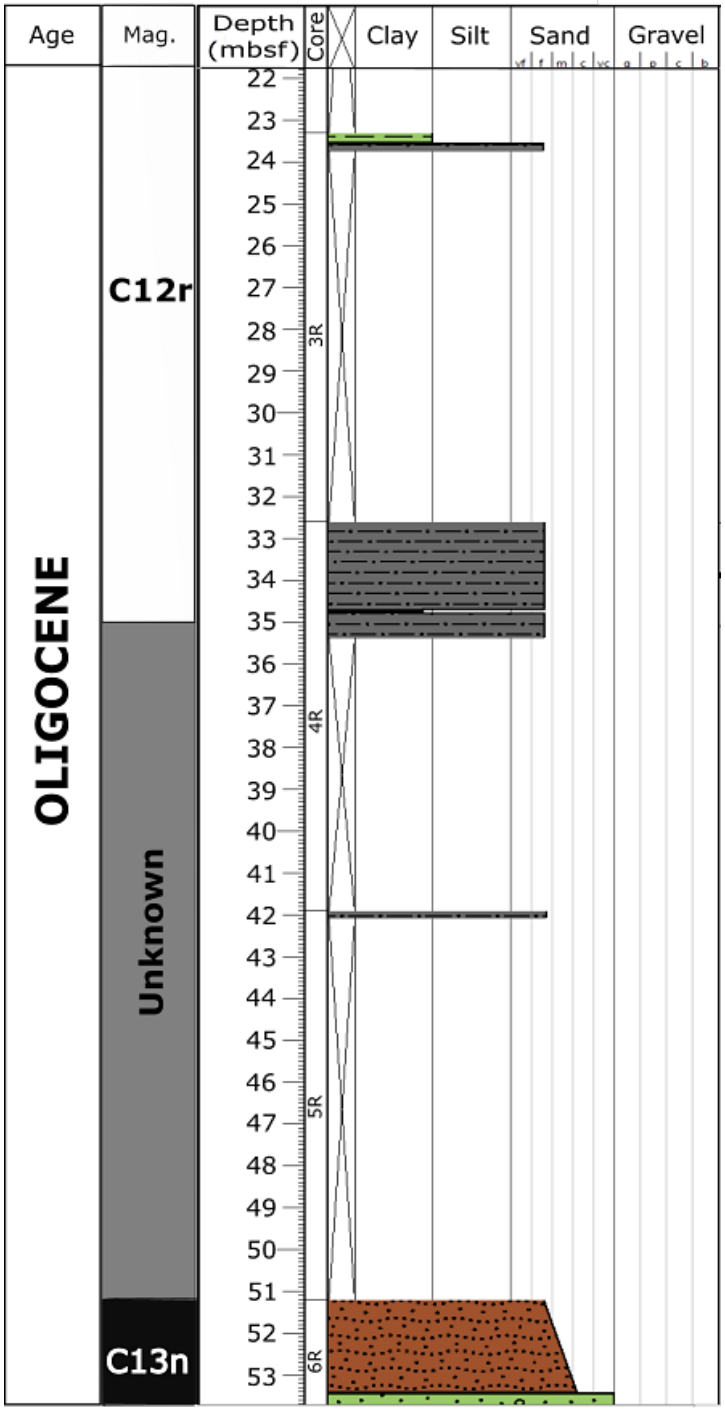

Figure 5: Lithology of Site U1360 Unit II, areas with X's are areas of no recovery. Chron ages are from Houben et al. [2013].

1.2.2 **Age Model**

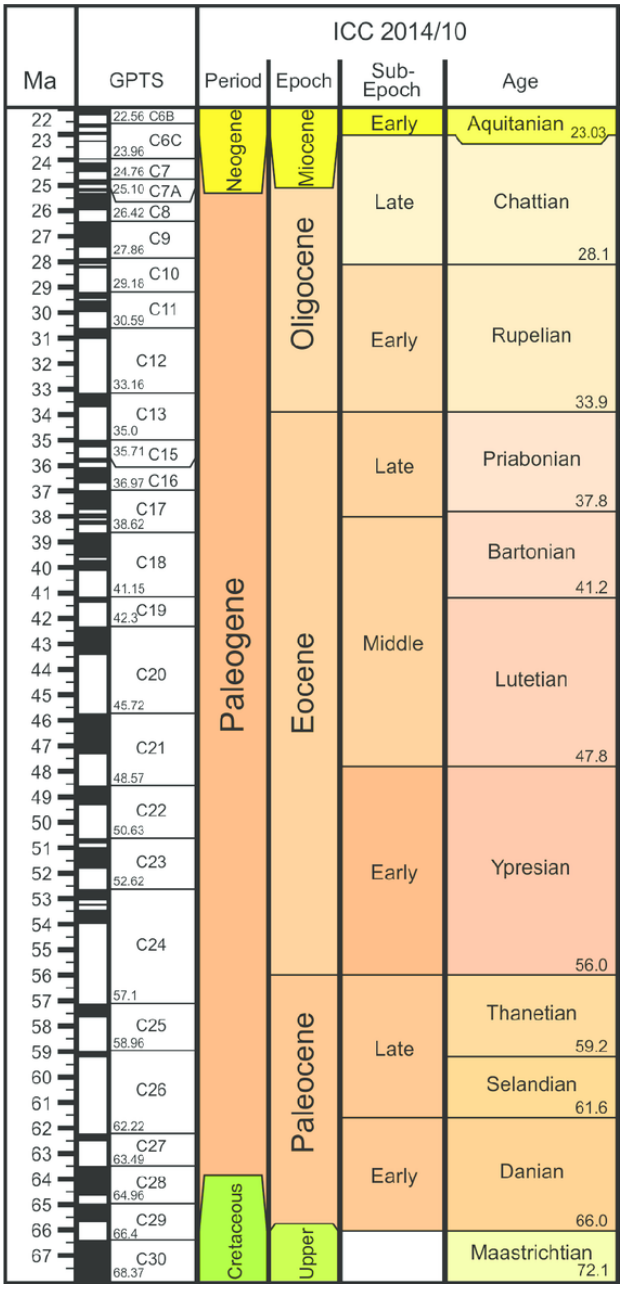

Figure 6: Chronostratigraphic chart for the Paleogene from Raine et al. [2015]. Showing the correlation between ages in Ma, Chrons (magnetic polarity reversals, under GPTS), and Epochs.

Recently, detailed magnetobiostratigraphic age models have been developed for Sites 696B [Barker et al., 1988], 1166A [O'Brien et al., 2001], and Site U1360 [Expedition 318 Scientists, 2010]. Originally, Site 1166A was thought to contain late Eocene to early Oligocene sediment in what was classified as lithostratigraphic Unit II [O'Brien et al, 2001]. Florindo et al.

[2003] conducted a paleomagnetic study, creating a more precise age model for Site 1166A by constraining paleomagnetic data with diatom and radiolarian assemblages. Based on the paleomagnetic data and diatom assemblages, it was interpreted that Unit II could have coincided with Chron 12r and Chron 13n, or Chron 15r through Chron 17 [Florindo et al., 2003] (for Chron information see Figure 6). Further study by Passchier et al. [2017] has placed Unit II in the latter category using the first occurrence of the dinoflagellate *Deflandrea* sp. A., correlating the lower part of Unit II to Chron 16n.1n. The reversal located in the upper section of Unit II would then be Chron 15r, indicating that Unit II is late Eocene in age and does not contain Oligocene age sediment [Passchier et al., 2017]. Based on the first occurrence of *Deflandrea* sp. A at 238 mbsf and the magnetic reversal at 136.32 mbsf, it was possible to calculate more precise ages for Unit II that span from 35.745 Ma to 35.705 Ma, calibrated to the Vandenberghe et al., [2012] time scale. This interval therefore, represents a snap-shot of time immediately preceding the EOT.

Initial ages for sediments from Site 696B Unit VII, specifically subunits B, C, and D were dated from the Early Miocene to Eocene based on fossil taxa and select paleomagnetic analysis [Barker et al., 1988]. Initial ages for Unit II of Site U1360 were dated as lower Oligocene based on diatoms and dinocysts [Expedition 318 Scientists, 2010]. Reversed polarity was found in two samples from Site U1360 that correlated to Chron 12r, in combination with the biostratigraphy it provided a reliable Oligocene age [Expedition 318 Scientists, 2010].

In 2013, Houben et al. published updated magnetobiostratigraphic age models for Sites 696B and U1360. The updated age model was based on the first occurrence of the fossil taxa *Malvinia escutiana* that coincides with the Oi-1 oxygen isotope excursion event [Houben et al., 2013]. The updated age models show that subunits B, C, and D from site 696B encompass a complete Eocene to Oligocene succession, not containing Miocene aged sediments [Houben et al., 2013]. More precise ages were calculated using three age tie points based on the first occurrence of three taxa: *Istmolithis recurvus* at 616.6 mbsf dated to 36.27 Ma, *Stoveracysta kakanuien* at 571.2 mbsf dated to 34.1 Ma, and *Malvinia escutiana* at 568.8 mbsf dated to 33.6 Ma [Houben et

al., 2013: Supplemental Data]. Calculated ages ranged from 33.63 to 35.84 Ma, providing a time interval that spans the EOT.

The Houben et al., [2013] model also provided a better magnetobiostratigraphic age control for sediments from Site U1360. *Malvinia escutiana* was found to have a first occurrence 42.02 mbsf in core 5R, and from 5R to 3R other Oligocene diatoms were found [Houben et al., 2013]. Magnetic polarity showed a normal interval in Core 6R and a reversal interval in cores 4R and 3R; based on the taxa and polarity intervals, it was determined that core 6R likely matched Chron 13n, which would suggest that the reversal located above, was dated to Chron 12r [Houben et al., 2013]. While the core has been dated to earliest Oligocene (ranging between 33.705 and 33.157 Ma [Vandenberghe et al., 2012]) more exact ages cannot be determined as it is unclear where Chron 13n ends and Chron 12r begins in the hole due to low core recovery. The new age models allow for a more reliable high-resolution temporal look at cores from around the Antarctic margin with larger spatial coverage than previous analysis.

1.2.3 **Regional Geology**

Antarctica has a complicated tectonic and geologic history. It is divided into Eastern and Western regions by the ~3000 km long Transantarctic Mountains that stretch from the Weddell Sea to the Ross Sea [Fitzsimons, 2000]. These two regions were separate until the breakup of Gondwana (Early Cretaceous) that began their shift to the present geographic location at the South Pole [Fitzgerald, 2002]. The Late Cretaceous marked the final shift to the South Pole, and the formation of the Antarctic continent as it is known today [Fitzgerald, 2002].

The western Antarctic region is made-up of multiple microplates, including the Ellsworth-Whitmore Mountains block, Thurston Island, Antarctic Peninsula, Marie Byrd Land, Haag Nunatak, Berker, and the Filchner, [Fitzgerald, 2002]. During the breakup of Gondwana these microplates shifted and rotated, moving close to their present location by ~110 Ma [Fitzgerald, 2002]. The South Orkney Microcontinent (SOM) is thought to have also been a part of this shift, as it was likely a part of the tip of the Antarctic Peninsula during this time [Carter et al., 2016].

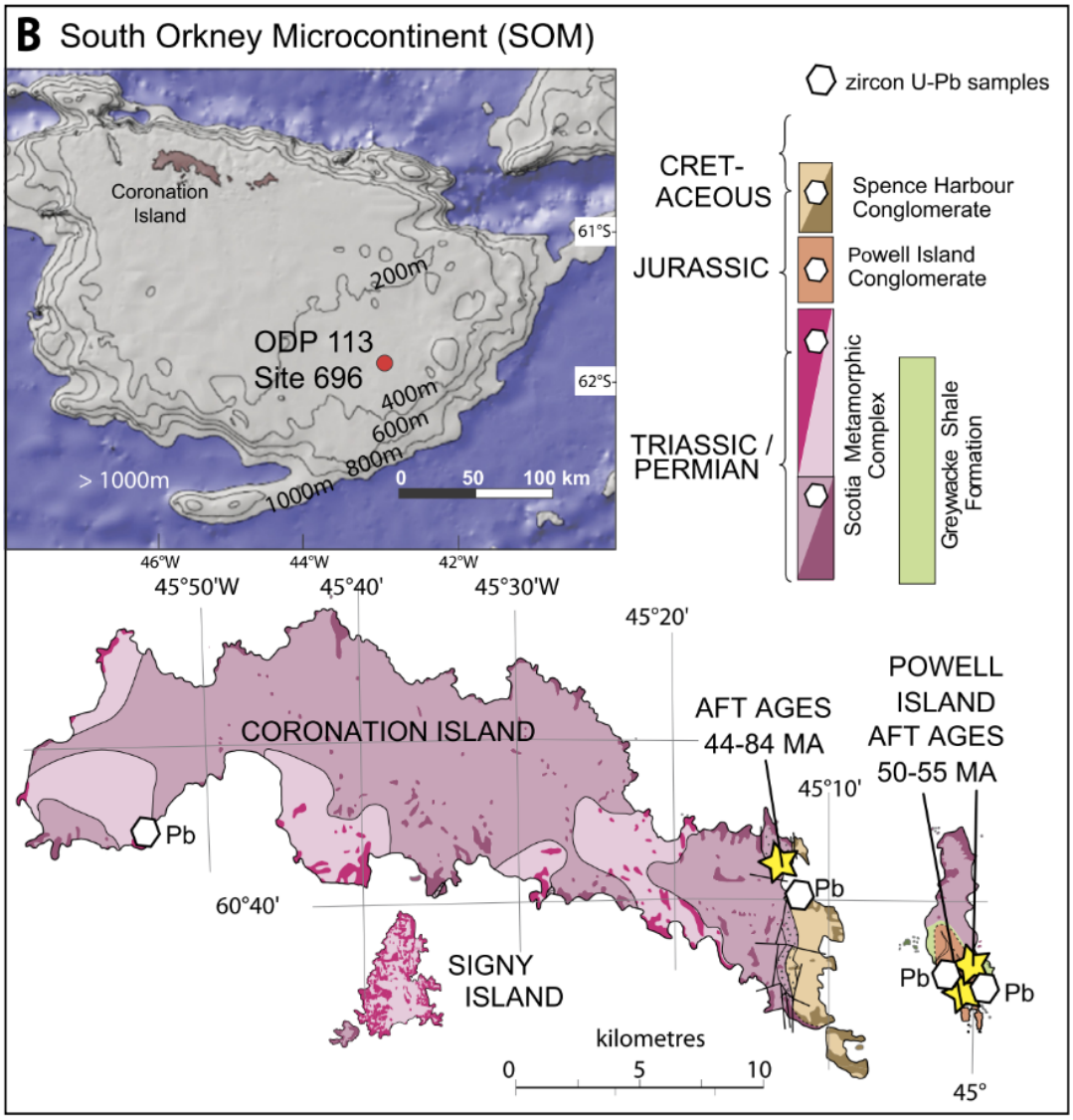

Figure 7: Regional Geology of the South Orkney Islands including the shelf Site ODP 696 from Carter et al., 2016.

Site 696 lies on the southern continental shelf margin of the SOM. The islands that comprise the continental portion of the SOM are made up of igneous and sedimentary rocks that were metamorphosed through accretion during the Mesozoic, along the margin of Gondwana (Figure 7) [King & Barker, 1988]. They also contain conglomerates that are Jurassic to Cretaceous in age and intruded dykes [King & Barker, 1988]. The SOM underwent late Eocene rifting from the Antarctic Peninsula creating the beginning of what would become the Powell Basin [Carter et

al., 2016]. The subsequent isolation of the SOM would have caused Site 696 to receive localized sediment from the South Orkney Islands or Ice Rafted Debris (IRD) sourced from Eastern Antarctica [Carter et al., 2016].

The eastern Antarctic region consists of a craton that contains metamorphosed Precambrian - Ordovician igneous and sedimentary basement that is host to granitic intrusions [Fitzsimons, 2000]. In some areas, the basement is covered by the Beacon Supergroup, consisting of Devonian - Jurassic undeformed sediments that also contain Jurassic intrusions of the Ferrar Group (volcanic and plutonic mafic rocks) [Fitzsimons, 2000]. Locally, rock types near Sites 1166 and U1360 differ, as do the local depositional environments.

Site 1166 is located in Prydz Bay, the main drainage basin for the Lambert Glacier-Amery Ice Shelf that today drains ~20% of the of the EAIS [van de Flierdt et al., 2008]. The Amery Ice Shelf and Prydz Bay are located in the Lambert Graben, a failed arm of a triple junction, formed during the late Paleozoic to early Mesozoic as India began to rift from Antarctica [Whitehead, 2005]. On the Western edge of the Graben are the Northern and Southern Prince Charles Mountains (NPCM and SPCM), containing outcrops of Archean mafic dykes [Mikhalsky et al., 2013], Precambrian: granitic basement, metasedimentary rocks, high-grade metamorphic rocks, granitoids and volcanics, Cambrian granites, and Permian sedimentary rocks [Sheraton et al., 1996; Munksgaard et al., 1992]. To the East of the Lambert Graben are the Grove Mountains that consist of Precambrian felsic orthogneisses, mafic granulites, and paragneiss (Figure 8) [Liu et al., 2007]. Located South of the Prince Charles Mountains and inland from the Lambert Graben are the Gamburtsev Subglacial Mountains (GSM). The GSM's are ~3000 m in elevation and reside in the middle of the East Antarctic craton; they are believed to be an important nucleation point for EOT ice growth [van de Flierdt et al., 2008, DeConto and Pollard, 2003]. The rock types of the GSM's remain unknown due to thick ice cover; however, recent studies suggest that they may be composed of mafic granitoids that have two age ranges, 650-500 Ma and 1100-800 Ma [Veevers et al., 2008].

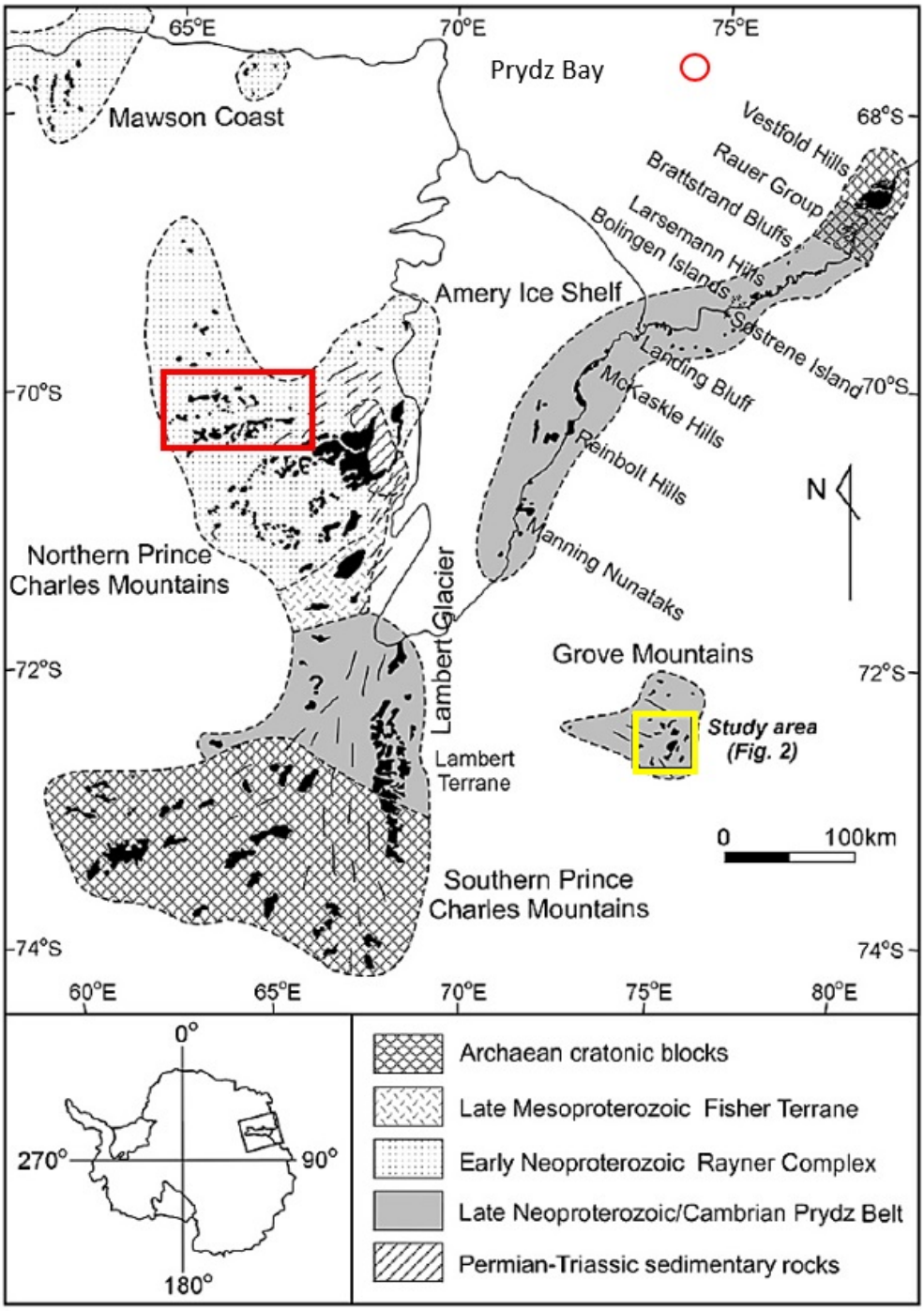

Figure 8: Geologic map of the Prydz Bay region from Liu et al., 2007. Including the Grove Mountains study area outlined in yellow, and the Northern Prince Charles Mountains [Munksgaard et al., 1992] outlines in red. The red circle shows the location of ODP drill Site 1166 [O'Brien et al., 2001]

Through age dating of Eocene fluvial sediments from Site 1166, van de Flierdt et al., [2008] suggest a Proterozoic to Cambrian age of source rocks, consistent with the previous study.

Sediment transport to Site 1166 is dominantly glacio-fluvial, glacial textures on quartz grains were found, indicating a proglacial environment [Strand et al., 2003]. As sediment is likely to have been derived from the GSM's, possibly the Prince Charles and Grove Mountains during the Eocene; geochemical signatures of bulk sediments will be studied to better understand the provenance of the sediments from Unit II, which could have implications for ice growth in Prydz Bay.

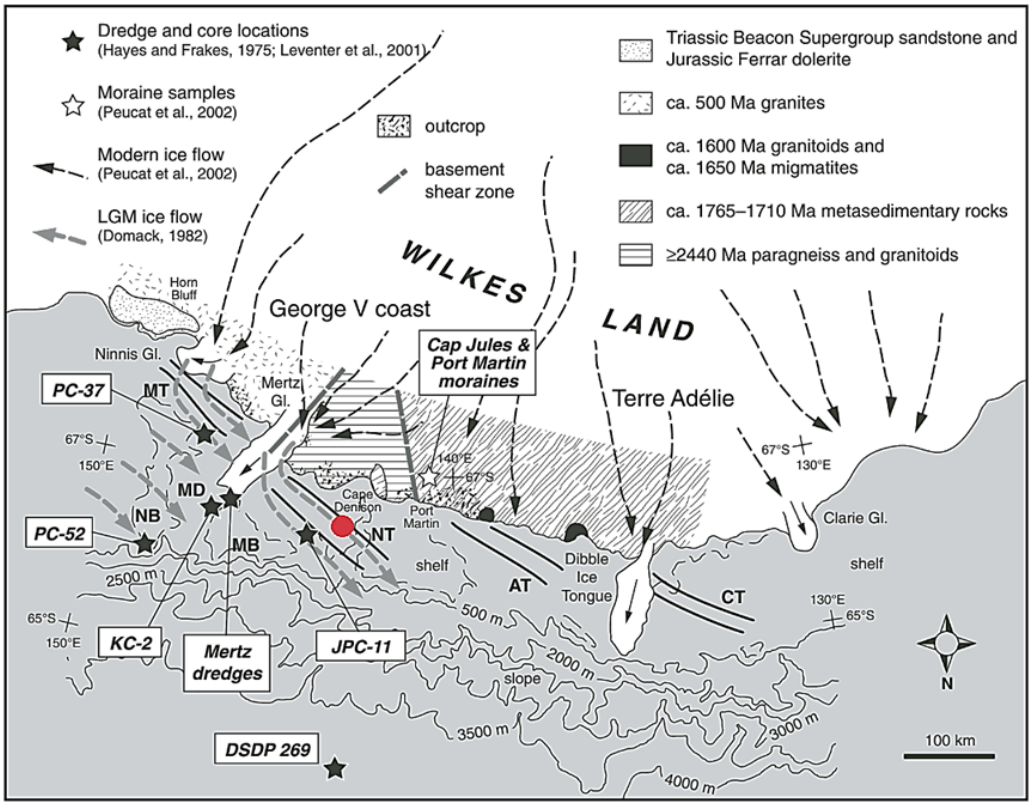

Figure 9: Geological Map of the Wilkes Land Coast from Goodge and Fanning, (2010). Red dot indicates the approximate location of IODP Site U1360.

Site U1360 is found off the Terra Adélie coast of the Wilkes Land province (Figure 8). During the late Cretaceous this region underwent rifting from Australia creating the continental margin, as spreading continued through the Eocene an open marine environment formed [Expedition 318 Scientists, 2010]. The shelf in this region is fed by sediments transported from the Wilkes Basin [Expedition 318 Scientists, 2010]. Inland the bedrock geology of the region is dominated by Late Archean and Early Proterozoic paragneisses and granitoids, Early Proterozoic metasedimentary rocks, Early to Mid-Proterozoic granitoids and migmatites, Cambrian granites, Triassic sandstones, and Jurassic dolerites (Figure 9) [Goodge and Fanning, 2010], and rhyolites from further inland (Peucat et al., 2002)

1.2.4 **Paleoclimate**

Paleoclimate studies have been conducted to better understand and reconstruct the climatic and environmental conditions in Antarctica at the onset of glaciation. A study done in 2013 by Passchier et al. encompassed a time span from the Eocene to the Miocene, using ODP continental shelf Site 1166, IODP continental rise Site U1356 (Wilkes Land), and various other sites around Antarctica to broadly investigate the chemical weathering histories of sediments. Using bulk geochemical data, they calculated Mean Annual Temperatures (MAT) and Mean Annual Precipitation (MAP) affecting the sediments for each region [Passchier et al., 2013]. Results showed an overall cooling from the Eocene to the Miocene of ≥8˚C with terrestrial calculated MAT values between ≤4 to 14˚C, and calculated MAP values between ~400 and 1200 mm [Passchier et al, 2013]. Macphail and Truswell, [2004] determined based on palynology from Site 1166 that during the Eocene the region contained rainforest scrub lands indicating warmer wetter environments.

1.2.5 **Ice Growth During the Eocene Oligocene Transition**

The inception of the East Antarctic Ice Sheet (EAIS) is still poorly understood, and therefore has been extensively modeled to better understand not only how the ice began but the

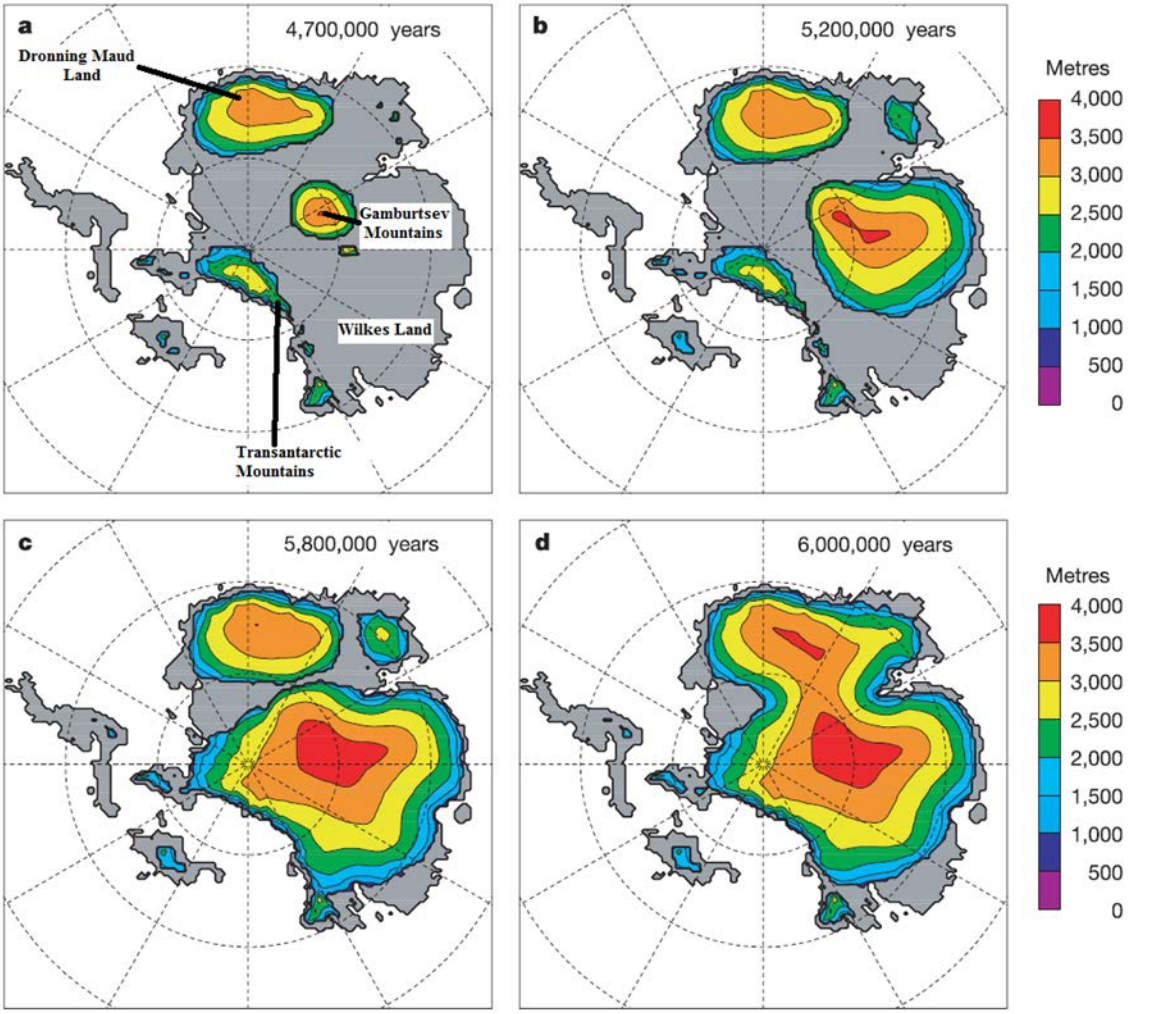

Figure 10: DeConto and Pollard, (2003) model results showing the nucleation and growth of ice through time. Model based on a 10 million year simulation from greenhouse conditions to icehouse conditions, dates indicate ice conditions at specific run times from time zero. Regional labels have been added for clarity. It is likely that the Prydz Bay sediments are being deposited in a scenario seen in box 'a' while the Wilkes Land sediments are likely being deposited in a scenario like 'c' or 'd'.

direction and timing of growth. Through modeling, DeConto et al. [2003] posit that the onset of glaciation was likely due to a decrease in atmospheric CO_2, which could have caused the initial cooling necessary for ice caps to begin growing. The opening of the Tasman and Drake passages and subsequent isolation of the Antarctic continent along with the Miocene formation of the Antarctic Circum-polar Current (ACC) would have been a secondary mechanism for cooling [DeConto et al., 2003, Expedition 318 Scientists, 2010], potentially allowing for ice sheet growth. Their model suggests that under these conditions the growth of the EAIS would have nucleated in

areas of high topographic relief and expanded outward toward the coasts, reaching the marine environment first in the Dronning Maud Land, then Prydz Bay and finally the Wilkes Land/Terra Adélie coast (Figure 10) [DeConto et al., 2003]. This project will focus on sediment samples from three sites, associated with deposition from the three regions outlined by DeConto et al. [2003]. These sites were drilled specifically in hopes of better understanding changes in the EAIS through the EOT.

2. METHODOLOGY

2.1 GEOCHEMICAL ANALYSIS

Previous geochemical analysis of shelf Sites 1166 and U1360 through the EOT was sparse; only four samples were analyzed for Site 1166 and only one sample for Site U1360 within the EOT interval [Expedition 318 Scientists, 2010; Passchier et al., 2013]. Recently developed magnetobiostratigraphic age models for both sites have made it worthwhile to gather more geochemical data for marginal sediments through the EOT, allowing for a more detailed picture of ice development. This study used bulk geochemical analysis of major, trace, and Rare Earth Elements (REE) to look at terrestrial weathering conditions through the EOT. Preparation and analysis of samples was based on the shipboard guidelines of Murray et al. [2000] and analysis was carried out on a Horiba Jobin-Yvon Ultima inductively coupled plasma-optical emission spectrometer (ICP-OES) and Thermo Scientific iCap Q inductively coupled plasma-mass spectrometer (ICP-MS) at Montclair State University. Major, trace, and REE intensities were used to calculate paleoclimate proxies, changes in provenance, and elemental enrichments for Sites 1166 and U1360.

2.1.1 **Sample Preparation**

ICP-OES was conducted on 27 samples from Site 1166 and 9 samples from Site U1360. Samples were first powdered using a mortar and pestle. Powdered samples were then weighed to 100 mg and dry mixed with 400 mg of lithium metaborate. Blanks of lithium metaborate alone were also weighed, and the sample mixtures, along with the blanks, were placed in graphite

crucibles and heated in a furnace to 1050˚C for 30 minutes. Crucibles were removed from the furnace, swirled, and replaced for an additional 10 minutes. Crucibles were then removed from the furnace, and the samples were digested in 50 mL of 7% nitric acid, and filtered into 60 mL Nalgene sample bottles to acquire a concentration of 500x sample solution. From the 500x solution, a 4,000x solution was created for the sample analysis on the OES, by pipetting 6.5 mL of 500x solution into a bottle and adding 50 mL of 2% nitric acid. Both the 500x solution and the 4,000x solution sample bottles were stored in a refrigerator to reduce the chance of chemical reactions occurring in the samples. Later, the 4,000x solutions were poured into test tubes and placed in an organized rack formation for analysis. Twelve calibration standards from the United States Geological Survey (USGS) (i.e., MAG-1, DNC-1, BHVO2, W2, BCR2, AGV2, SCO1, GSP2, BIR, G2, QLO1, and RGM-1) were also prepared in the same manner and added to the rack for analysis.

ICP-MS was conducted on 27 samples from Site 1166. Samples for ICP-MS analysis were diluted to a 10,000x solution from the original 500x solution used for ICP-OES analysis. The 10,000x solution was prepared by pipetting .5 mL of 500x solution into a test tube and diluting it with 9.5 mL of 2% nitric acid. Samples were placed in a rack and organized according to a premade map for analysis.

2.1.2 **Data Acquisition**

For ICP-OES analysis the sample rack is placed in an auto sampler, and a map of the rack is created in the ICP-OES software, which includes sample names, blanks, and standards. The ICP-OES uses the auto sampler to extract solution from each sample test tube for analysis. Before and after each row of samples, a drift solution is tested to later determine if there is any effect on the samples due to error in the machine. Solution is extracted, and pumped into a nebulizer; it is then aspirated into the torch where the mist solution is introduced to the argon plasma [Murray et al., 2000]. The contact with the plasma excites elemental atoms; as the electrons return to their ground state, they give off an element-specific emission ray that is detected as an intensity [Murray et al., 2000]. The intensities of each element are measured three times for each sample and recorded; an

average of the intensities is then entered into a spread sheet to correct for any contamination and instrument drift during sample analysis.

The ICP-MS analyses elements in a similar fashion; the solution is again introduced to the argon plasma as an aerosol, the plasma then ionizes the elements and the ions are introduced to the mass spectrometer [Wolf, 2005]. From this point, the ions are filtered based on a ratio of their mass to their charge [Wolf, 2005]. They are filtered by the changing of current that only allows for a particular ion to be captured at any given time [Wolf, 2005]. Like the ICP-OES the intensities of the ions are recorded for each sample three times and the averages are reported. The averages are again entered into a template to correct for any contamination and instrument drift.

Major element intensities were analyzed using an excel spreadsheet that calculates the amount of drift, the calibrations of each standard that was run, and corrects the intensities for any drift in the instrument, including any potential contamination. The spreadsheet then calculates the weight percent (wt.%) oxides of major elements by calculating the dilution factor, using the weight of the acid and the weight of the solution. From this, there are three outputs: the final wt.%, a normalized wt.%, and the oxides and trace elements in parts per million (ppm).

ICP-OES analysis was performed on both sites while ICP-MS analysis was only performed on samples from Site 1166, as time and feasibility did not allow for ICP-MS analysis of site U1360. Calibrations calculated from the USGS standards showed an inadequate R^2 value for Ni from the ICP-OES for both sites and therefore Ni values from the OES data were not used. ICP-MS calibrations show inadequate R^2 values for Si and Al, and therefore it was determined that for Site 1166 major element data would be used from ICP-OES, trace and rare earth element data would be used from the ICP-MS.

Carbonate Correction

Many of the major element proxies used in the geochemical analysis rely on the amount of calcium in the silicate fraction. To make sure that the calcium present was not due to calcium carbonate, a carbonate correction was done. First, each sample was tested under a microscope,

using a small amount of powdered sample and 10% hydrochloric acid to determine if there was a reaction, as hydrochloric acid reacts with carbonate. Samples that showed a reaction were then set aside to correct for the amount of carbonate present in the samples. To do this, 2-3 grams of sample was added to an Erlenmeyer flask, and a test tube of 10% HCl was inserted into the flask and weighed. The flask was then tipped to pour the HCl into the sample, and the samples were allowed to react under a fume hood for three hours. After the three hours had passed, the flasks were weighed once again and the final weight was subtracted from the original. A blank of strictly HCl was used alongside the samples to correct for any evaporation that may have occurred over three hours. The amount of evaporation was then added back to the final weights of the samples and the difference of the original to the final was calculated. The difference was then divided by the sample weight to determine the wt.% of CO_2 that was reacted from the sample, and the wt.% of $CaCO_3$ was calculated using the equation (1) [Passchier, 2000].

$$\text{wt.\% } CaCO_3 = \text{wt.\% } CO_2 * 100/44 \quad (1)$$

2.1.3 **Geochemical Proxies**

Chemical Index of Alteration

The Chemical Index of Alteration [Nesbitt and Young, 1982] is used on mud-rocks to calculate the degree of chemical weathering from the molar concentrations of Al_2O_3, CaO, Na_2O and K_2O, using equation (2).

$$CIA = \left[\frac{Al_2O_3}{Al_2O_3+CaO+Na_2O+K_2O}\right] * 100 \quad (2)$$

CIA values greater than 65 indicate an environment prone to chemical weathering likely warmer and more humid. While values below 65 indicate an environment prone to physical weathering and an increase in glacial rock flour [Nesbitt and Young, 1982; Passchier et al., 2017] likely an indication of glacial growth.

The molar value of CaO in the CIA calculation needs to be the silicate mineral contribution of CaO. The samples from this study are bulk samples and therefore may contain calcium in the

form of calcium carbonate ($CaCO_3$). To correct for this a carbonate correction is done using the method in equation (1). In calculating the final wt.% $CaCO_3$, it was determined that one or more conditions during experimentation caused the values to be drastically larger than observed reaction results. Therefore, results from the carbonate correction were not used for either site 1166 or U1360 and instead a range of CIA values was calculated using various $CaCO_3$ values from shipboard logs.

Mean Annual Precipitation/Mean Annual Temperature

MAP and MAT were calculated using mudrocks from Sites 1166 and U1360 according to methods from Passchier et al. [2013] and Sheldon et al. [2002]. MAP for each site was calculated using equation (3).

$$MAP = 143.75e^{0.0232(CIA-K)} \quad (3)$$

To calculate MAP, the equation requires a version of the CIA in which K_2O is removed to account for the possibility of potassium metasomatism; known as the CIA-K [Passchier et al, 2013, Sheldon et al., 2002].

MAT was calculated using equation four [Passchier et al, 2013; Sheldon et al 2002], in which S is the molar ratio of K_2O and Na_2O to Al_2O_3 [Sheldon et al, 2002].

$$MAT = -18.5(S) + 17.3 \quad (4)$$

Once values were calculated for both MAP and MAT they were compared to previously published precipitation and temperature data [Passchier et al., 2013; Macphail and Truswell, 2004], based on both terrestrial climofunctions and palynology.

Provenance Tracing

Aluminum and titanium are conservative elements, meaning they are not easily altered in the water column during sedimentation and carry the signature of their source rock. This allows the ratio of Al_2O_3/TiO_2 to show changes in source rock over time throughout the core. Calculated values were compared to ratios from source rocks in the regions around Sites 1166 and U1360 to better narrow provenance. Al_2O_3 was plotted against TiO_2 to determine if the samples showed differences in grouping that would indicate a change in provenance.

To better constrain provenance at Site 1166, trace and REE elements were used to create ratios of Cr/V and Y/Ni, and plotted with previously published data [Sheraton et al, 2000; Liu et al, 2007; Munksgaard et al., 1992] from around the region to see where the different rock types would plot in comparison to the study samples. To exclude grain size effects on the data, the diamict was plotted separately from sand, and mud samples. In this instance, a sample was considered a sand if more than 20% of the total volume was greater than 63 microns. Sc/Th and Cr/Th plots were also created and plotted with average basalts and average granites [Faure, 1991] to see the proportion of mafic versus felsic material in the samples from Site 1166. Previously published Nd ratios from van de Flierdt et al. [2008] suggest that the upper part of Unit II at Site 1166 was likely sourced from an older potentially Archean/Paleoproterozoic parent material. Therefore, plots were created to show whether the samples from this interval were more mafic or more felsic in composition. A Th/Sc and Zr/Sc plot was also produced to determine if the samples showed recycling [McLennan, 1993].

For Site U1360 a plot of Cr/V against Al_2O_3/TiO_2, site samples were plotted with previously published data [Goodge and Fanning, 2010; Peucat et al., 2002] was used to determine mafic or felsic composition. Y/Ni ratios would have been used, if the Ni for this site had had an acceptable calibration in ICP-OES measurements.

Elemental Enrichments

Enrichments of elements were calculated using the normalized wt.% and normalized ppm of elements in each sample divided by the average upper crustal abundance [Rudnick and Gao, 2003]. Rare Earth Elements (REE) were divided by average chondrites [Nakamura, 1974]. Values were then set to a logarithmic scale; values above 1 indicate enrichment, while values below 1 indicate a depletion of that element in the sample.

2.2 PARTICLE SIZE ANALYSIS

Particle size analysis using laser diffraction was conducted on samples from Site 696. Previously the age model from Houben et al., [2013] showed that Site 696 contains an intact

succession of Eocene to Oligocene sediments. Particle size analysis was done on select samples to compare sedimentation at various sites around the margin spanning the EOT.

2.2.1 **Sample Selection**

Samples for Site 696 were selected based on an applied age model to encompass the time periods represented at Sites 1166 and U1360. Nineteen samples in total were selected from the top, middle, and bottom of sections from cores 55R, 56R, 57R, 58R, and 59R. Certain samples were unable to be disaggregated because of cementation and were not measured, a full list of samples can be found in the appendix.

2.2.2 **Sample Preparation**

A small amount of each sample was first placed in a 250 mL glass beaker and labeled with the sample site, core, section, and interval. Next, 10 mL of 30% H_2O_2 was added to the beaker and swirled to disaggregate the sample. If the sample did not disaggregate, it was placed in a mortar and rubbed with a rubber scrapper until broken down, then rinsed back into the glass beaker using Millipore water. Roughly 50 mL of Millipore water was added, and the solution was heated to 300 degrees until the reaction ceased. Throughout the heating process sediment was rinsed down the sidewalls of the glass beaker to make sure that all sediment took place in the reaction. Once the reaction ceased, 2 mL of 10% HCl was added to the solution and brought to a boil for 10-15 minutes or again until the reaction stopped; the sediment that was splattered onto the sides was rinsed back into the beaker and the beakers were removed from the hot plate and allowed to cool. At this point each sample was transferred to a 50 mL centrifuge tube, if the samples did not reach the 50 mL mark Millipore water was added, to make sure that all centrifuge tubes were similar weights when added to the machine. Samples were spun for 30 minutes at 2000 rpm; the samples were then decanted and refilled with Millipore water to rinse off any excess H_2O_2 and HCl. The samples were centrifuged again for 30 min at 2000 rpm. When the second run was finished, the fluid was again decanted and the samples were rinsed back into their original beakers. A small amount of sodium pyrophosphate was added to the sample in Millipore water and heated to just boiling, to dissolve

the dispersant agent. If the sample appeared to be completely disaggregated, it was ready to be run through the particle sizer; however, some samples required sonication before being run through the particle sizer. In this case, the samples were placed in the sonicator for between 5 and 15 minutes to break up any clumps of sample that may have remained.

2.2.3 **Data Acquisition**

Particle size data was acquired using a Malvern Mastersizer 2000. After the machine was turned on, the laser was allowed to warm up for 15 minutes before use. During this time, the computer was set to process the samples using a "marine sediments" standard operating procedure. The particle sizer was set to 2000 rpm, and using two 800 mL beakers containing Millipore water, the machine was quickly rinsed to avoid contamination from other samples.

To begin, a background measurement is taken using only Millipore water, so that it may be subtracted from the sample after it is run. Sample was then added to another 800 mL beaker containing ~650 mL of Millipore water and introduced to the particle sizer. The machine collects data by cycling the sample between two transparent cell windows, and a laser is used to create diffraction. Differing grain sizes show different diffraction angles [Sperazza et al, 2004]. These patterns are collected and filtered into 28 different size bins. Each bin represents a narrow range of grain-size values; bins range in size from 0.02 microns (μm) to 2000 microns (μm). The clay fraction ranges from 0.02-3.9 μm, the silt fraction ranges from 3.9-62.5 μm, and the sand fraction ~62.5-2000 μm. Samples need to show an obscuration value of between 10 and 40%, samples outside of this range need to be prepared again and re-run. Between samples, the machine was rinsed twice to avoid contamination; when all samples were finished, the data was exported for further analysis.

2.2.4 **Data Processing**

Data processing for particle size consists of determining the percentage of clay, silt, and sand in the samples. To find these values, the data is exported into an Excel spreadsheet and the frequency of volume percent is added for those bins included in the sand, silt, and clay fractions.

The data is also processed in Gradistat version 8: statistical calculator, that gives the Mean, Sorting, Skewness and Kurtosis of each sample and determines the texture and the sediment type based on its particle size [Blott and Pye, 2010].

3. **RESULTS**

3.1 GEOCHEMICAL ANALYSIS

3.1.1 **Chemical Index of Alteration**

Site 1166, Unit II, shows CIA values for the Late Eocene to be between 68 and 81 (Figure 11). The overlying Neogene glacial diamict shows a value of 57. Shipboard logs for Site 1166 show carbonate values up to 3.340% [O'Brien et al., 2001]. However, in correcting for $CaCO_3$ from 1-3.5% values of CaO became negative; therefore, for the purposes of this study a carbonate correction was not used on samples from Site 1166.

The shipboard logs for Site U1360 show carbonate values up to 0.683%. Due to this, a carbonate correction was done at 0% and 1% $CaCO_3$. CIA values calculated at 0% carbonate range from 56- 59 (Figure 12), while CIA values calculated with 1% carbonate range from 58 -61 for the Early Oligocene (Figure 12).

At Site 1166, Late Eocene values are greater than 65 and are consistent with a chemical weathering regime [Nesbitt and Young, 1982]. In contrast, Early Oligocene sediments from Site U1360 contain values less than 65, consistent with a dominant physical weathering regime.

3.1.2 **Mean Annual Precipitation/Mean Annual Temperature**

Calculated MAP in Prydz Bay during the late Eocene showed values between ~860 mm and ~1200 mm (Figure 11), while the Neogene diamict showed a lower value of 663.98 mm (Figure 11). Due to the carbonate correction for Site U1360, two MAP ranges were produced, that show lower values for the Oligocene than the Eocene. Values with no carbonate correction range from 630.02 mm to 653.82 mm, while values that were carbonate corrected ranged from 673.16 mm to 702.33 mm (Figure 12). The 1% change in carbonate accounts for a difference of between 43 mm

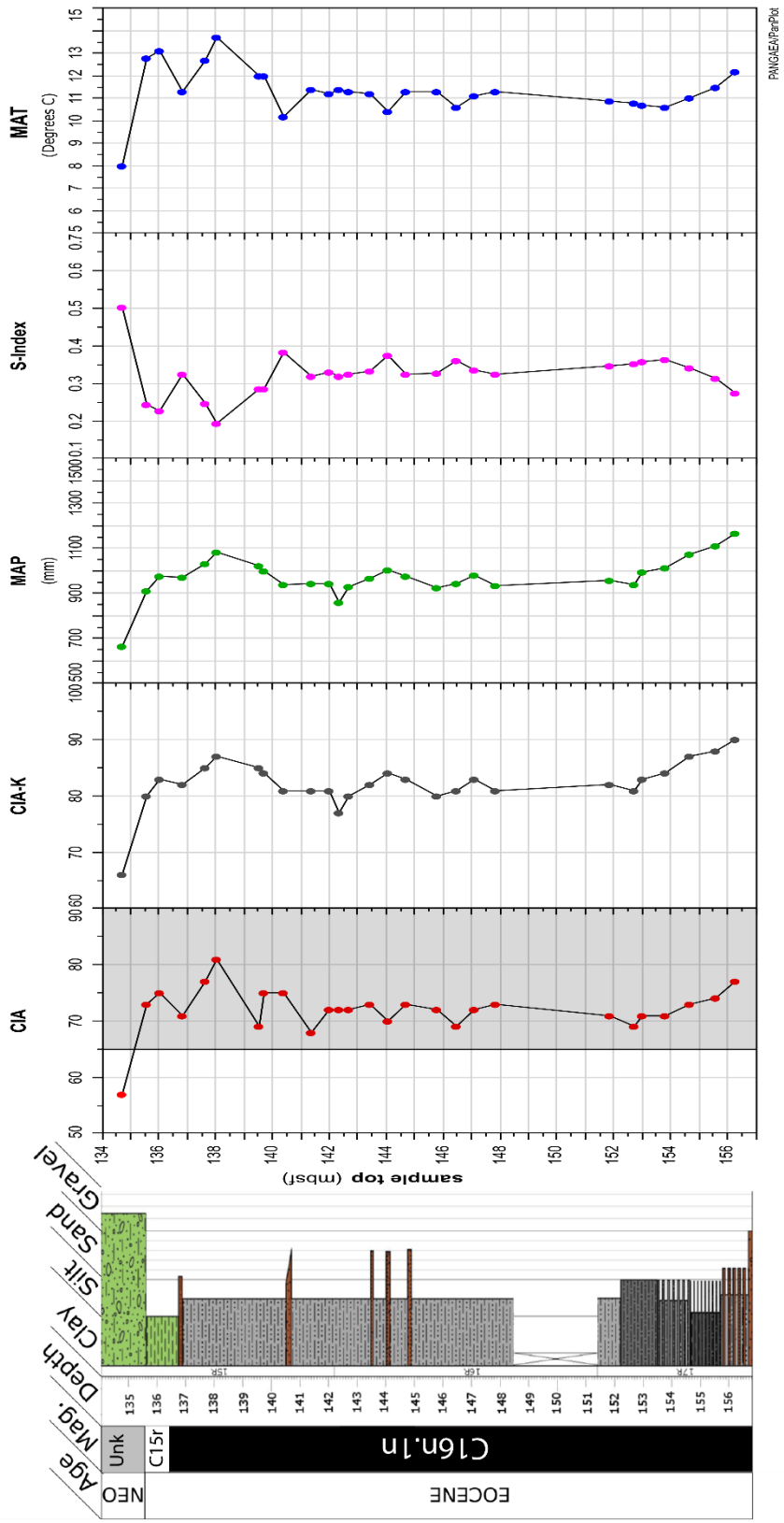

Figure 11. Paleoclimatic Proxy results shown downcore with lithology for Unit II at Site 1166. Grey section in CIA indicates samples with high chemical weathering. NEO = Neogene, Unk = unknown, Mag = Magnetostratigraphy.

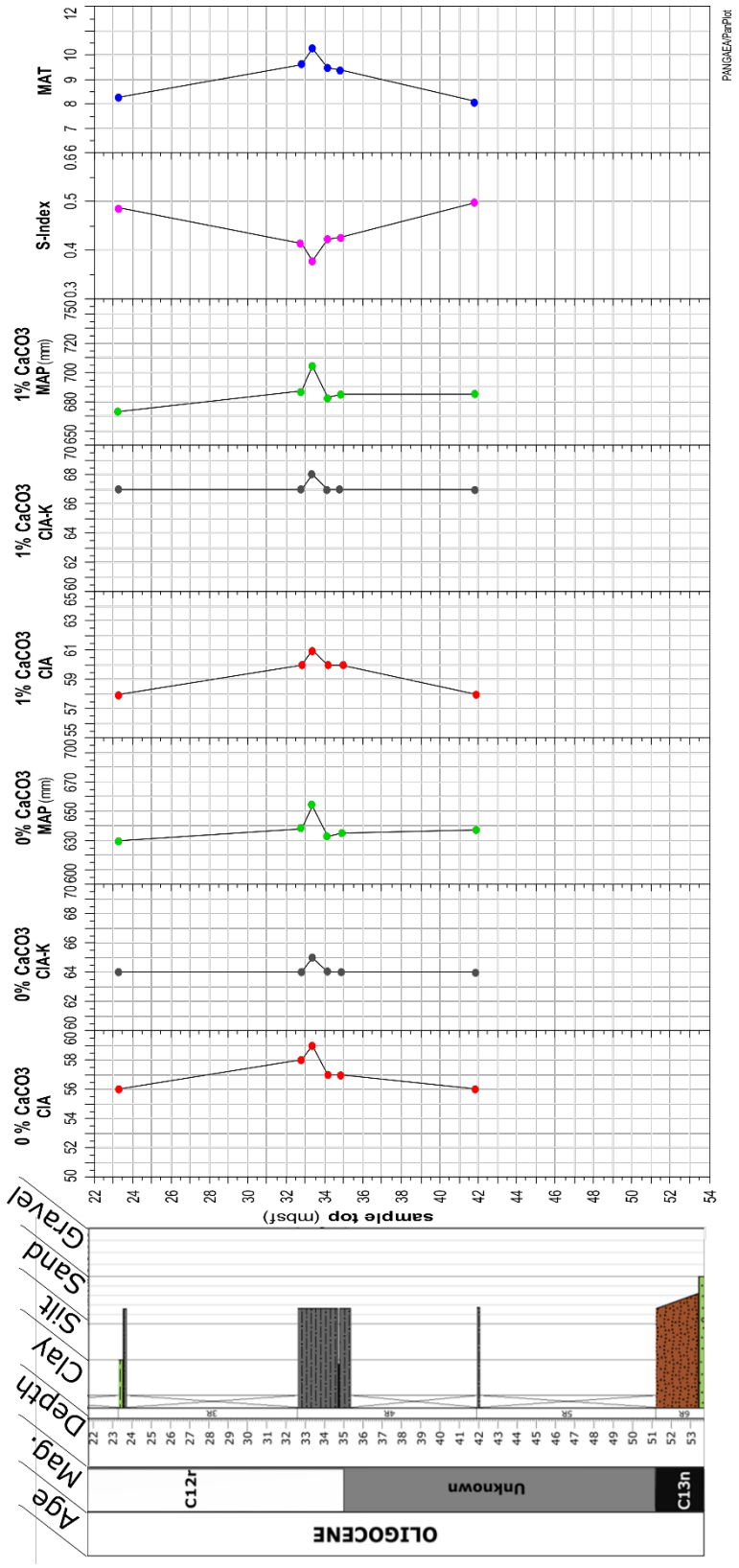

Figure 12. Paleoclimate proxy results shown down core with the lithology of Unit II for Site U1360. Figure shows values for a 1% CaCO3 correction as well as values with no CaCO3 correction.

and 51 mm annually. Standard errors were calculated for both MAP and MAT proxies by Sheldon et al., [2002] and show values of +/- 182 mm and +/- 4.4˚C, respectively.

Calculated MAT in the Prydz Bay late Eocene samples fluctuate between 10.2°C and 13.7°C (Figure 11). The trend plots similarly to CIA values, showing a drop of ~2°C from 156.26 to 153.81 mbsf, and fluctuations between 10°C and 11.5°C up-core. There is a marked upward increase to 13.7°C at ~138 mbsf, consistent with peaks in CIA values and precipitation. Fluctuations in the degree of warmer temperatures continue up core until a ~4°C drop between Eocene temperatures and Neogene temperatures across an unconformity.

In comparison to the Eocene samples from Site 1166 the Oligocene samples from Site U1360 show lower temperatures ranging from 8.1°C to 10.3°C (Figure 12). The trend in temperature appears to show a ~2°C warming up core and later a similar amount of cooling (Figure 12).

3.1.3 **Provenance Tracing**

The first step in provenance tracing was to calculate the Al_2O_3/TiO_2 ratios at each site to determine if there were drastic changes in the values, that would indicate a change in source material. Values at Site 1166 ranged from 18.9 to 24.5, which is not a major difference, suggesting little change in source material. The Al_2O_3/TiO_2 ratios from Prydz Bay sediments are consistent with felsic rocks from the Southern Prince Charles Mountains and the Eastern Amery Ice shelf [Sheraton et al, 1996], as well as the Grove Mountains [Liu et al, 2007]. A chart of Al_2O_3 to TiO_2 shows some separation in groupings for samples from Site 1166 indicating little source change, but possibly the addition of another rock type (Figure 13.A). In contrast, the same ratio applied to Site U1360 revealed values ranging from 21.4 to 45.1, this large range suggests that the sediment was sourced from different material. The plot of Al_2O_3 against TiO_2 clearly outlines three distinct groupings (Figure 13.B).

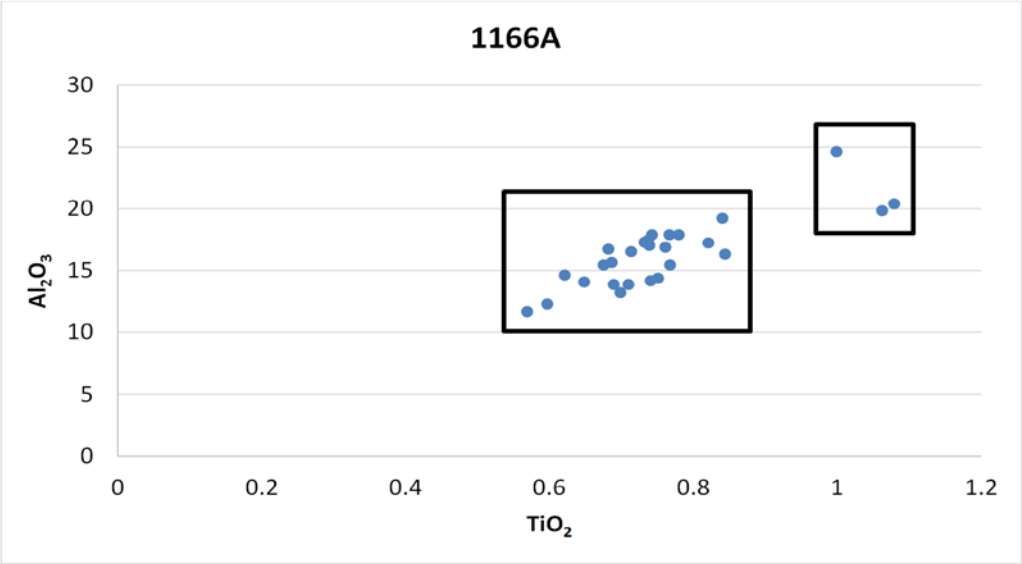

Figure 13.A. Chart showing groupings for Al_2O_3 and TiO2 from Site 1166. Separate groupings may indicate a change in source material.

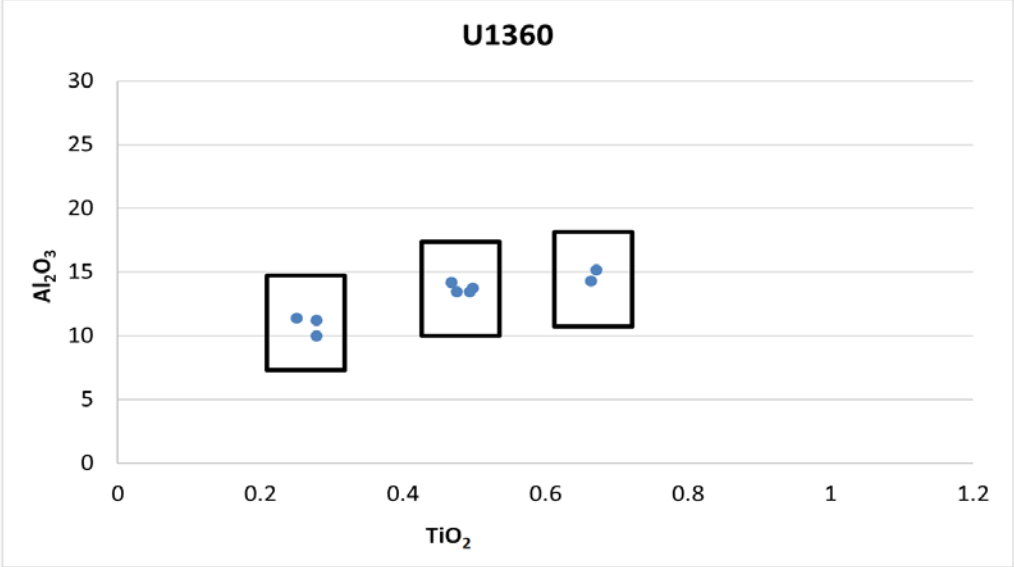

Figure 13.B. Chart showing groupings for Al_2O_3 and TiO_2 from Site U1360. Separate groupings may indicate a change in source material.

Mafic versus felsic diagrams were used to determine the proportions of mafic or felsic material from the samples, and compared with various rock sample sets from around each region.

Cr/V against Y/Ni plots for Site 1166 were put on a logarithmic scale to better represent the data. In each plot samples from Site 1166 show relatively consistent low ratios of Cr/V and more spread out Y/Ni that plot similarly to felsic metamorphic rocks (Figure 14.A) [Reategui et al., 2005], showing a dominant felsic component.

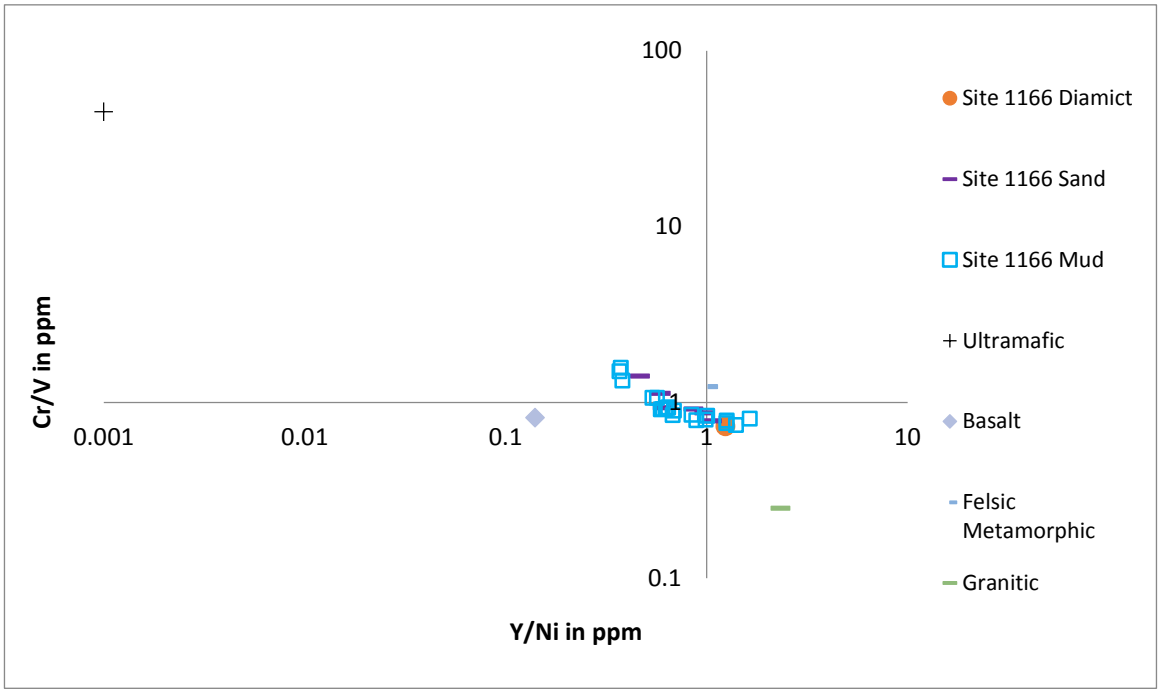

Figure 14.A. Cr/V vs. Y/Ni chart showing where Site 1166 samples plot relative to ultramafic, granitic, felsic metamorphic rocks [Reategui et al., 2005] and basalt [Faure, 1991].

Plotted with data from Liu et al. 2007 (Figure 14.B), the granulites from the Grove Mountains appear to contain slightly more felsic material than the samples from Site 1166. When plotted with various rocks from the Prince Charles Mountains (Figure 14.C), one sample plotted with the 1166 data, an orthopyroxene-granodiorite [Sheraton et al, 1996]. However, most of the rock types plot as more mafic or more felsic than the samples from Site 1166. When compared with samples from the Northern Prince Charles Mountains [Munksgaard et al. 1992] four of the published samples plotted similarly to the samples from Site 1166, two felsic-mafic granulites, and two leucogneisses (Figure 14.D).

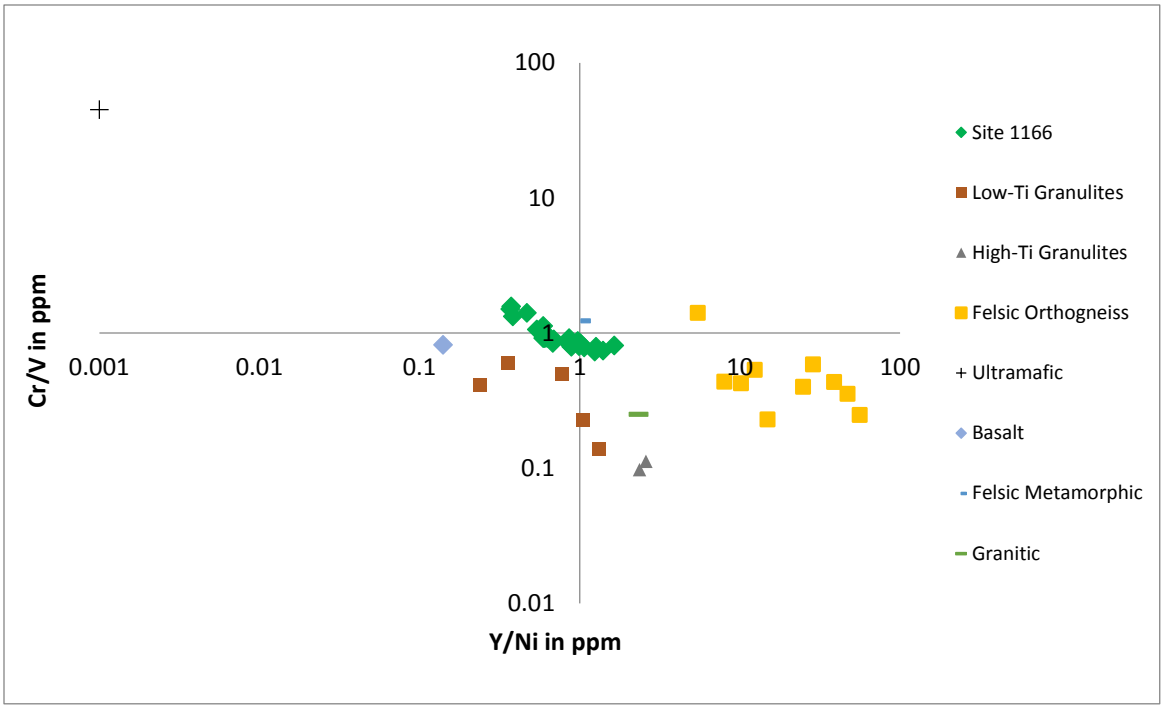

Figure 14.B. Cr/V vs. Y/Ni chart showing where Site 1166 samples plot in relation to samples from the Grove Mountains [Liu et al., 2007] with ultramafic, granitic, felsic metamorphic rocks [Reategui et al., 2005] and basalt [Faure, 1991] for reference.

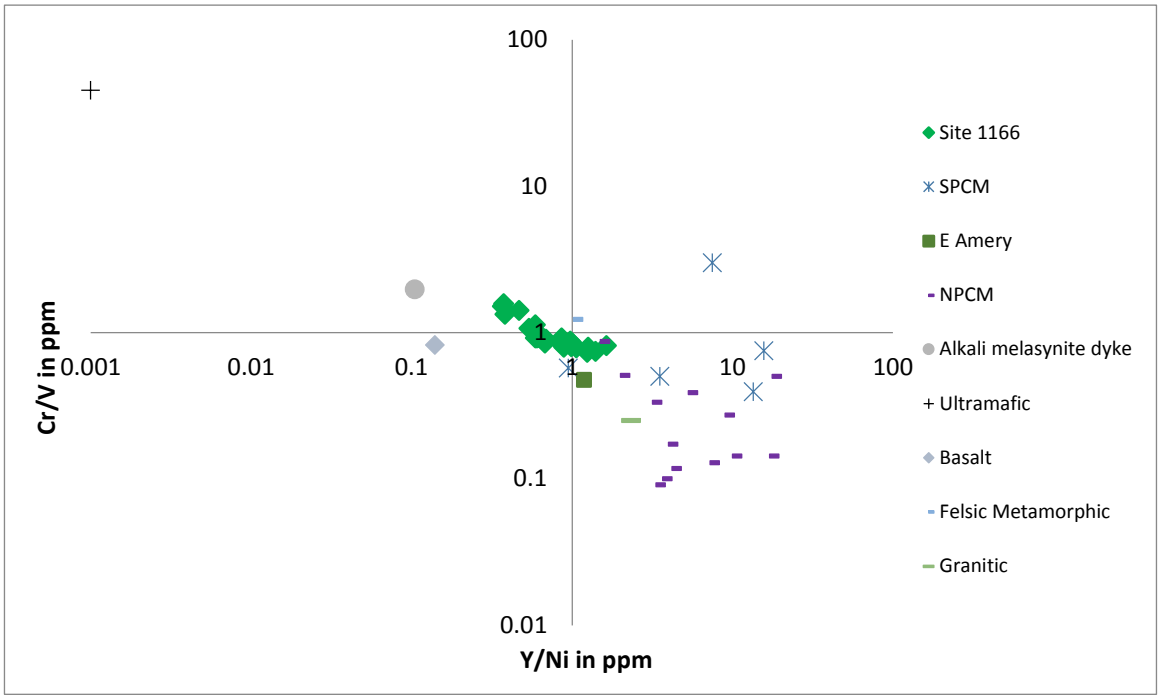

Figure 14.C. Cr/V vs. Y/Ni chart showing where Site 1166 samples plot in relation to samples from around the Prydz Bay region including the Southern Prince Charles Mountains (SPCM) and the Northern Prince Charles Mountains (NPCM) [Sheraton et al., 1996] with ultramafic, granitic, felsic metamorphic rocks [Reategui et al., 2005] and basalt [Faure, 1991] for reference.

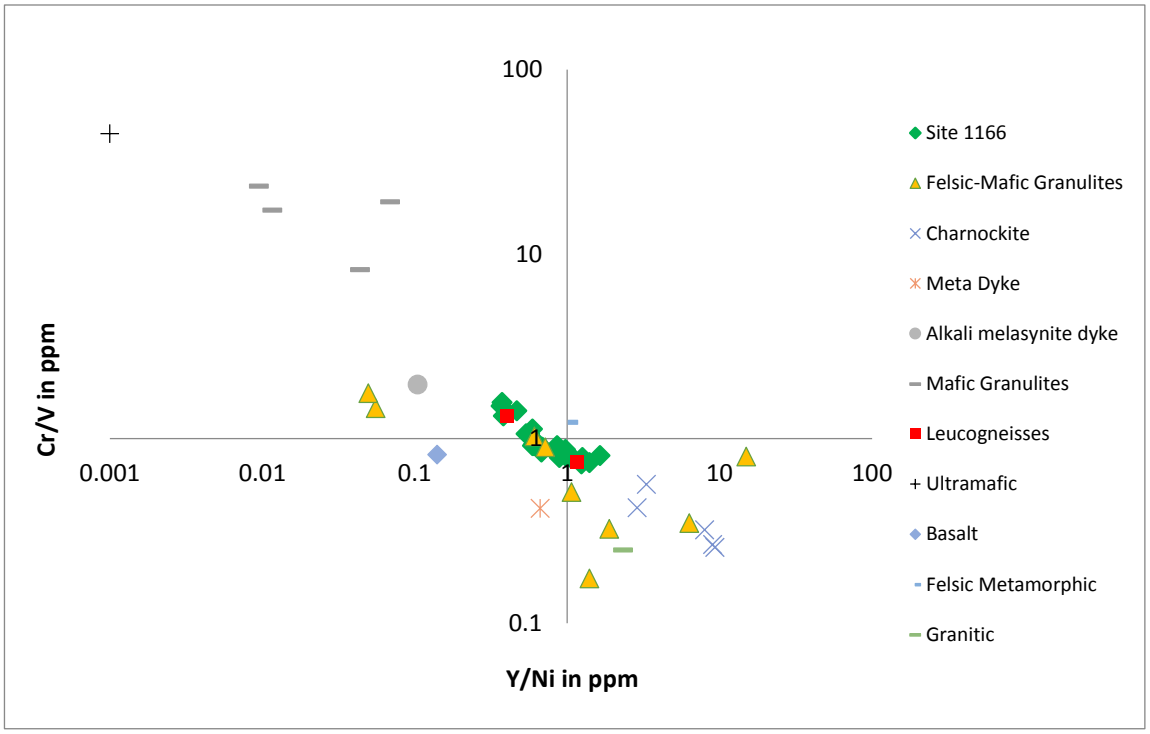

Figure 14.D. Cr/V vs. Y/Ni chart showing where Site 1166 samples plot in relation to samples from the Northern Prince Charles Mountains [Munksgaard et al., 1992] with ultramafic, granitic, felsic metamorphic rocks [Reategui et al., 2005] and basalt [Faure, 1991] for reference.

The felsic proportions for the study samples agree with the plot of Sc/Th against Cr/Th, where Sc and Cr are in higher abundance in mafic rocks, and Th is in higher abundance in felsic rocks. The samples plot to the lower left with average granites from Faure [1991] (Figure 15). The major felsic composition is also seen in the Th/Sc against Zr/Sc chart after McLennan et al. [1993], in which smaller ratios of Th/Sc and Zr/Sc indicate a mafic source material; following the line upward the source material becomes more felsic. It is noted that as ratios of Zr/Sc become larger the increased amount of Zr is thought to be a result of recycling (Figure 16) [McLennan et al., 1993].

Results for Site U1360 show that the samples contain more felsic material, with low Cr/V values and higher Al_2O_3/TiO_2 values (Figure 17). When compared to rock types from the region the samples plot well with muscovite and biotite granites [Goodge and Fanning, 2010], rhyolites, and rhyodacites [Peucat et al., 2002], confirming their felsic nature.

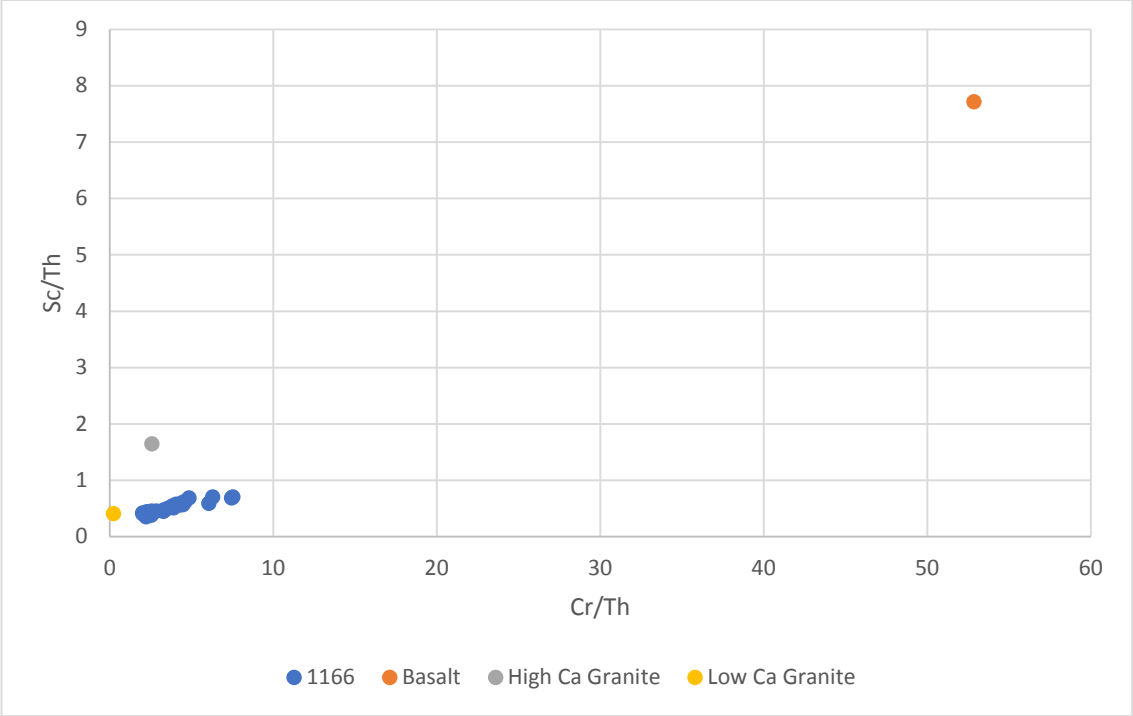

Figure 15. Graph of Sc/Th vs. Cr/Th [Potter et al., 2005], showing the relationship between mafic and felsic compositions for samples from Site 1166 and average basalts and granites [Faure, 1991].

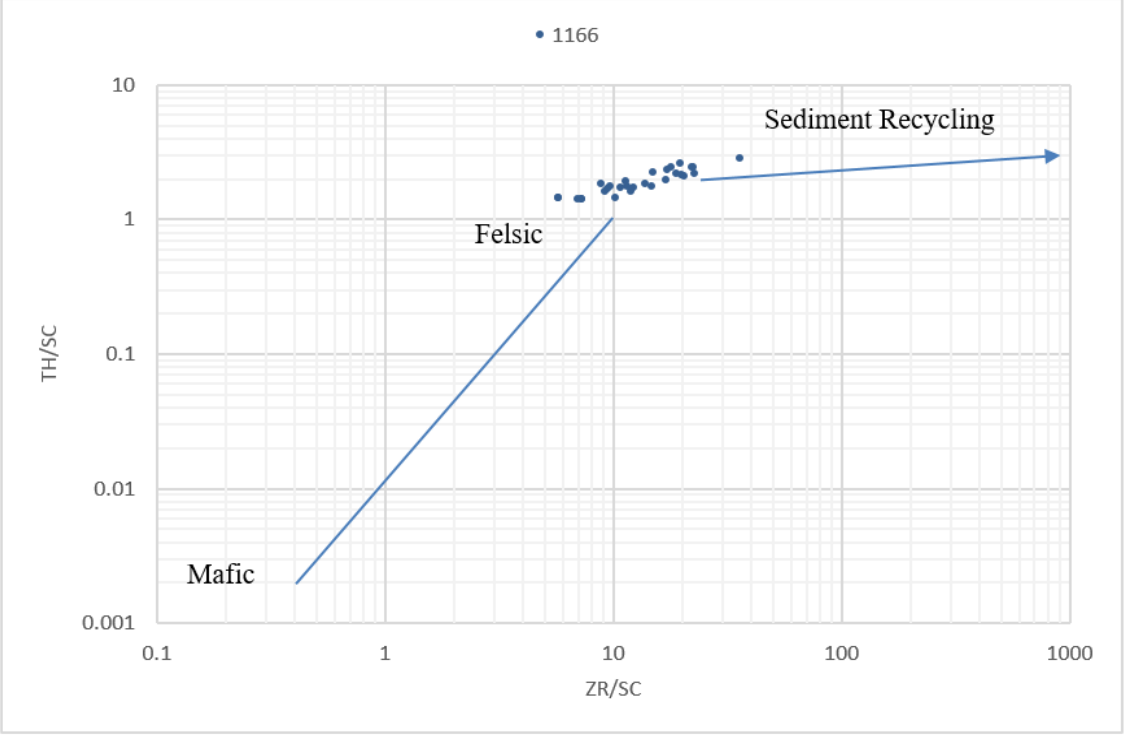

Figure 16. Th/Sc vs. Zr/Sc plot after McLennan et al., [1993] showing compositional change trend lines and sediment recycling trend lines.

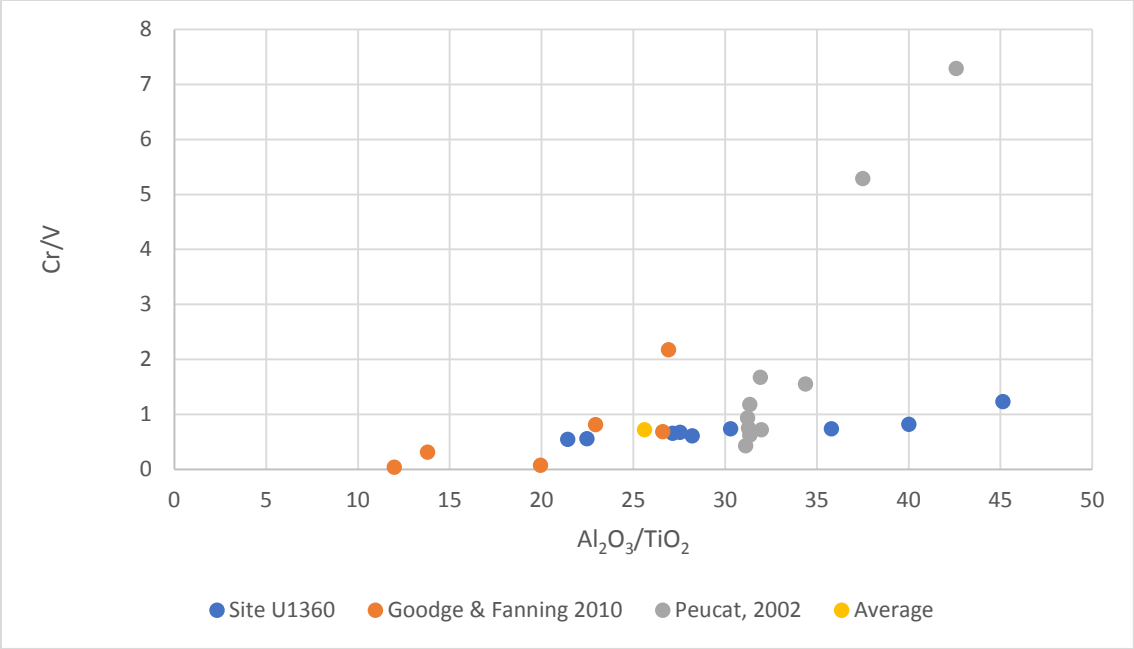

Figure 17. Plot of Cr/V vs. Al_2O_3/TiO_2 showing the relationship between mafic and felsic compositions for samples from Site U1360, plotted with data from Goodge and Fanning [2010] and Peucat et al., [2002], along with an average of the data from both authors.

3.1.4 **Elemental Enrichments**

Site 1166

Elemental spider diagrams were created for major, trace, and REE elements; charts were divided by core to show minor differences. All samples showed depletions in the major element oxides of Fe_2O_3, MnO, MgO, CaO, Na_2O, and P_2O_5 (see example Figure 18). CaO has the greatest amount of depletion followed by MnO. Other depleted elements vary in degree based on core (see appendix). In core 15R the overall trend shows that Fe_2O_3 and Na_2O are relatively similar in depletion value, as are K_2O and MgO. Three samples stand out from Core 15R that also show depletions in Al_2O_3 and TiO_2. This is opposite of the rest of core 15R in which Al_2O_3 and TiO_2 are slightly enriched. The Neogene diamict sample from core 15R also shows an enrichment of K_2O not seen in the other samples. All but three cores had a slight enrichment in SiO_2, the three outlier samples in core 15R showed only marginal depletion and were still very close to upper crustal values. Cores 16R and 17R show similar overall trends to core 15R, but with slight variations in TiO_2, Al_2O_3, and MnO.

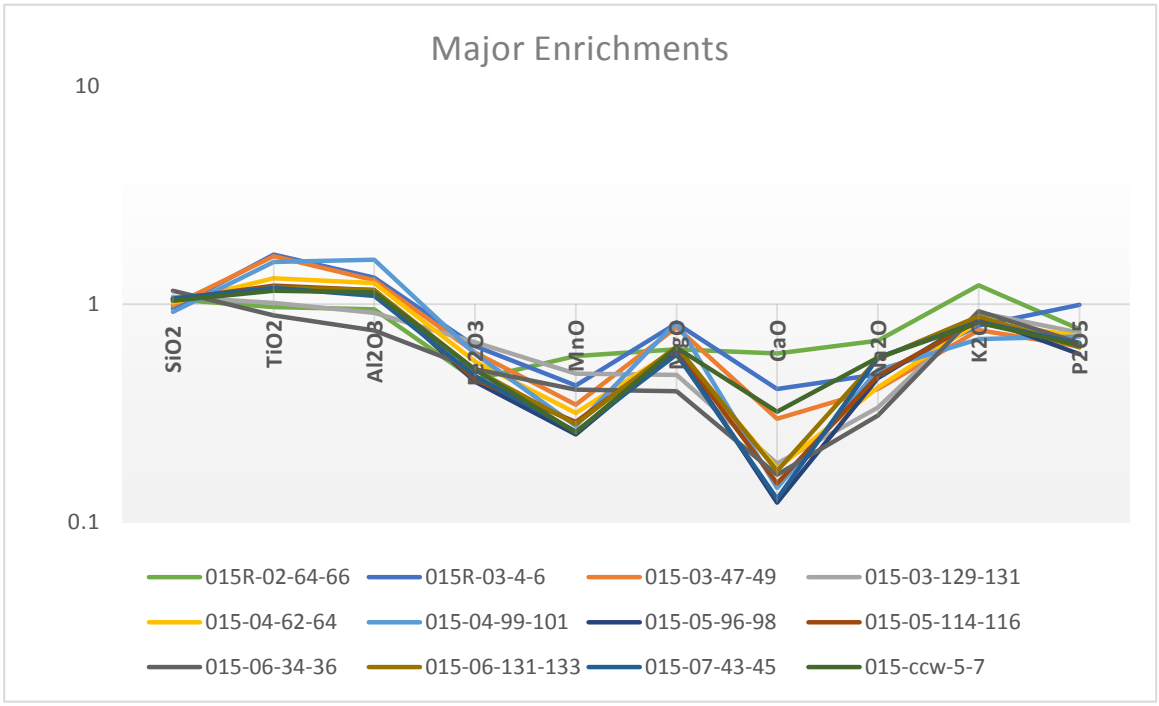

Figure 18: Major element enrichments over upper crust [Rudnick and Gao, 2004] for core 15R at Site 1166. Values over 1 indicate enrichment while values under 1 indicate depletion from the bulk sample.

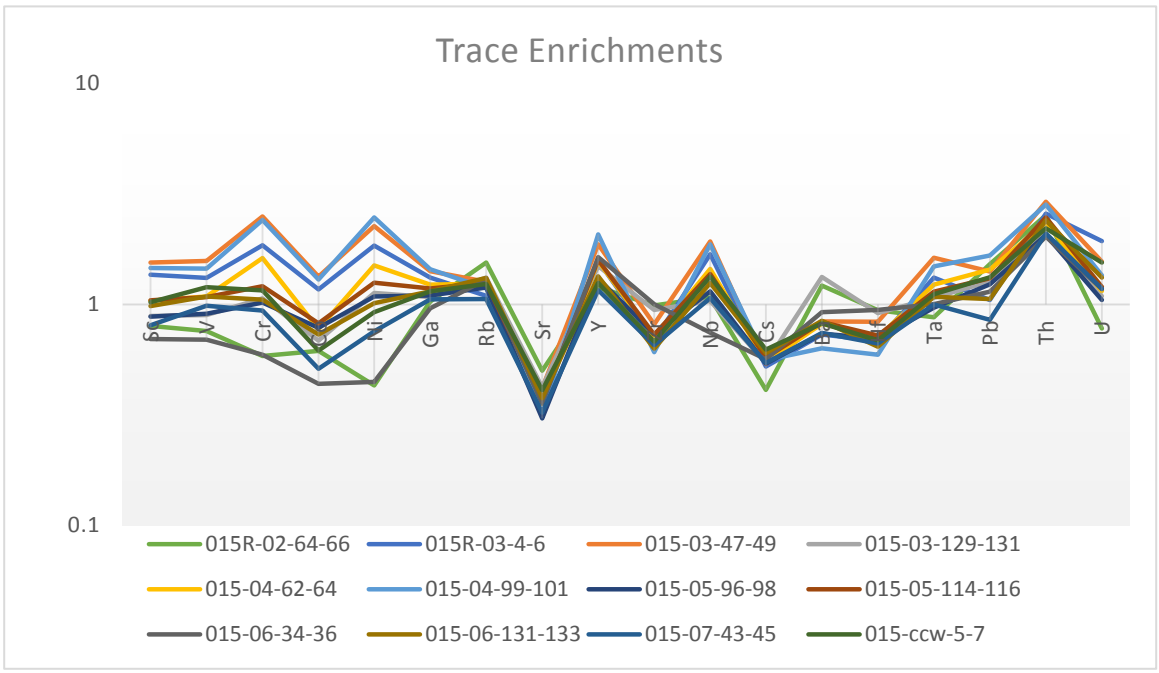

Figure 19: Trace element enrichments over upper crust [Rudnick and Gao, 2004] for core 15R at Site 1166. Values over 1 indicate enrichment while values under 1 indicate depletion from the bulk sample.

For all samples, the trace elements Sr and Cs are depleted and Th is enriched. Similar to the major elemental enrichment trends, enrichments and depletions for trace elements vary by core. In core 15R four samples stand out as enriched in Cr, Ni, V, and Sc and the overall trend for these elements shows increased depletion down hole; though two samples from core 15R stand out as depleted in both of these elements (Figure 19). Cobalt is enriched in three samples from core 15R and depleted in all other samples from this site. Zirconium becomes more enriched down hole as sediments become more laminated.

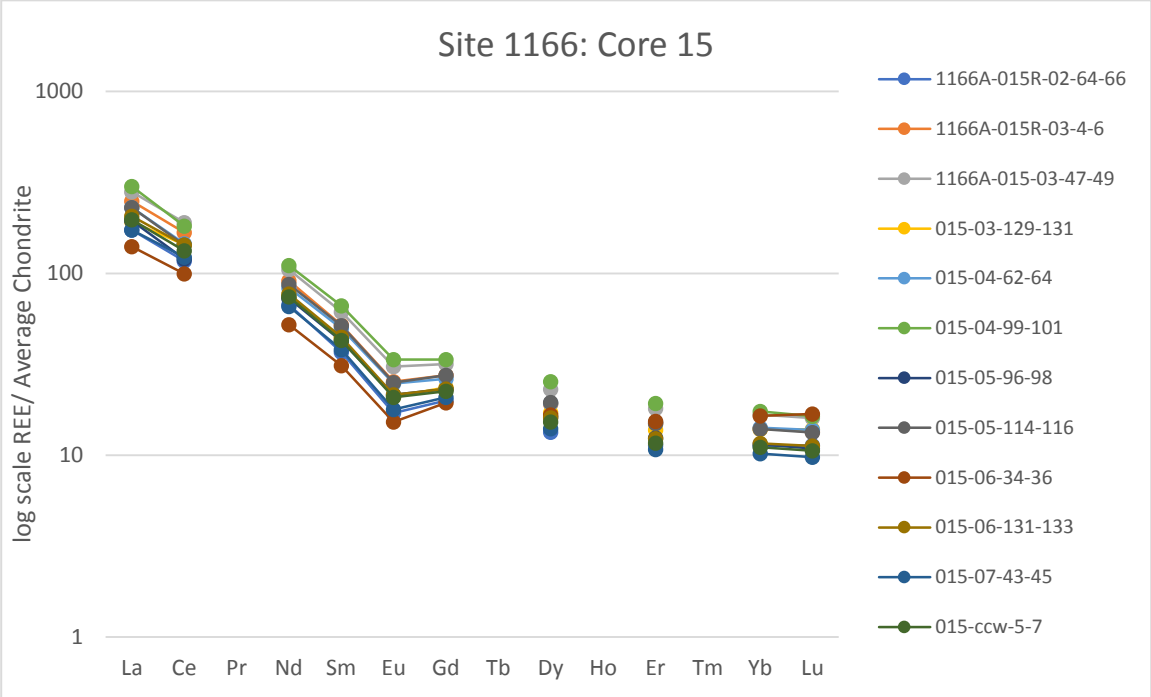

Figure 20: Rare Earth Elements normalized to an average chondrite [Nakamura, 1974] for core 15R at Site 1166.

REE shows a similar tend down hole from core 15R to core 17R. In core 15R the amount of enrichment decreases from lighter REE elements to heavier REE elements but still indicates enrichment (Figure 20). All samples show minor negative Eu/Eu* anomalies (* indicates Eu of samples, normalized to the Eu of an average chondrite [Nakamura, 1974]). Core 16R follows the same trend as core 15R but with a lesser degree of enrichment. core 17R plots similarly to 16R indicating little variation between the three cores in terms of REEs.

Site U1360

Major element enrichment trends differ by core and show similar grouping to the samples separated by the Al_2O_3 versus TiO_2 graphs. Core 4R is depleted in all major element oxides except for SiO_2, most so in Fe_2O_3 and to a lesser extent Na_2O (Figure 21). Cores 3R and 5R have a somewhat similar trend to core four but do show depletion in TiO_2 or K_2O, they also show a lesser extent of MgO depletion. The sample from core 3R, is the only sample enriched in P_2O_5. core 6R, like core four is depleted in all elements with the exception of SiO_2; however, the degree of depletion is much higher than that of core 4R.

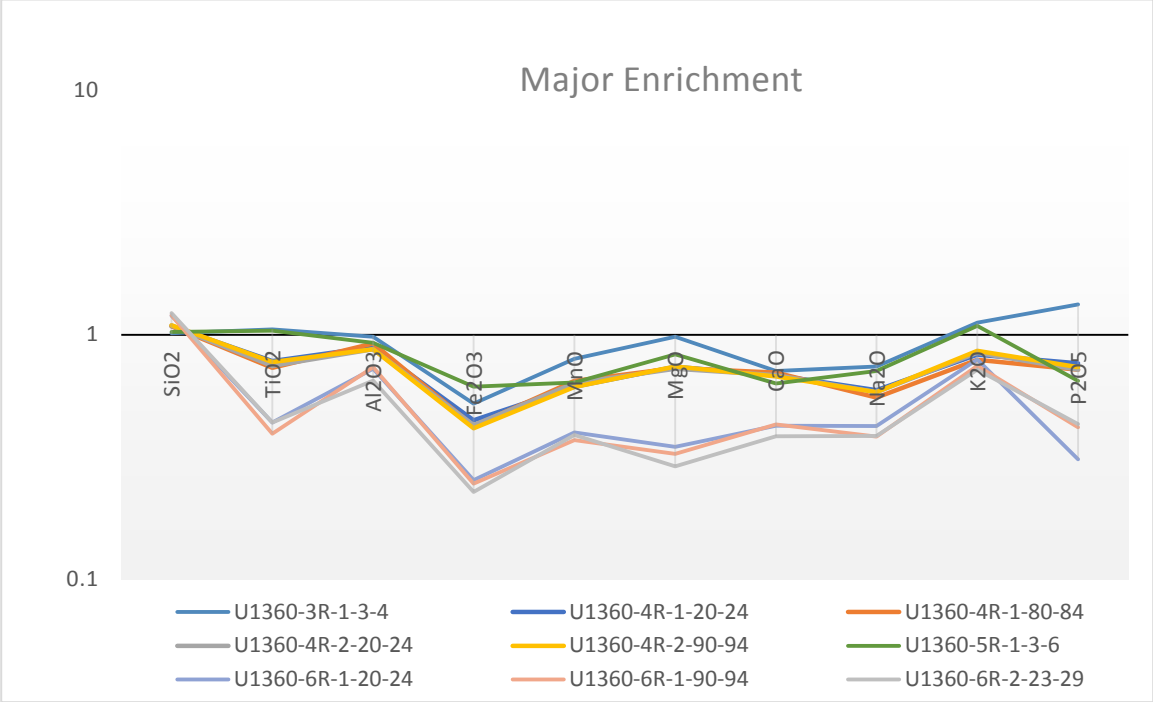

Figure 21. Major element enrichments over upper crust [Rudnick and Gao, 2004] for cores 3R, 4R, 5R and 6R from Site U1360.

Trace element enrichment trends are similar between cores 3R, 4R, and 5R, indicating depletions in Ba, Cr, and Sr. Trace elements V, Y, Zr, and Sc vary marginally, with cores 3R and 5R showing enrichment is Sc, V, and Y, with depletion in Zr (Figure 22). While core 4R shows little enrichment in Sc, Y, and Zr, with depletion in V. Core 6R differs from the other cores in that all elements except Zr are depleted.

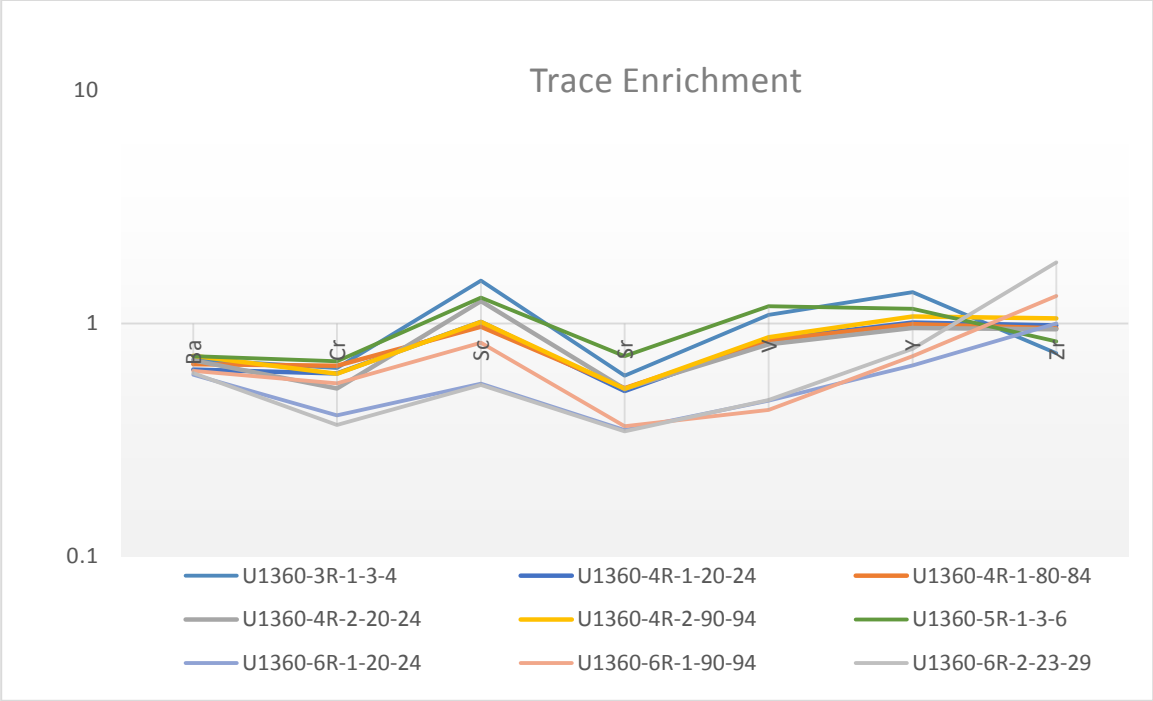

Figure 22. Major element enrichments over upper crust [Rudnick and Gao, 2004] for cores 3R, 4R, 5R, and 6R from Site U1360.

3.2 LASER PARTICLE SIZE DISTRIBUTION

Particle size analysis was done on samples from cores 55R to 59R from Site 696, core 55R was divided by section number as sections differed in mode of material, though all samples are classified as poorly sorted. Detailed particle size distributions can be found in the appendix.

3.2.1 **Particle Size Comparison**

The particle size percentages from Site 696 were plotted with the particle size percentages from Sites 1166 and U1360 [Ciarletta, 2014], and are compared on a ternary diagram of sand, silt, and clay as seen in Figure 23. The majority of samples from Site 1166 plot > 60% silt, with a few outliers plotting in the range of 50-60%. Similarly, the majority of samples at this site plot <20% clay, although, there are two outliers between 30-40%. All samples from this site are <40% sand. Similar to Site 1166, samples from U1360 contain <20% clay, and the majority are >60% silt; however, three samples are >50% sand. Unlike Sites 1166 and U1360, Site 696 shows a wider

distribution of particle sizes, that overall indicates finer grained sediment than that of the other two sites, and all three sites show a fining upward sequence.

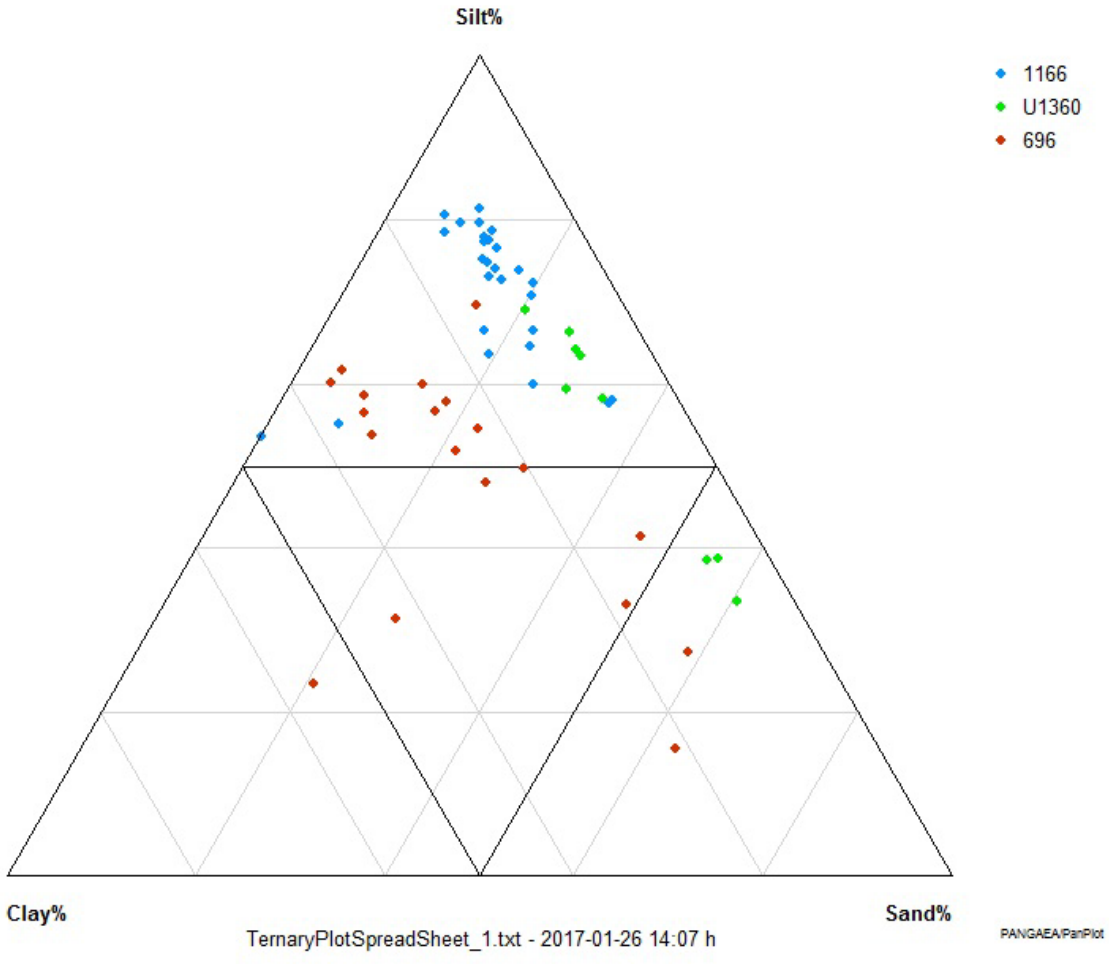

Figure 23. Ternary plot showing the grain size distributions between samples from Site 696, 1166, and U1360.

4. **DISCUSSION**

4.1 PALEOCLIMATIC CONDITIONS

The calculated CIA values for late Eocene sediments of Unit II in Prydz Bay indicate a dominant chemical weathering regime, with values exceeding 65. Contrastingly, the Neogene diamict that sits on top of these sediments indicates a dominant physical weathering regime, with a value of 57, as is expected with a significant glacial influence [Passchier et al., 2013]. The Eocene

values are consistent with previous studies from the area that range from ~67 to 80 [Passchier et al, 2013, Passchier et al., 2017]. Lower values of 68 may indicate an increase in physical weathering [Passchier et al., 2017], but does not likely indicate ice sheet growth. Higher values of 77-80 indicate a more intense chemical weathering period, consistent with higher temperatures and increased precipitation as seen in Figure 11.

MAT values calculated from the S-index, range from ~10 to ~14˚C for the late Eocene and show a ~8˚C temperature for the Neogene diamict. Showing an overall temperature drop from warmest late Eocene in Prydz bay to cooler Neogene ice cover of ~6˚C. These temperatures are likely to represent summer temperatures as mentioned in Passchier et al., [2017]. MAP values for the Prydz Bay region during the Eocene range from ~860 mm to ~1166 mm. These values are consistent with a warmer more humid environment, in agreement with the dominant kaolinite clay mineralogy found at the base of Unit II at Prydz Bay [O'Brien et al, 2001, Potter et al., 2005]. Macphail and Truswell [2004] discovered a low diversity of angiosperm species in the Eocene sediments of Site 1166, which suggest a rainforest scrub environment. It is mentioned that similar modern-day taxa are found in regions with 1200-2500 mm/yr precipitation, and it shows that the Eocene taxa could survive in a somewhat harsher environment than its modern-day counterpart. [Macphail and Truswell, 2004].

Carter et al. [2016] suggest based on apatite fission track and zircon U-Pb ages of ice rafted debris (IRD) found at distal Site 696, that widespread glaciation would have been present by ~36 Ma, enough so that glacial ice would have reached the ocean near the southern Weddell Sea sector. The combined CIA, temperatures, and precipitation from this study on Site 1166 in Prydz Bay (~35.7 Ma) do not suggest a significant glacial flour contribution from East Antarctica [Nesbitt and Young, 1982, Passchier et al., 2013], meaning, it is likely that during the late Eocene the main contribution of glacial material to shelf sites came from localized mountain glaciers, as is thought

to be the case in Prydz Bay [Passchier et al., 2017], and not the formation of a larger ice sheet at this time.

Contrastingly, Early Oligocene sediments from Site U1360 on the Wilkes Land margin show a dominant physical weathering regime, as CIA values for samples that were carbonate corrected as well as samples that were not, are still well below 65 (Figure 12). This suggests an environment with a larger contribution of glacial rock flour. Temperatures between ~8 and ~10˚C and annual precipitation ranging between ~360 mm and ~700 mm, suggest that the early Oligocene at the Wilkes Land was a cooler and more arid environment. This is in agreement with clay mineralogy showing dominant illite and smectite [Expedition 318 Scientists, 2010, Potter et al., 2005]. Recently a study was done by Galeotti et al. [2016] using sediment cores from the Ross Sea, that indicate a full-scale ice sheet was not present until ~32 million years at their study sites. However, the paleoclimate data recovered from the Wilkes Land site, indicates a significant amount of ice present at the beginning of the Oligocene (~34 Ma). The geochemical proxy data indicates a substantial difference between the Late Eocene warm and semi-humid environment at Prydz Bay and the cold and more arid environment of the Wilkes Land during the Early Oligocene.

4.2 SOURCE MATERIAL

4.2.1 **Site 1166**

At Site 1166, Al_2O_3/TiO_2 ratios show a slight offset in groupings amongst the samples as seen in Figure 13.A, suggesting that there is not a drastic change in provenance, but there is a slight increase in both TiO_2 and Al_2O_3. Overall Al_2O_3/TiO_2 are similar to rocks found in the Southern Prince Charles Mountains (SPCM) and the Eastern Amery Ice shelf [Sheraton et al, 1996], as well as the Grove Mountains [Liu et al., 2007].

Initial analysis of the elements downcore showed an increase in mafic elements Cr, Ni, and V in core 15R toward the top. To better understand both provenance and these increases, Cr/V ratios were plotted against Y/Ni ratios to determine whether the sediment had a mafic or

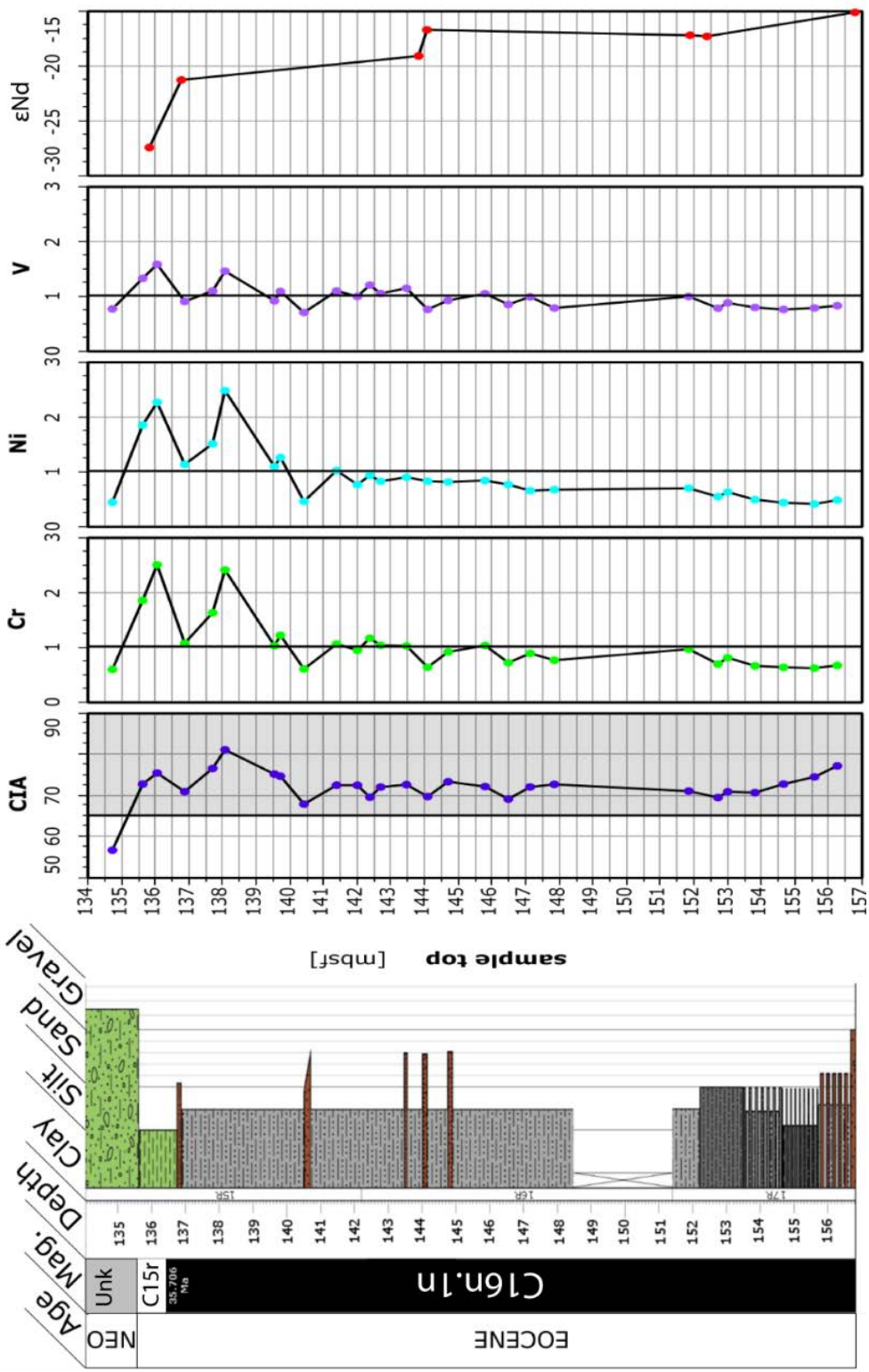

Figure 24: Ferromagnesian elemental enrichments of Cr, Ni, V, plotted against calculated CIA values from this study and εNd values from van de Flierdt et al., [2008]. Shaded CIA values indicate a chemical weathering regime.

felsic signature. Ultramafic rocks plot with very high Cr/V ratios and low Y/Ni ratios; whereas, granitic rocks plot higher in Y/Ni and lower in Cr/V.

Plots to determine the proportions of mafic to felsic material show that all samples are dominantly composed of felsic material. Rocks for the region were plotted similarly against the study samples to see which regions showed similar proportions of mafic material. The region that plotted similar was the Northern Prince Charles Mountains (NPCM) [Sheraton et al, 1996, Munksgaard et al., 1991]. However, samples from the NPCM that overlap the higher Cr, Ni, and V samples only have a similar ratio, and in most cases, do not contain comparable concentrations of the elements [Munksgaard et al., 1991; Sheraton et al., 1996]. While these plots cannot be used to compare elemental concentrations, they do provide an idea of the mafic vs felsic proportions in each region, which can be used to better understand the provenance.

A particle size influence was ruled out by plotting the data as different size fractions (Figure 14.A), as the data plotted as well mixed. A change in the mafic elements up-core due to chemical weathering was also ruled out, as Cr, Ni, and V are leached out of mafic minerals during chemical weathering. It would be expected that at times of peak chemical weathering the abundance of these elements would be lower, showing an inverted trend to the CIA. Also, if the Cr, Ni, and V were enriched due to weathering it would be expected that they would be enriched at the base of Unit II as well. As the elements covary with higher CIA values in core 15R (Figure 24), it was determined that the elevated ppm was likely due to a slight change in provenance and not the degree of chemical weathering.

The NPCM and the Grove Mountains, both contain mafic granulites [Munksgaard et al., 1991; Liu et al., 2007], and the SPCM contains a swarm of mafic dykes [Mikhalsky et al., 2013]; in these regions, geochemical analysis shows that certain rock types contain similar proportions to the study samples of the aforementioned mafic elements (Figure 7). Eocene topographic reconstructions (Figure 25) [Wilson et al., 2012] show that the NPCM region was of higher elevation and likely contributed to sediment supply, as were the Grove Mountains to the

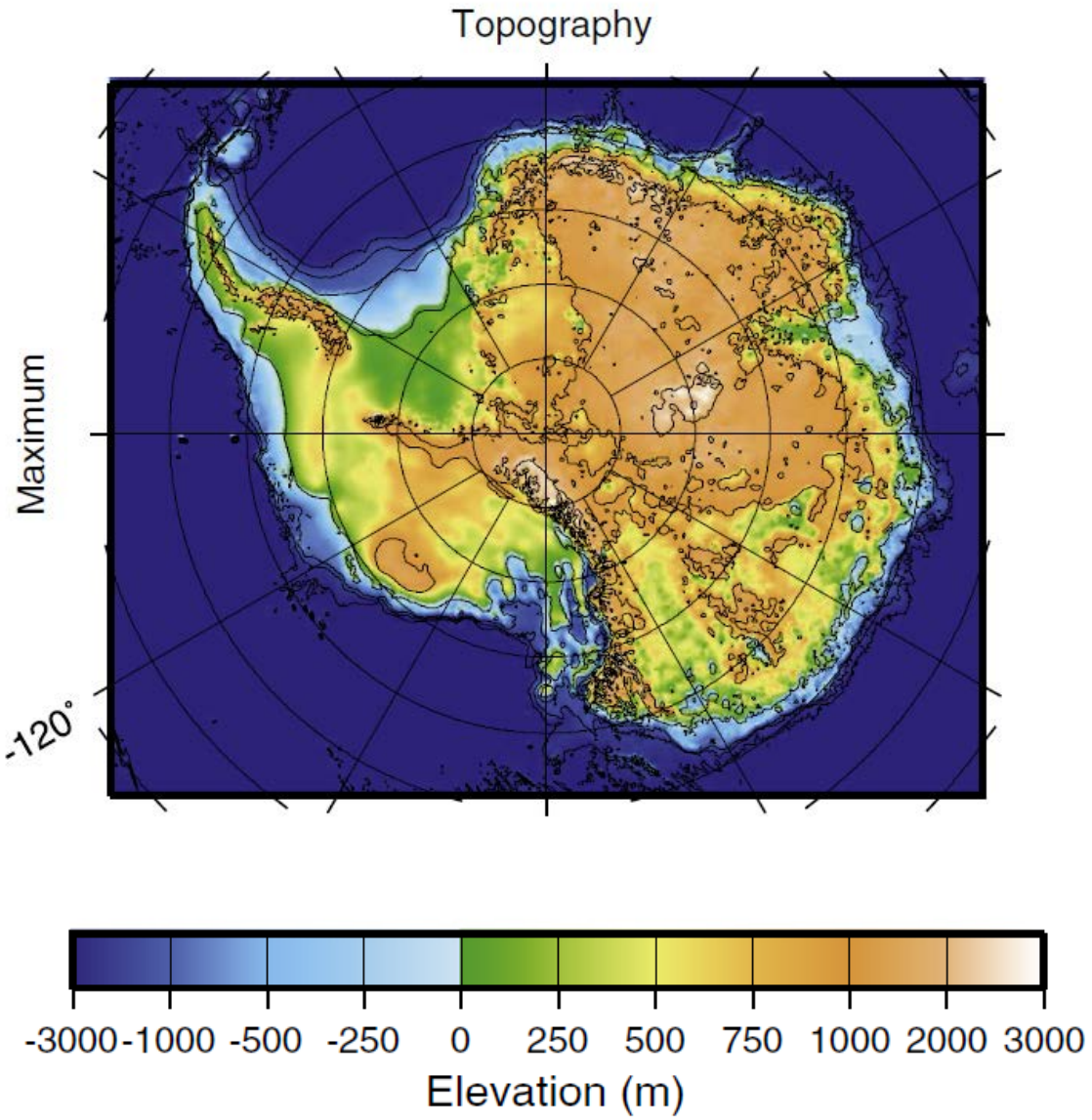

Figure 25: Maximum elevation Eocene-Oligocene topographic reconstruction from Wilson et al., [2012] showing the topographic high points around Prydz Bay.

East. However, the NPCM region also contains Cretaceous aged rocks [Thomson et al., 2013], and according to apatite fission track ages taken from Unit II at Site 1166, the coarse sediment fraction in this unit does not contain material of Cretaceous age, and is likely sourced from further inland [Thomson et al., 2013]. This makes a reasonable case for the Grove Mountains and the SPCM as possible sources for the mafic material.

Nd isotopic ratios (εNd) from van de Flierdt et al., [2008] show large negative εNd values for Unit II, with calculated crustal residence ages of 2.0-3.0 Ga suggesting a very old Proterozoic/Archean upper crustal source material. The ages increase from the bottom of Unit II upward, with the oldest ages coinciding with the peak of mafic enrichment (Figure 24). The εNd crustal residence ages from the Grove Mountains show the majority of rocks ranging from 1.76-1.65 Ga, with the exception of felsic orthogneisses that range from 2.46- 2.27 Ga, and a 50 m wide paragneiss outcrop that contains spinel and has a εNd value of -24.5, with a residence age of 2.99 Ga [Liu et al., 2007]. The SPCM region shows εNd values that range from -0.5 to -23 with residence ages from 1660 – 3850 Ma [Mikhalsky et al., 2013]. Based on the εNd values, crustal residence ages and the amount of source material available, it is more likely that the SPCM are the source material for the mafic component. This source material is further supported by the Archean age of the rocks in this region (Figure 8); McLennan et al., [2000] mention that Archean continental crust contains much higher concentrations of ferromagnesian trace elements, which supports the SPCM as the most likely source of enrichments in core 15R.

The Gamburtsev Mountains are considered to be the nucleation point for ice growth in the Prydz Bay region [DeConto and Pollard., 2003]. Eocene drainage and topographic reconstructions [van de Flierdt et al., 2008; Wilson et al., 2012] indicate that a glacial path from this nucleation point would travel through the SPCM and the Lambert Graben, eventually draining into Prydz Bay. It has been established that Site 1166 during the Eocene was ice proximal [Strand et al., 2003], meaning that a glacier was present in the hinterland of Prydz Bay. One explanation as to why the mafic component is not seen earlier may lie with the amount of felsic material in the region, the mafic material from the SPCM was likely diluted by the amount of felsic material being entrained in the drainage basin. At ~138 mbsf based on upward increasing temperature and weathering proxies it is likely that the glacier was retreating (Figure 24). The glacier could have retreated to a point in which the amount of felsic material added to the system decreased enough for the localized

mafic signature to increase. The drop in temperatures, and increase in particle size at ~137 mbsf could indicate an advance of the glacier with more felsic material, and another retreat at ~136 mbsf. Though this is one possible interpretation for the source material, the Grove Mountains cannot be ruled out as a possible source at this time.

Enrichments

The majority of elemental depletions at this site can be attributed to weathering. Initial mineralogical analysis from smear slides and X-ray diffraction show dominant quartz and clay minerals (Kaolinite), with plagioclase, K-feldspar, and some pyrite [O'Brien et al., 2001]. Due to a high chemical weathering regime, the depletions in CaO and Na_2O are likely a loss of Ca and Na ions as anorthite and albite convert to kaolinite [Faure, 1991]. Sr often substitutes for Ca in anorthite, and Cs for Na in albite [Heier, 1962], these trace elements also become soluble in the creation of kaolinite, accounting for the depletion seen in all samples. Chemical weathering is also likely the cause of depletions in MnO and Fe_2O_3 as Mn and Fe are easily mobile in surface waters [Post, 1999; Faure, 1991]. Depletions of Cr, Ni, V, Sc, and Co in cores 16R and 17R are consistent with a material that is slightly more felsic than the average upper crust (Wedepohl, 1978), as is the enrichment of Th seen is all samples. Core 15R shows enrichment of Sc, Cr, V, Ni, and Co consistent with a change in the source material, including a more mafic component. Interestingly, the three cores showed little variation in REE chondrite normalized data, though enrichments do seem to be slightly higher in core 15R than 17R. The slight negative Eu/Eu* anomaly suggests a more felsic source material [Potter et al., 2005], that is consistent with all other geochemical proxies.

4.2.2 **Site U1360**

At Site U1360 the Al_2O_3/TiO_2 ratios showed small clusters that indicate a change in source material. The proportions of mafic to felsic material in two groups of the study samples overlap with Muscovite-Biotite and Biotite Granite clasts found off the coast [Goodge and Fanning, 2010], sourced from the Mertz Glacier. The trace element enrichment diagram (Figure 22) shows an

enrichment of Sc and V, which have been found to preferentially inhabit muscovite over biotite [Yang and Rivers, 2000]. This may indicate that muscovite-biotite granites dominate the source material for cores 3R and 5R, while core 4R could be dominantly sourced from biotite granites. The group of samples that show the highest ratios of Al_2O_3/TiO_2 and are the most different from the other samples are the three samples from core 6R. These samples contain a >50% sand fraction and it is likely that the difference in Al_2O_3/TiO_2 ratios and elemental enrichments and depletions is due to a grainsize effect. Essentially, during transport from the Mertz Glacier, there is a loss of finer material that consists of weathered alkali feldspars, micas, and mafic minerals, leaving behind a greater overall concentration of quartz. This is consistent with depletions in most of the major elements and trace elements as well as the enrichment of SiO_2. To fully determine the provenance of the sediments a more in depth mineralogical study will need to be conducted, however based on the data from this study it can loosely be interpreted that during the Oligocene the dominant sediment source to Site U1360 came from granites to the East of the Mertz Glacier region.

4.3 SEDIMENTOLOGICAL CONDITIONS

In comparing the particle size from all three sites (Figure 23), sediment at Site 696 skews noticeably toward clay indicating that it may have been at a greater shelf depth than Sites 1166 and U1360. Sedimentological analysis of Site 696 shows a steady fluctuation between sand and silt throughout the sampling, and overall shows a fining upward sequence from the bottom of the section at 607.06 mbsf to the top at 568.9 mbsf. With a dominant sand influence near the bottom and decreasing in particle size to a dominant silt influence at the top. Fining upward sequences are indicative of a transgressive system [Boggs Jr., 2011]. Two of the most common causes for sea level rise are local subsidence and the melting of large amounts of ice [Boggs Jr., 2011]. As the EOT was a time of ice growth, it is likely that the transgressive system is attributed to subsidence. A study done in 2013 by Stocchi et al., explains that while far field studies show a eustatic sea level drop as the EAIS grows, modeling and near field shelf sites (i.e. Sites 1166 and U1360) show an increase in relative sea level, as the ice sheet depresses the continental crust. While this is a

plausible explanation for the fining upward sequence, the Stocchi et al., [2013] model did not include more distant West Antarctic records. One other explanation is that local subsidence is occurring due to tectonic deepening from the creation of the Powell Basin.

Figure 26.A, 26.B, and 26.C show the particle size distributions for each site in percentages downcore from left to right. Based on applied age models it was determined that Unit II of Site 1166 is similar in age to the section of Site 696 that lies between ~598 and ~607 mbsf. Therefore, at ~35.7 Ma, East Antarctic deposition was dominantly silt (Figure 26.B); while the West Antarctic deposition was dominantly silty sand; similar clay percentages could indicate a similar water depth for both sites. Site 1166 shows a fining upward sequence indicating a transgressive system [O'Brien et al., 2001] as well; however, glacial retreat can also account for the deposition of finer sediments and therefore it cannot be differentiated as specifically due to relative sea level rise. Though it can be said that the relative sea level rise happened over a longer period of time at the distal Site 696.

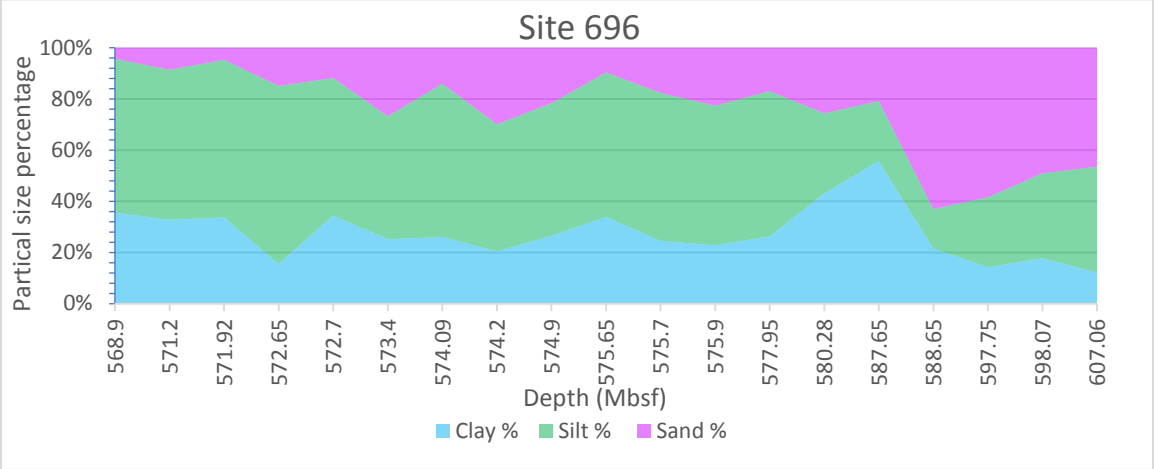

Figure 26.A. Particle size percentages down core plotted with depth in meters below sea floor for Site 696. In terms of Age Site U1360 falls between 568.9 and 571.2 mbsf, while Site 1166 falls between 598.07 and 607.06 mbsf.

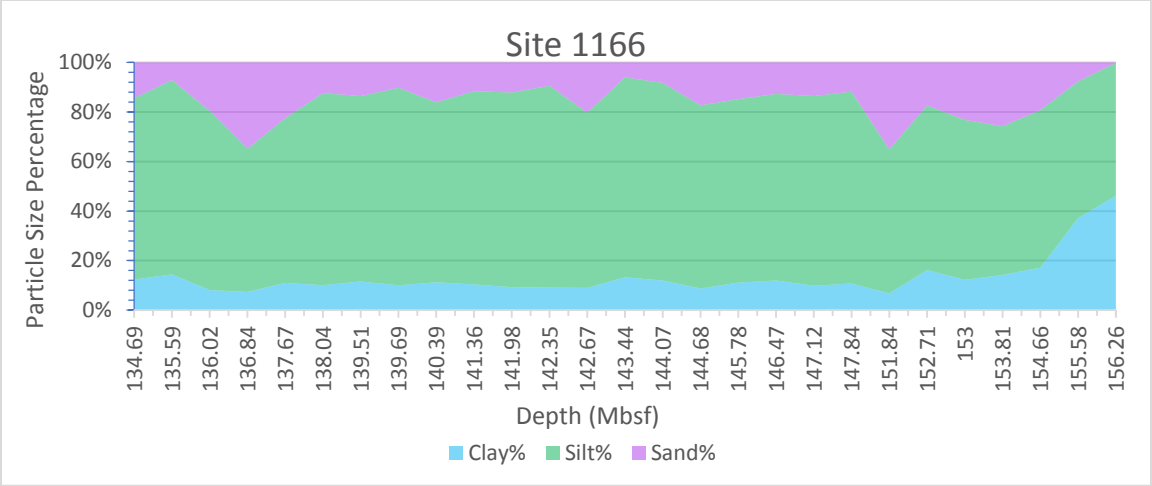

Figure 26.B. Particle size percentages down core plotted with depth in meters below sea floor for Site 1166.

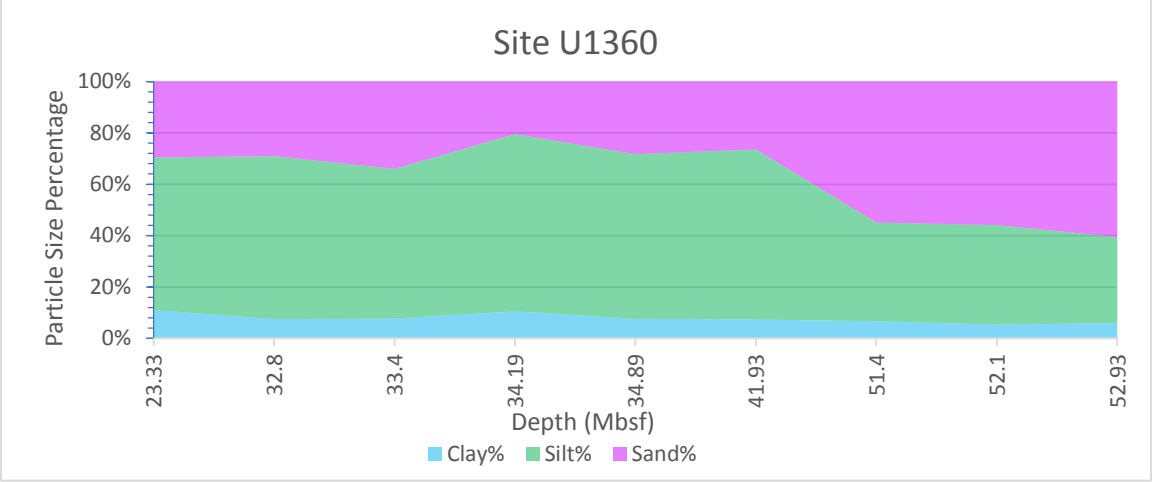

Figure 26.C. Particle size percentages down core plotted with depth in meters below sea floor for Site U1360.

The Oligocene section at Site 696 lies somewhere above ~571 mbsf, and consists of dominantly silt and clay, with very little sand (Figure 26.A), again indicating a deeper depositional environment. Contrastingly, Site U1360 contains dominant silt and sand with very little clay, but overall shows a fining upward sequence that is probably more an influence of glacial erosion and sediment supply.

5. **CONCLUSIONS**

By applying updated age models to new geochemical records from around the East Antarctic margin it was possible to reconstruct paleoclimatic conditions and better understand the

provenance for two different sites and time periods: The Late Eocene leading up to the EOT and the Early Oligocene immediately following the EOT. It was determined that during the late Eocene (~35.7 Ma), significant ice expansion was not present based on CIA values > 65 (dominant chemical weathering regime) and temperatures reaching ~14˚C. Multiple warming events were captured from the mudstones of Prydz Bay, which coincide with changes in Al_2O_3/TiO_2 ratios and an increase in mafic trace element geochemistry, indicating a slight change in dominantly felsic source material. One interpretation of the data is a glacial advance and retreat cycle that changes the amount of felsic material supplied to the region; however, the Prydz Bay geology contains at least two possible source areas and cannot be narrowed further without a more in depth isotopic geochemical study.

Contrastingly, Oligocene Site U1360 showed CIA values <65 and cooler temperatures indicating a dominantly physical weathering regime, and a change to a cooler more arid terrestrial environment. Al_2O_3/TiO_2 ratios suggested a change in provenance; however, based on grain size data and elemental enrichments it is interpreted that the provenance for this site remains the same and that the separation is likely the result of particle size. Overall the geochemical study allowed for a more complete picture of glacial dynamics in the Prydz Bay region during the late Eocene, as well as the change from Eocene warm humid conditions to Oligocene cool arid conditions, consistent with the growth of continental ice.

Sedimentological study of West Antarctic Site 696 showed overall finer sediment than the East Antarctic Sites indicating that it was likely a deeper shelf site. The samples showed an overall fining upward sequence in the hole from Eocene to Oligocene, consistent with a marine transgression, similar to sediments in Prydz Bay. The relative sea level rise is likely due to crustal subsidence from the weight of a continental ice sheet [Stocchi et al., 2013].

As the inception and spatial distribution of the EAIS through time is still poorly understood, it is important to study sedimentological and paleoclimatic conditions at high resolution time scales to better decipher and model ice sheet growth. In a broader sense, it is important to study the

inception of the EAIS during a time of elevated atmospheric CO_2 levels and warmer polar conditions to better understand how the ice sheet may react if global temperatures and atmospheric CO_2 continue to rise.

6. **REFERENCES**

Anderson, J. B. Antarctic Marine Geology. Cambridge: Cambridge UP, 1999. Print

Barker, P.F., Kennett, J.P., et al., 1988. Proceedings of the Ocean Drilling Program, Initial Reports, 113. Ocean Drilling Program, College Station, Texas.

Blott, S. J., and Pye, K. "GRADISTAT version. 8." A Grain Size Distribution and Statistics Package for the Analysis of Unconsolidated Sediments by Sieving or Laser Granulometer (2010).

Boggs, Jr, S. *Petrology of Sedimentary Rocks*. 2nd ed., Cambridge, Cambridge University Press, 2009. Print

Boggs, Jr, S. *Principles of Sedimentology and Stratigraphy*. 5th ed., Pearson, 2011. Print.

Carter, A., Riley, T.R., Hillenbrand, C., and Rittner, M. "Widespread Antarctic Glaciation during the Late Eocene." *Earth and Planetary Science Letters* 458 (2017): 49-57.

Ciarletta, D., "*Characterization of Eocene-Oligocene Depocenters in Prydz Bay, East Antarctica: A Lithostratigraphic Correlation of ODP Sites 739,742, and 1166*". Montclair: Montclair State University, 2014. Print.

DeConto, R. M., and Pollard, D. "Rapid Cenozoic Glaciation of Antarctica Induced by Declining Atmospheric CO2." *Nature* 16 Jan. 2003: 245-48.

Expedition 318 Scientists, 2010. Wilkes Land Glacial History: Cenozoic East Antarctic Ice Sheet evolution from Wilkes Land margin sediments. IODP Prel. Rept., 318. doi:10.2204/iodp.pr.318.2010

Fitzgerald, P. A. U. L. "Tectonics and landscape evolution of the Antarctic plate since the breakup of Gondwana, with an emphasis on the West Antarctic Rift System and the Transantarctic Mountains." *Royal Society of New Zealand Bulletin* 35 (2002): 453-469.

Fitzsimons, I. C. W. "A review of tectonic events in the East Antarctic Shield and their implications for Gondwana and earlier supercontinents." Journal of African Earth Sciences 31.1 (2000): 3-23.

Florindo, F., Bohaty, S.M., Erwin, P.S., Richter, C., Roberts, A.P., Whalen, P.A., and Whitehead, J.M. "Magnetobiostratigraphic Chronology and Palaeoenvironmental History of Cenozoic Sequences from ODP Sites 1165 and 1166, Prydz Bay, Antarctica." *Palaeogeography, Palaeoclimatology, Palaeoecology* (2003): 69-100.

Faure, G. *Principles and applications of inorganic geochemistry: a comprehensive textbook for geology students.* Macmillan Publ., 1991. Print.

Galeotti, S., DeConto, R., Naish, T., Stocchi, P., Florindo, F., Pagani, M., Barrett, P.,Bohaty, S.M., Lanci, L., Pollard, D., Sandroni, S., Talarico, F.M., and Zachos, J.C. (2016). Antarctic Ice Sheet variability across the Eocene-Oligocene boundary climate transition. *Science*, *352*(6281), 76-80.

Goodge, J. W., and Fanning, C.M. "Composition and age of the East Antarctic Shield in eastern Wilkes Land determined by proxy from Oligocene-Pleistocene glaciomarine sediment and Beacon Supergroup sandstones, Antarctica." *Geological Society of America Bulletin* 122.7-8 (2010): 1135-1159.

Heier, K. S. "Trace elements in feldspars—a review." *Norsk geol. tidsskr* 42.2 (1962): 415-466.

Houben, A.J., Bijl, P.K., Pross, J., Bohaty, S.M., Passchier, S., Stickley, C.E., Rohl, U., Sugisaki, S., Tauxe, L., van De Flierdt, T., Olney, Sangiorgi, M.F., Sluijs, A., Escutia, C., and Brinkhuis, H. "Reorganization of Southern Ocean Plankton Ecosystem at the Onset of Antarctic Glaciation." *Science* (19 Apr. 2013): 341-44.

King, E. C., and Barker, P.F. "The margins of the South Orkney microcontinent." *Journal of the Geological Society* 145.2 (1988): 317-331.

Ladant, J. B., Donnadieu, Y., Lefebvre, V., & Dumas, C. "The respective role of atmospheric carbon dioxide and orbital parameters on ice sheet evolution at the Eocene-Oligocene transition." *Paleoceanography* 29.8 (2014): 810-823.

Liu, X., Jahn, B.M., Zhao, Y., Zhao, G., & Liu, X. "Geochemistry and geochronology of high-grade rocks from the Grove Mountains, East Antarctica: evidence for an Early Neoproterozoic basement metamorphosed during a single Late Neoproterozoic/Cambrian tectonic cycle." *Precambrian Research* 158.1 (2007): 93-118.

Macphail, M.K., and Truswell, E.M. “Palynology of Site 1166, Prydz Bay, East Antarctica.” *In* Cooper, A.K., O'Brien, P.E., and Richter, C. (Eds.), *Proc. ODP, Sci. Results,* 188 (2004) [Online]. Available from World Wide Web: <http://www-odp.tamu.edu/publications/188_SR/013/013.htm>. [Cited 2017-06-12]

McLennan, S. M. "Relationships between the trace element composition of sedimentary rocks and upper continental crust." *Geochemistry, Geophysics, Geosystems* 2.4 (2001).

McLennan, S. M., Hemming, S., McDaniel, D.K., & Hanson, G.N. “Geochemical approaches to sedimentation, provenance, and tectonics." *Geological Society of America Special Papers* 284 (1993): 21-40.

McLennan, S. M., Taylor, S.R.., McCulloch, T., & Maynard, J.B. "Geochemical and Nd/ Sr isotopic composition of deep-sea turbidites: Crustal evolution and plate tectonic associations." *Geochimica et Cosmochimica Acta* 54.7 (1990): 2015-2050.

Murray, R.W., Miller, D.J., & Kryc, K.A. “Analysis of major and trace elements in rocks, sediments, and interstitial waters by inductively coupled plasma–atomic emission spectrometry (ICP-AES).” *ODP Tech. Note, 29* (2000).

Munksgaard, N. C., Thost, D.E., & Hensen, B.J. "Geochemistry of Proterozoic granulites from northern Prince Charles Mountains, East Antarctica." *Antarctic science* 4.01 (1992): 59-69.

Mikhalsky, E. V., Boger, S.D., & Henjes-Kunst, F. "The geochemistry and Sm–Nd isotopic systematics of Precambrian mafic dykes and sills in the southern Prince Charles Mountains, East Antarctica." *Journal of Petrology* 54.12 (2013): 2487-2520.

Nakamura, N. "Determination of REE, Ba, Fe, Mg, Na and K in carbonaceous and ordinary chondrites." *Geochimica et Cosmochimica Acta* 38.5 (1974): 757-775.

Nesbitt, W., & Young., G.M. "Early Proterozoic Climates and Plate Motions Inferred from Major Element Chemistry of Lutites." *Nature* 21 Oct. 1982: 715-17.

O’Brien, P.E., Cooper, A.K., Richer, C. "Prydz Bay–Cooperation Sea, Antarctica: glacial history and palaeoceanography." *Proceedings of the Ocean Drilling Program, Part A*. Vol. 188. (2001).

Passchier, S. "Sedimentology, mineralogy and geochemistry of the sirius group and other cenozoic glacigenic sediments from Antarctica: implications for climate and ice sheet history." Electronic Thesis or Dissertation. Ohio State University, (2000). *OhioLINK Electronic Theses and Dissertations Center*. 08 Jun 2017.

Passchier, S., Ciarletta, D.J., Miriagos, T.E., Bijl, P.K., & Bohaty, S.M. "An Antarctic stratigraphic record of stepwise ice growth through the Eocene-Oligocene transition." *Geological Society of America Bulletin* 129.3-4 (2017): 318-330.

Passchier, S., Bohaty, S.M., Jiménez-Espejo, F., Pross, J., Röhl, U., Van De Flierdt, T., Escutia, C., & Brinkhuis, H. "Early Eocene to Middle Miocene Cooling and Aridification of East Antarctica." *Geochemistry, Geophysics, Geosystems Geochem. Geophys. Geosyst.* 14.5 (2013): 1399-1410.

Peucat, J. J., Capdevila, R., Fanning, C. M., Ménot, R. P., Pécora, L., & Testut, L "1.60 Ga felsic volcanic blocks in the moraines of the Terre Adélie Craton, Antarctica: comparisons with the Gawler Range Volcanics, South Australia." *Australian Journal of Earth Sciences* 49.5 (2002): 831-845.

Post, J.E. "Manganese oxide minerals: Crystal structures and economic and environmental significance." *Proceedings of the National Academy of Sciences* 96.7 (1999): 3447-3454.

Potter, P.E., Maynard, J.B., & Depetris, P.J. *Mud and mudstones: Introduction and overview*. Springer Science & Business Media, 2005.

Pross, J., Contreras, L., Bijl, P.K., Greenwood, D.R., Bohaty, S.M., Schouten, S., …& Huck, C.E. "Persistent near-tropical warmth on the Antarctic continent during the early Eocene epoch." *Nature* 488.7409 (2012): 73-77.

Raine, J. I., Beu, A. G., Boyes, A. F., Campbell, H., Cooper, R. A., Crampton, J. S., ... & Morgans, H. E. G. *Revised Calibration of the New Zealand Geological Timescale: NTGT2015/1*. Lower Hutt: GNS Science, 2015

Reátegui, K., Martínez, M., Esteves, I., Gutiérrez, J. V., Martínez, A., Meléndez, W., & Urbani, F."Geochemistry of the Mirador Formation (Late Eocene-Early Oligocene), southwestern Venezuela: Chemostratigraphic constraints on provenance and the influence of the sea level." *Geochemical Journal* 39.3 (2005): 213-226.

Rudnick, R. L., & Gao, S. "Composition of the Continental Crust." *Treatise on Geochemistry*. Vol. 3. Oxford: Elsevier Science, (2004): 1-64. Print

Ryan, W.B.F., Carbotte, S.M., Coplan, J.O., O'Hara, S., Melkonian, A., Arko, R., Weissel, R.A., Ferrini, V., Goodwillie, A., Nitsche, F., Bonczkowski, J., & Zemsky, R. (2009), Global Multi-Resolution Topography synthesis, Geochem. Geophys. Geosyst., 10, Q03014, doi:10.1029/2008GC002332.

Sheldon, N. D., Retallack, G.J., & Tanaka, S. "Geochemical Climofunctions from North American Soils and Application to Paleosols across the Eocene Oligocene Boundary in Oregon." *The Journal of Geology* 110.6 (2002): 687-96.

Sheraton, J. W., Tindle, A.G., & Tingey, R.J. "Geochemistry, origin, and tectonic setting of the Prince Charles Mountains, Antarctica." *AGSO Journal of Australian Geology and Geophysics* 16 (1996): 345-370.

Sperazza, M., Moore, J.N., & Hendrix, M.S. "High-resolution particle size analysis of naturally occurring very fine-grained sediment through laser diffractometry." *Journal of Sedimentary Research* 74.5 (2004): 736-743.

Stocchi, P., Escutia, C., Houben, A.J., Vermeersen, B.L., Bijl, P.K., Brinkhuis, H., DeConto, R.M., Galeotti, S., Passchier, S., Pollard, D. & Klaus, A "Relative sea-level rise around East Antarctica during Oligocene glaciation." *Nature Geoscience* 6.5 (2013): 380-384.

Strand, K., Passchier, S., & Näsi, J. "Implications of Quartz Grain Microtextures for Onset Eocene/Oligocene Glaciation in Prydz Bay, ODP Site 1166, Antarctica." *Palaeogeography, Palaeoclimatology, Palaeoecology* (2003): 101-11. Print.

Thomson, S.N., Reiners, P.W., Hemming, S.R., & Gehrels, G.E. "The contribution of glacial erosion to shaping the hidden landscape of East Antarctica." *Nature Geoscience* 6.3 (2013): 203-207.

van de Flierdt, T., Hemming, S. R., Goldstein, S. L., Gehrels, G. E., & Cox, S. E. "Evidence against a young volcanic origin of the Gamburtsev Subglacial Mountains, Antarctica." *Geophysical Research Letters* 35.21 (2008): 1-6. doi:10.1029/2008GL035564

Vandenberghe, N., Hilgen, F.J., & Speijer, R. "The Paleogene Period." The Geologic Time Scale 2012. By Felix M. Gradstein. Amsterdam: Elsevier Science, 2012. 855-921. Print.

Veevers, J. J., A. Saeed, and P. E. O'Brien. "Provenance of the Gamburtsev Subglacial Mountains from U–Pb and Hf analysis of detrital zircons in Cretaceous to Quaternary sediments in Prydz Bay and beneath the Amery Ice Shelf." *Sedimentary Geology* 211.1 (2008): 12-32.

Wilson, D. S., Jamieson, S. S., Barrett, P. J., Leitchenkov, G., Gohl, K., & Larter, R. D. "Antarctic topography at the Eocene–Oligocene boundary." *Palaeogeography, Palaeoclimatology, Palaeoecology* 335 (2012): 24-34.

Wedepohl, K. H. "*Handbook of Geochemistry, 2 vols*." (1978). Print

Wolf, Ruth E. “What Is ICP-MS?... and More Importantly, What Can It Do?” Introduction to ICP-MS, USGS, crustal.usgs.gov/laboratories/icpms/intro.html. Accessed 6 June 2017.

Yang, P., & Rivers, T. "Trace element partitioning between coexisting biotite and muscovite from metamorphic rocks, Western Labrador: structural, compositional and thermal controls." *Geochimica et Cosmochimica Acta* 64.8 (2000): 1451-1472.

Zachos, J. "Trends, Rhythms, and Aberrations in Global Climate 65 Ma to Present." *Science* (2001): 686-93. Print.

Zachos, J, Wara, M.W., Bohaty, S., Delaney, M.L., Petrizzo, M.R., Brill, A., Bralower, T.J., & Premoli-Silva, I. "A Transient Rise in Tropical Sea Surface Temperature during the Paleocene-Eocene Thermal Maximum." *Science* 302.5650 (2003): 1551-1554

8.APPENDIX

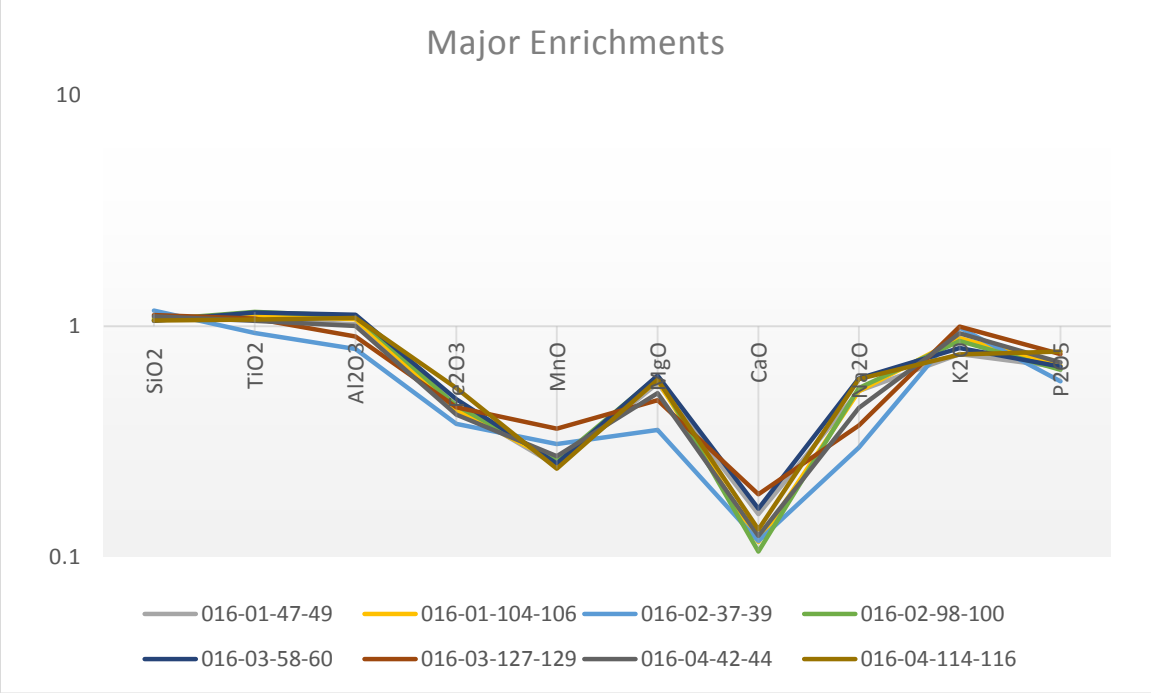

Figure A.1: Major element enrichments over upper crust [Rudnick and Gao, 2004] for Core 16R at Site 1166.

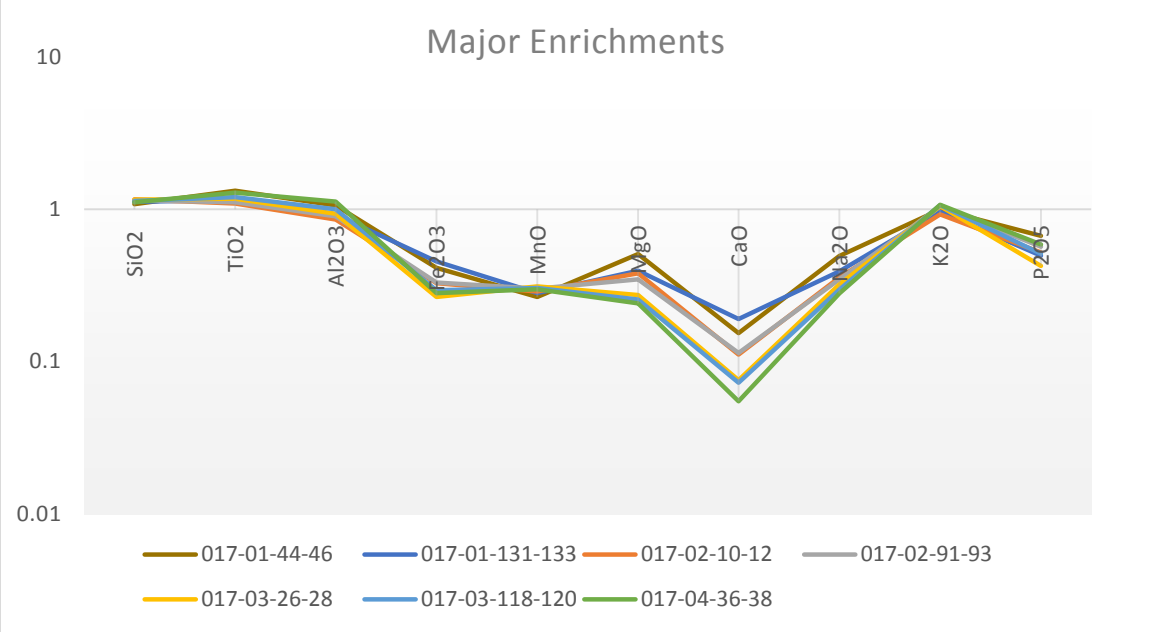

Figure A.2: Major element enrichments over upper crust [Rudnick and Gao, 2004] for Core 17R at Site 1166.

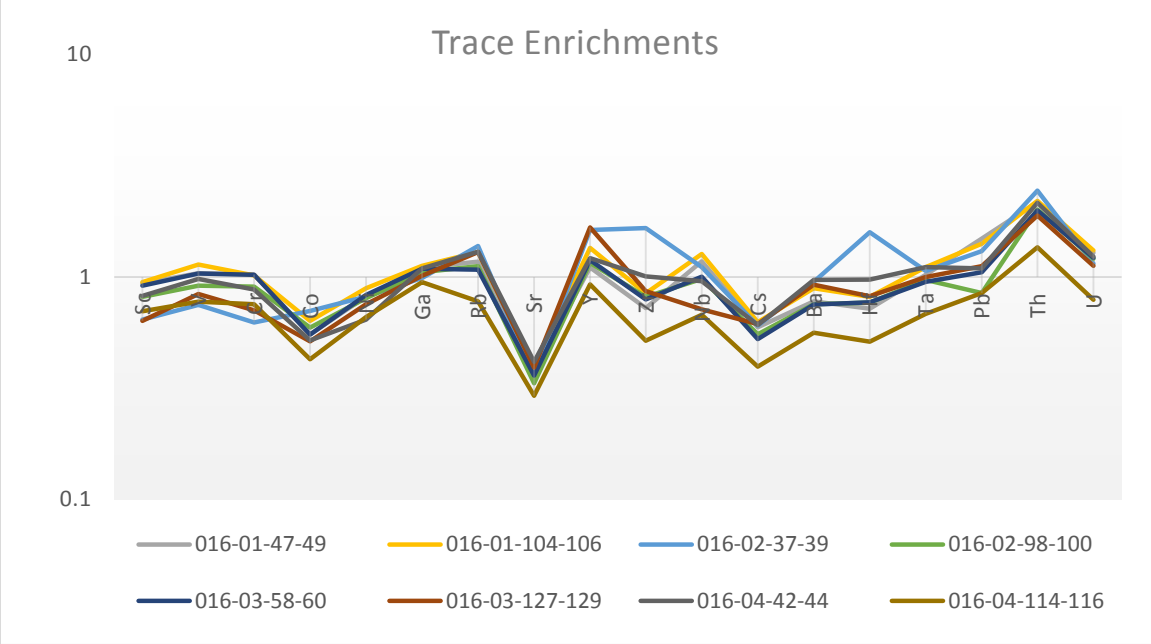

Figure A.3: Trace element enrichments over upper crust [Rudnick and Gao, 2004] for Core 16R at Site 1166.

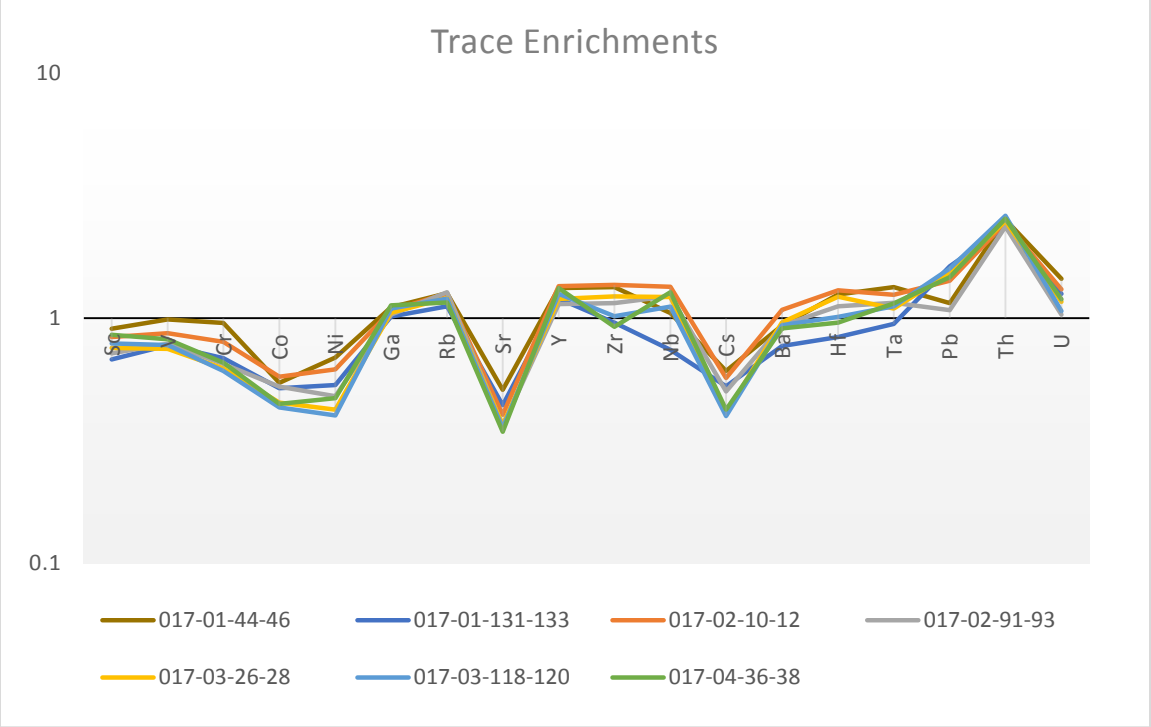

Figure A.4: Trace element enrichments over upper crust [Rudnick and Gao, 2004] for Core 17R at Site 1166.

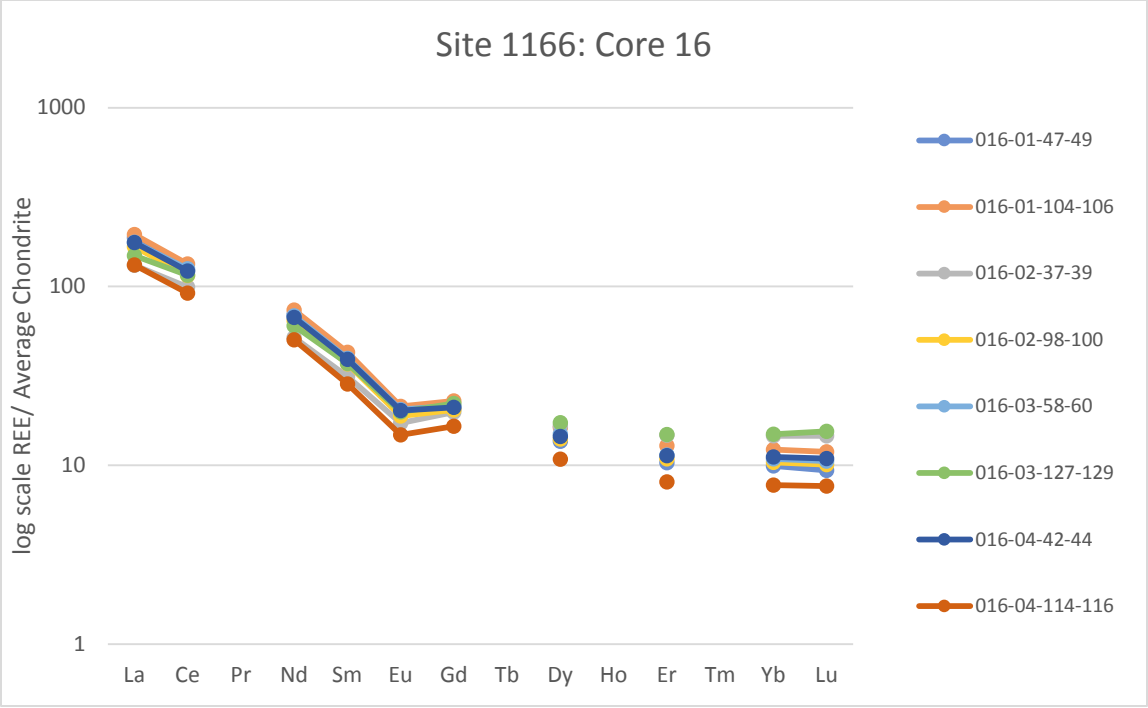

Figure A.5: Rare Earth Elements normalized to an average chondrite [Nakamura, 1974] for Core 16R at Site 1166.

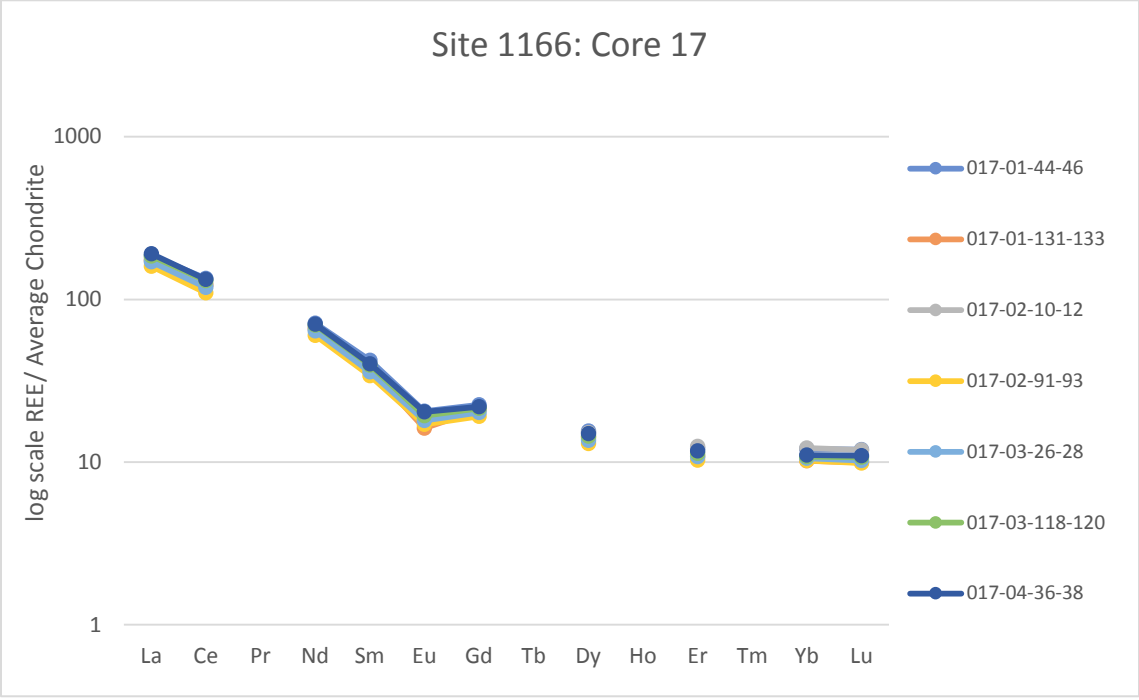

Figure A.6: Rare Earth Elements normalized to an average chondrite [Nakamura, 1974] for Core 17R at Site 1166.

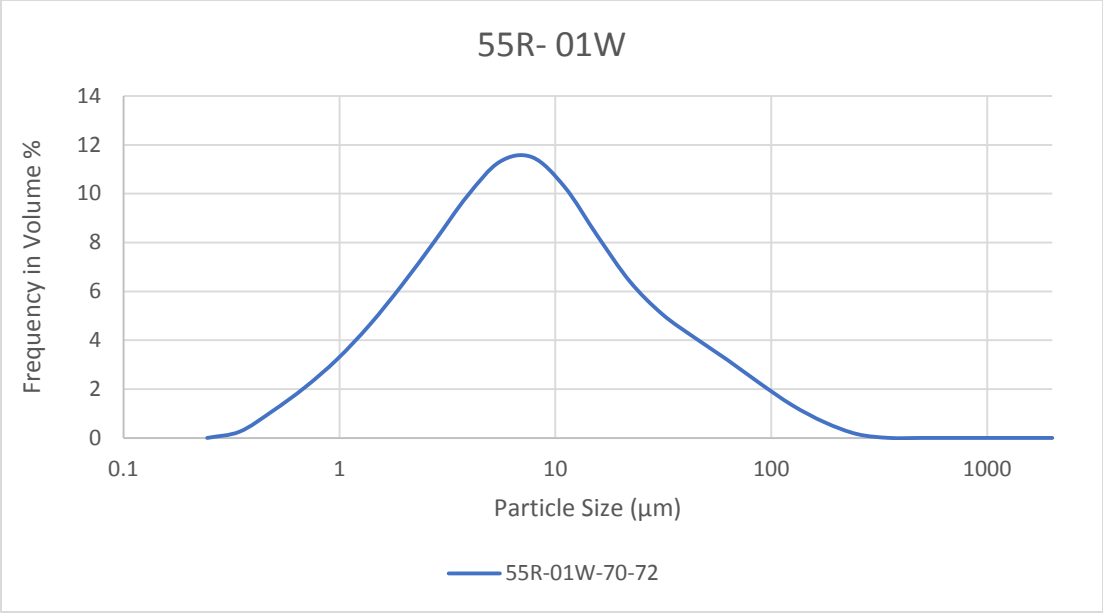

Figure A.7. Frequency in volume percent of Particle size (microns) for Section 01W of Core 55R at Site 696.

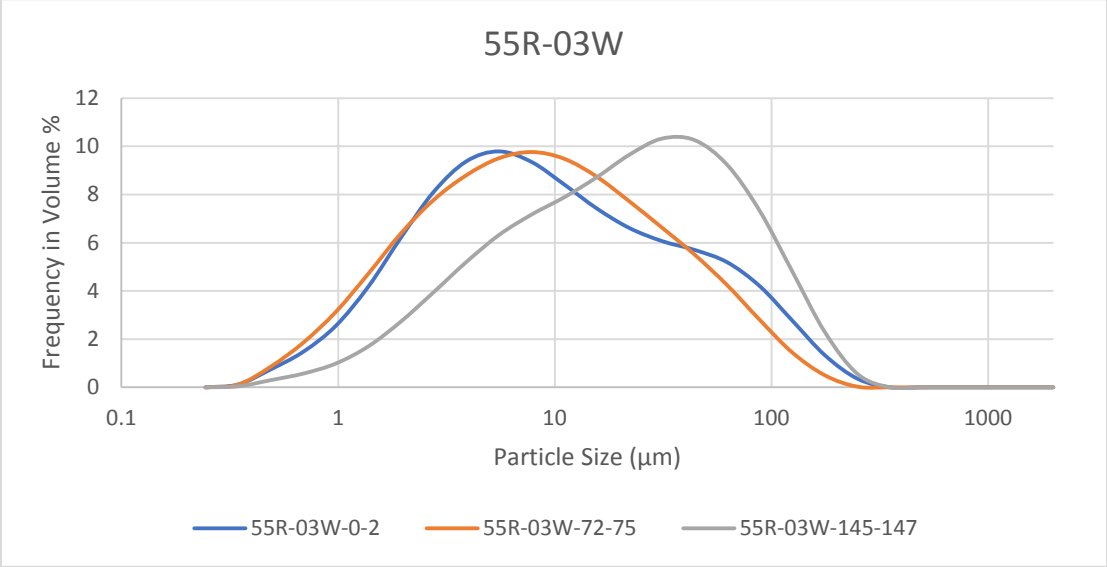

Figure A.8: Frequency in volume percent of Particle size (microns) for Section 03W of Core 55R at Site 696.

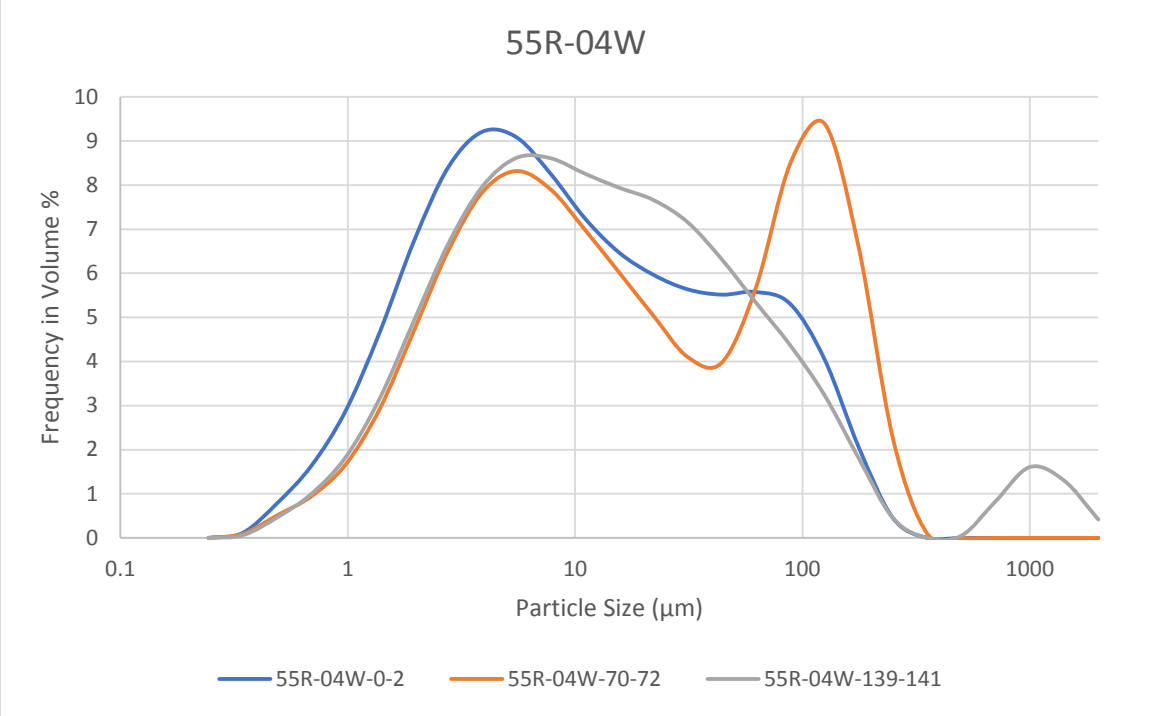

Figure A.9: Frequency in volume percent of Particle size (microns) for Section 04W of Core 55R at Site 696.

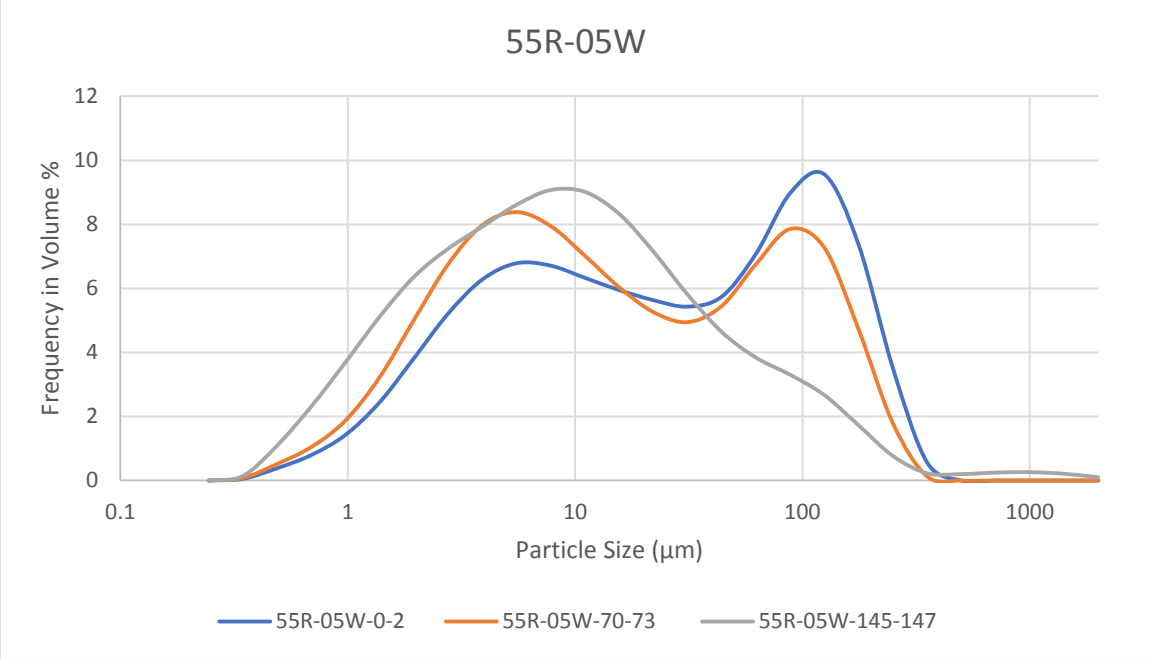

Figure A.10: Frequency in volume percent of Particle size (microns) for Section 05W of Core 55R at Site 696.

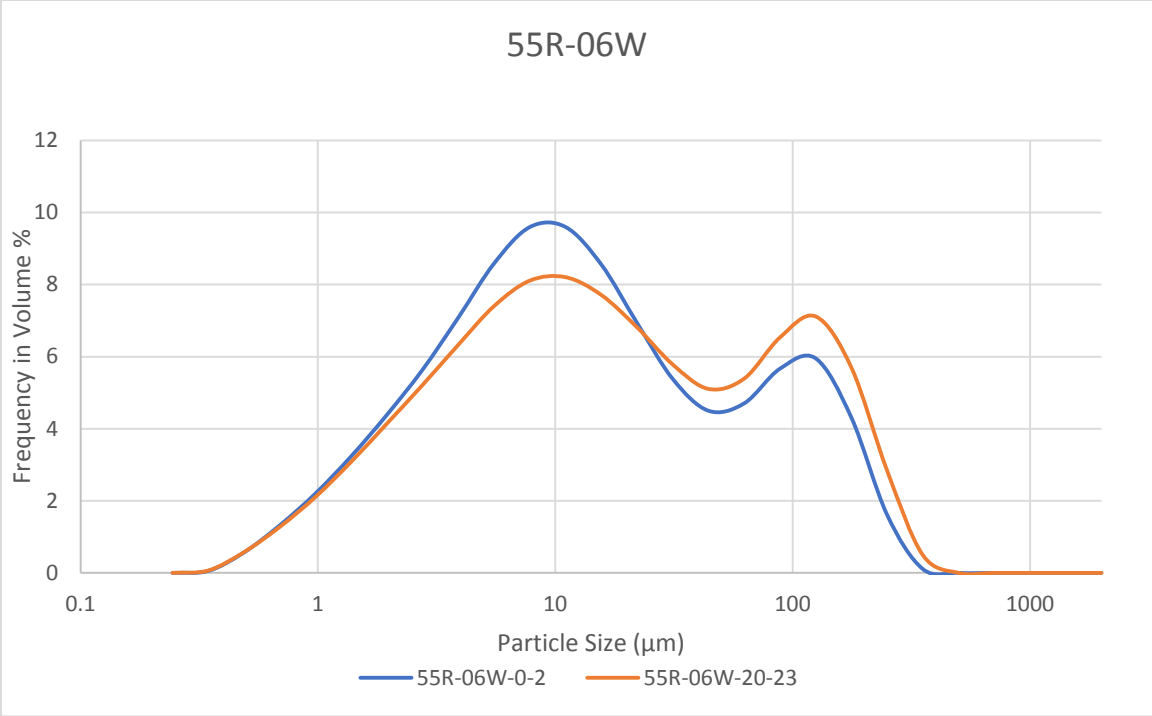

Figure A.11: Frequency in volume percent of Particle size (microns) for Section 06W of Core 55R at Site 696.

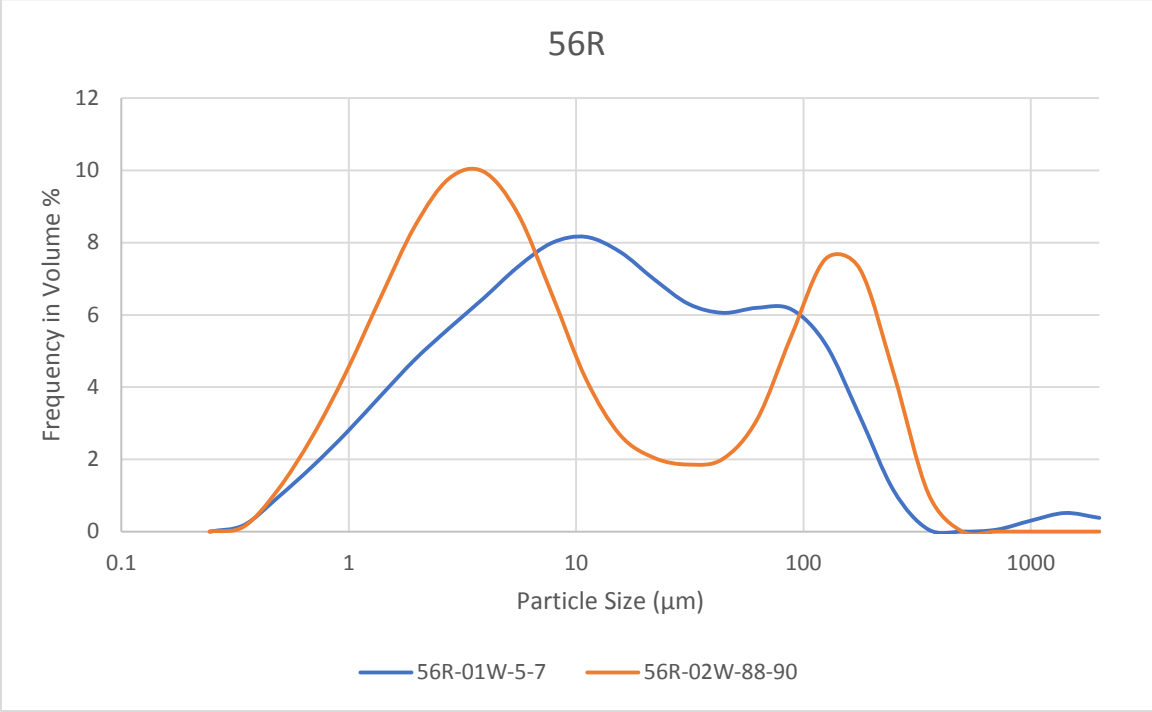

Figure A.12: Frequency in volume percent of Particle size (microns) for Core 56R at Site 696.

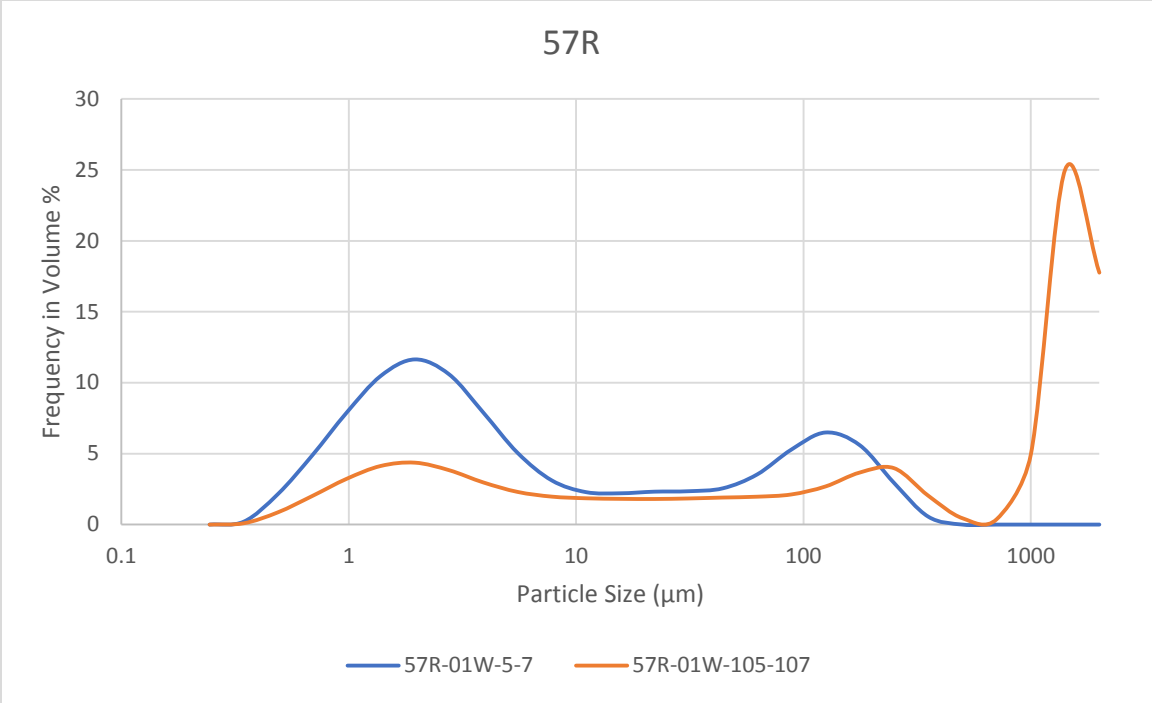

Figure A.13: Frequency in volume percent of Particle size (microns) for Core 57R at Site 696.

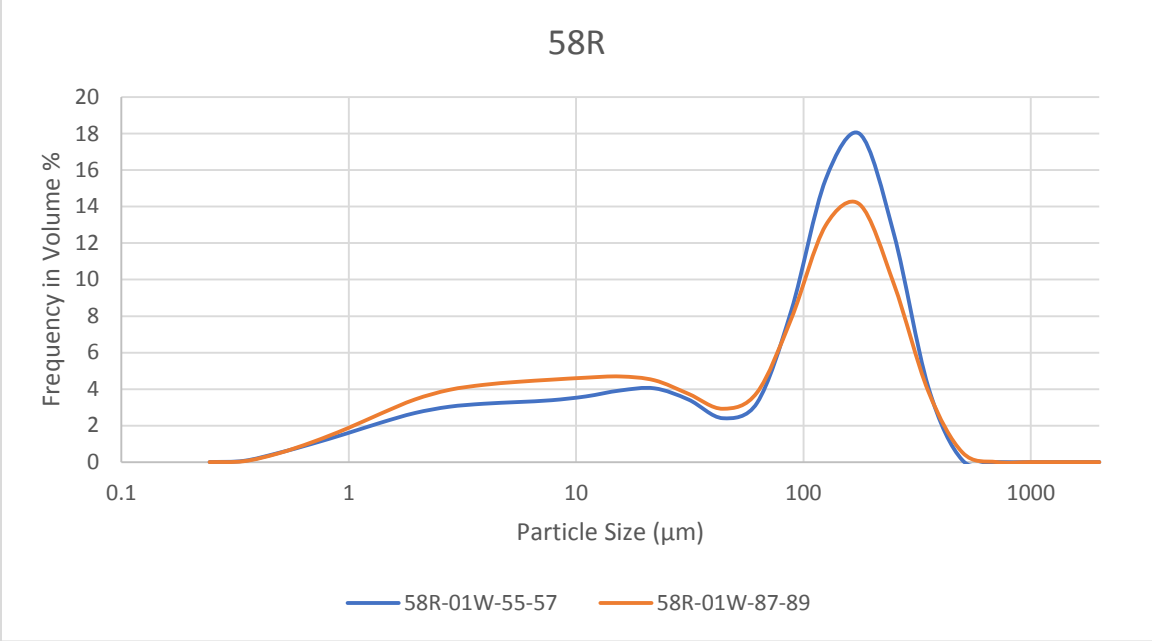

Figure A.14: Frequency in volume percent of Particle size (microns) for Core 58R at Site 696.

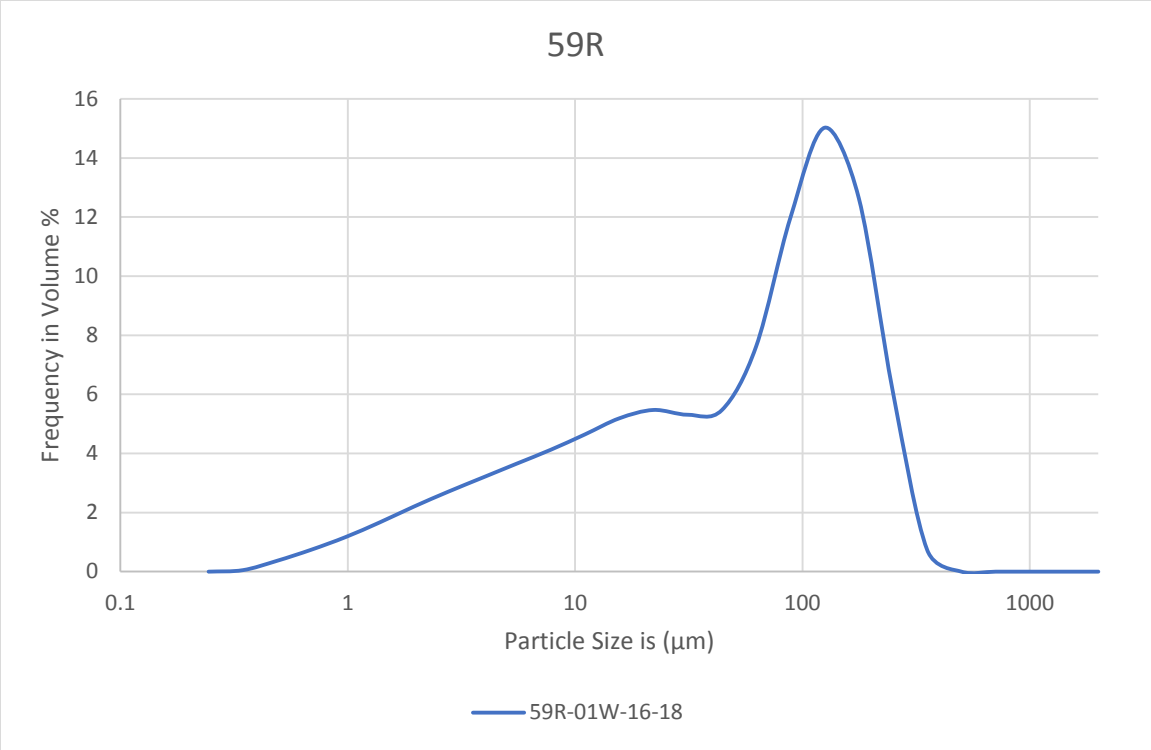

Figure A.15: Frequency in volume percent of Particle size (microns) for Core 59R at Site 696.

Table A.1. Normalized Major elements in weight percent oxides for Site 1166.

Sample ID	SiO2	TiO2	Al2O3	Fe2O3	MnO	MgO	CaO	Na2O	K2O	P2O5	Total
015R-02W 64-66 cm	70.21	0.62	14.61	5.07	0.06	1.54	2.14	2.22	3.41	0.12	100.00
015R-03W 4-6 cm	63.86	1.08	20.38	7.20	0.04	2.02	1.47	1.56	2.23	0.15	100.00
015R-03W 47-49 cm	65.76	1.06	19.83	6.73	0.03	1.95	1.07	1.34	2.14	0.10	100.00
015R-03W 129-131 cm	72.09	0.65	14.09	7.51	0.05	1.18	0.67	1.10	2.56	0.11	100.00
015R-04W 62-64 cm	67.79	0.84	19.24	6.13	0.03	1.55	0.63	1.36	2.32	0.11	100.00
015R-04W 99-101 cm	61.48	1.00	24.60	6.64	0.03	2.06	0.52	1.64	1.94	0.11	100.00
015R-05W 96-98 cm	70.40	0.74	17.87	4.96	0.03	1.53	0.44	1.50	2.44	0.09	100.00
015R-05W 114-116 cm	70.17	0.78	17.87	5.06	0.03	1.56	0.54	1.54	2.36	0.10	100.00
015R-06W 34-36 cm	76.75	0.57	11.70	5.65	0.04	0.99	0.59	1.01	2.60	0.10	100.00
015R-06W 131-133 cm	69.08	0.77	17.91	5.61	0.03	1.59	0.62	1.84	2.47	0.10	100.00
015R-07W 43-45 cm	70.89	0.76	16.85	5.26	0.03	1.46	0.46	1.86	2.33	0.10	100.00

Sample ID	SiO2	TiO2	Al2O3	Fe2O3	MnO	MgO	CaO	Na2O	K2O	P2O5	Total
015R-CCW 5-7 cm	69.16	0.74	17.45	5.64	0.03	1.57	1.16	1.87	2.30	0.10	100.00
016R-01W 47-49 cm	72.70	0.69	15.68	5.03	0.02	1.40	0.55	1.71	2.12	0.10	100.00
016R-01W 104-106 cm	71.73	0.71	16.52	4.86	0.03	1.44	0.42	1.71	2.48	0.10	100.00
016R-02W 37-39 cm	77.76	0.60	12.28	4.22	0.03	0.88	0.42	0.97	2.76	0.09	100.00
016R-02W 98-100 cm	71.00	0.74	17.01	5.07	0.03	1.50	0.38	1.76	2.42	0.10	100.00
016R-03W 58-60 cm	70.20	0.73	17.26	5.40	0.03	1.51	0.58	1.94	2.25	0.10	100.00
016R-03W 127-129 cm	74.44	0.69	13.89	4.98	0.04	1.19	0.67	1.21	2.79	0.11	100.00
016R-04W 42-44 cm	73.36	0.68	15.44	4.64	0.03	1.27	0.44	1.45	2.61	0.10	100.00
016R-04W 114-116 cm	70.46	0.68	16.73	6.03	0.02	1.45	0.47	1.93	2.11	0.12	100.00
017R-01W 44-46 cm	71.86	0.84	16.33	4.62	0.03	1.26	0.55	1.61	2.79	0.10	100.00
017R-01W 131-133 cm	74.23	0.74	14.20	5.09	0.03	0.98	0.68	1.28	2.70	0.07	100.00
017R-02W 10-12 cm	77.22	0.70	13.22	3.66	0.03	0.94	0.40	1.17	2.58	0.08	100.00

Sample ID	SiO2	TiO2	Al2O3	Fe2O3	MnO	MgO	CaO	Na2O	K2O	P2O5	Total
017R-02W 91-93 cm	76.28	0.71	13.87	3.70	0.03	0.86	0.41	1.14	2.92	0.09	100.00
017R-03W 26-28 cm	76.90	0.75	14.36	2.97	0.03	0.68	0.27	1.05	2.93	0.06	100.00
017R-03W 118-120 cm	75.56	0.77	15.43	3.30	0.03	0.63	0.26	0.97	2.98	0.08	100.00
017R-04W 36-38 cm	73.95	0.82	17.25	3.16	0.03	0.60	0.20	0.92	2.99	0.09	100.00

Table A.2. Trace Element Data for Site 1166 in Parts Per Million

Sample ID	Sc	V	Cr	Co	Ni	Ga	Rb	Sr	Y	Zr	Nb	Cs	Ba	Hf	Ta	Pb	Th	U
015R-02W 64-66 cm	11.20	73.56	53.81	10.67	20.24	18.02	127.07	160.28	25.16	191.05	12.93	2.01	764.36	4.99	0.79	25.88	26.64	2.10
015R-03W 4-6 cm	19.08	127.92	170.30	20.21	86.81	23.18	89.87	131.93	33.11	132.81	20.27	2.57	459.45	3.64	1.19	17.79	27.04	5.22
015R-03W 47-49 cm	21.65	152.92	230.52	23.17	106.49	24.75	103.93	133.41	39.27	157.11	23.18	2.64	526.42	4.43	1.46	23.98	30.63	4.22
015R-03W 129-131 cm	12.44	86.89	98.05	11.88	52.94	18.89	108.49	134.98	31.31	182.23	12.45	2.67	837.57	4.85	0.97	21.60	21.87	2.95
015R-04W 62-64 cm	14.57	105.63	149.47	13.41	70.72	21.53	101.89	113.70	33.01	137.15	17.41	2.69	513.73	3.76	1.11	24.43	24.67	3.11
015R-04W 99-101 cm	20.49	140.78	221.68	22.43	116.60	25.28	97.09	101.66	43.63	117.57	22.49	2.74	398.28	3.14	1.34	28.29	29.73	3.65
015R-05W 96-98 cm	12.33	88.13	93.85	13.59	51.13	19.20	97.78	97.84	27.55	141.80	13.76	2.64	464.56	3.71	0.87	20.99	21.69	2.83
015R-05W 114-116 cm	14.65	104.81	111.36	14.21	58.93	20.68	102.54	117.40	33.43	140.94	16.46	2.82	522.56	3.84	1.03	22.36	26.01	3.24
015R-06W 34-36 cm	9.77	67.20	54.47	7.56	21.01	16.83	106.48	113.72	34.45	193.56	8.96	2.78	580.57	5.00	0.90	19.44	21.32	3.17
015R-06W 131-133 cm	13.77	105.60	96.73	12.65	47.66	20.08	108.24	120.52	28.17	121.85	14.99	2.95	529.25	3.41	0.97	18.00	25.28	3.58
015R-07W 43-45 cm	11.27	95.87	86.25	8.85	35.49	18.48	86.81	103.55	24.40	126.59	12.82	2.67	466.15	3.53	0.90	14.51	22.05	3.18

Sample ID	Sc	V	Cr	Co	Ni	Ga	Rb	Sr	Y	Zr	Nb	Cs	Ba	Hf	Ta	Pb	Th	U
015R-CCW 5-7 cm	14.32	116.06	106.53	10.72	43.46	20.05	101.38	131.18	26.26	131.20	16.03	3.07	515.65	3.65	1.00	22.56	23.21	4.18
016R-01W 47-49 cm	13.13	101.10	94.59	9.59	38.39	19.34	96.15	119.66	23.20	139.94	14.13	2.91	488.23	3.83	0.92	25.31	22.83	3.47
016R-01W 104-106 cm	13.28	110.44	93.56	11.01	41.89	19.64	106.28	126.29	28.42	163.06	15.23	3.07	560.14	4.32	1.00	24.02	23.12	3.56
016R-02W 37-39 cm	9.04	72.70	57.55	12.21	38.49	17.36	113.09	114.06	34.19	320.82	13.30	2.97	598.57	8.45	0.96	22.29	25.74	3.11
016R-02W 98-100 cm	11.43	88.85	83.35	10.27	37.81	18.38	91.79	106.57	24.32	157.37	11.78	2.71	474.84	4.08	0.87	14.44	21.11	3.27
016R-03W 58-60 cm	12.81	100.75	94.25	9.55	39.06	19.12	88.71	115.40	25.02	152.98	12.04	2.58	473.24	4.08	0.86	17.89	20.91	3.29
016R-03W 127-129 cm	8.91	81.58	65.20	8.89	35.55	17.72	106.35	125.28	35.15	166.82	8.59	3.01	580.18	4.35	0.90	19.07	19.85	3.03
016R-04W 42-44 cm	11.52	95.13	81.02	8.99	30.29	19.18	106.61	133.28	25.52	194.43	11.52	2.99	609.34	5.16	1.00	18.59	22.66	3.34
016R-04W 114-116 cm	9.82	75.16	69.41	7.40	31.14	16.59	63.75	93.67	19.47	99.96	8.12	1.94	353.20	2.72	0.62	14.44	14.32	2.14
017R-01W 44-46 cm	12.66	95.77	87.97	9.42	32.40	19.39	103.53	162.89	27.87	257.98	12.58	2.99	586.31	6.62	1.20	19.54	26.51	3.90
017R-01W 131-133 cm	9.49	74.95	63.06	8.96	25.06	17.73	91.58	141.12	25.23	185.10	8.90	2.58	482.34	4.43	0.85	27.63	24.73	3.39
017R-02W 10-12 cm	11.72	84.24	73.57	9.96	29.07	18.79	103.18	129.12	28.32	263.45	16.10	2.79	679.22	6.89	1.12	24.18	25.72	3.53

Sample ID	Sc	V	Cr	Co	Ni	Ga	Rb	Sr	Y	Zr	Nb	Cs	Ba	Hf	Ta	Pb	Th	U
017R-02W 91-93 cm	10.06	76.18	59.86	9.09	22.54	18.08	104.49	116.39	23.98	221.81	14.77	2.46	585.97	5.92	1.04	18.31	24.77	2.79
017R-03W 26-28 cm	10.57	72.62	57.40	7.81	19.90	18.42	98.91	117.08	25.10	236.63	14.60	2.01	604.16	6.48	0.98	25.93	26.09	3.14
017R-03W 118-120 cm	11.03	75.34	56.04	7.46	18.82	19.16	98.45	113.92	26.34	196.22	13.34	1.95	587.82	5.35	1.00	27.04	27.42	2.88
017R-04W 36-38 cm	11.96	79.39	60.56	7.72	22.17	19.71	94.90	109.81	27.82	177.93	15.31	2.07	570.45	5.08	1.03	24.95	26.75	3.22

Table A.3. Site 1166 Rare Earth Element Data

Sample ID	La	Ce	Pr	Nd	Sm	Eu	Gd	Tb	Dy	Ho	Er	Tm	Yb	Lu
015R-02W 64-66 cm	57.07	101.16	11.59	42.25	7.49	1.31	5.52	0.81	4.60	0.93	2.56	0.39	2.46	0.38
015R-03W 4-6 cm	81.95	145.05	15.52	57.32	10.57	1.96	7.60	1.17	6.57	1.26	3.37	0.49	3.09	0.46
015R-03W 47-49 cm	92.17	164.56	17.90	66.04	12.47	2.36	8.76	1.39	7.89	1.52	4.06	0.59	3.68	0.54
015R-03W 129-131 cm	63.40	124.24	12.65	46.94	8.86	1.62	6.51	1.01	5.88	1.15	3.10	0.47	3.06	0.47
015R-04W 62-64 cm	75.56	126.10	14.38	52.45	10.10	1.91	7.28	1.15	6.64	1.26	3.41	0.50	3.12	0.47
015R-04W 99-101 cm	99.05	157.29	18.83	69.57	13.49	2.58	9.29	1.52	8.70	1.64	4.34	0.62	3.84	0.56
015R-05W 96-98 cm	64.17	103.59	12.43	45.85	8.63	1.66	6.40	0.97	5.59	1.04	2.80	0.40	2.52	0.37
015R-05W 114-116 cm	75.76	124.08	14.85	54.85	10.50	1.93	7.60	1.17	6.70	1.28	3.36	0.49	3.06	0.45
015R-06W 34-36 cm	46.19	86.15	9.13	32.89	6.31	1.17	5.37	0.90	5.73	1.20	3.46	0.54	3.62	0.57
015R-06W 131-133 cm	67.82	123.82	13.39	48.58	9.06	1.65	6.39	0.98	5.51	1.04	2.78	0.40	2.56	0.38
015R-07W 43-45 cm	56.90	106.22	11.41	41.47	7.72	1.38	5.76	0.84	4.81	0.92	2.42	0.35	2.25	0.33

Sample ID	La	Ce	Pr	Nd	Sm	Eu	Gd	Tb	Dy	Ho	Er	Tm	Yb	Lu
015R-CCW 5-7 cm	64.84	115.04	12.89	46.82	8.70	1.60	6.20	0.95	5.22	1.01	2.63	0.39	2.44	0.36
016R-01W 47-49 cm	61.70	105.81	12.11	43.81	8.02	1.47	5.72	0.86	4.67	0.88	2.32	0.34	2.18	0.32
016R-01W 104-106 cm	64.10	115.38	12.78	46.39	8.69	1.64	6.32	0.98	5.58	1.09	2.89	0.43	2.69	0.40
016R-02W 37-39 cm	43.22	85.87	8.80	32.63	6.34	1.33	5.46	0.91	5.69	1.19	3.32	0.50	3.21	0.49
016R-02W 98-100 cm	54.78	99.73	10.98	40.56	7.51	1.45	5.63	0.84	4.81	0.93	2.44	0.37	2.28	0.34
016R-03W 58-60 cm	58.11	108.43	11.63	43.10	8.04	1.58	5.96	0.92	5.14	0.98	2.57	0.39	2.39	0.36
016R-03W 127-129 cm	48.91	99.99	10.23	38.02	7.52	1.53	6.11	0.99	5.93	1.24	3.34	0.51	3.28	0.52
016R-04W 42-44 cm	57.84	105.69	11.66	42.24	7.93	1.56	5.82	0.89	4.97	0.97	2.55	0.39	2.44	0.37
016R-04W 114-116 cm	43.49	79.49	8.78	31.68	5.77	1.14	4.56	0.67	3.71	0.71	1.81	0.28	1.70	0.26
017R-01W 44-46 cm	61.13	116.52	12.31	44.96	8.57	1.58	6.20	0.95	5.31	1.03	2.73	0.42	2.64	0.40
017R-01W 131-133 cm	56.98	105.81	11.23	41.44	7.58	1.24	5.79	0.86	4.86	0.93	2.44	0.36	2.24	0.34
017R-02W 10-12 cm	57.97	106.89	11.50	42.31	7.69	1.46	5.85	0.90	5.20	1.03	2.80	0.42	2.69	0.40

Sample ID	La	Ce	Pr	Nd	Sm	Eu	Gd	Tb	Dy	Ho	Er	Tm	Yb	Lu
017R-02W 91-93 cm	52.50	95.09	10.37	37.90	6.89	1.32	5.27	0.80	4.45	0.88	2.31	0.35	2.25	0.33
017R-03W 26-28 cm	56.14	102.42	11.12	40.31	7.29	1.39	5.55	0.84	4.67	0.93	2.43	0.37	2.32	0.35
017R-03W 118-120 cm	60.87	112.85	11.99	43.78	7.99	1.48	5.91	0.88	4.95	0.96	2.54	0.38	2.37	0.36
017R-04W 36-38 cm	62.70	114.76	12.17	44.36	8.13	1.57	6.03	0.91	5.12	1.00	2.64	0.40	2.43	0.37

Table A.4. Site 1166 Paleoclimate Data

Sample ID	sample top (mbsf)	Age (Ma)	CIA	CIA-K	MAP (mm)	S-Index	MAT (˚C)
015R-02W 64-66 cm	134.69	Unclear	57	66	663.98	0.50329888	8.0
015R-03W 4-6 cm	135.59	35.705	73	80	910.34	0.2446267	12.8
015R-03W 47-49 cm	136.02	35.705	75	83	978.51	0.227775464	13.1
015R-03W 129-131 cm	136.84	35.707	71	82	970.77	0.325220892	11.3
015R-04W 62-64 cm	137.67	35.708	77	85	1033.42	0.246958825	12.7
015R-04W 99-101 cm	138.04	35.709	81	87	1085.21	0.19477269	13.7
015R-05W 96-98 cm	139.51	35.712	69	85	1021.06	0.285997757	12.0
015R-05W 114-116 cm	139.69	35.712	75	84	998.75	0.284636592	12.0
015R-06W 34-36 cm	140.39	35.713	75	81	941.07	0.382858052	10.2
015R-06W 131-133 cm	141.36	35.715	68	81	945.65	0.317825472	11.4
015R-07W 43-45 cm	141.98	35.716	72	81	945.93	0.331263091	11.2
015R-CCW 5-7 cm	142.35	35.717	72	77	860.68	0.318788644	11.4
016R-01W 47-49 cm	142.67	35.718	72	80	929.06	0.32594889	11.3

Sample ID	sample top (mbsf)	Age (Ma)	CIA	CIA-K	MAP (mm)	S-Index	MAT (˚C)
016R-01W 104-106 cm	143.44	35.719	73	82	969.28	0.332347995	11.2
016R-02W 37-39 cm	144.07	35.720	70	84	1005.92	0.373653417	10.4
016R-02W 98-100 cm	144.68	35.721	73	83	976.46	0.324248492	11.3
016R-03W 58-60 cm	145.78	35.723	72	80	924.83	0.32613769	11.3
016R-03W 127-129 cm	146.47	35.725	69	81	945.65	0.36085607	10.6
016R-04W 42-44 cm	147.12	35.726	72	83	983.69	0.33716893	11.1
016R-04W 114-116 cm	147.84	35.727	73	81	932.69	0.325849232	11.3
017R-01W 44-46 cm	151.84	35.734	71	82	956.76	0.347483127	10.9
017R-01W 131-133 cm	152.71	35.736	69	81	939.92	0.353682804	10.8
017R-02W 10-12 cm	153	35.737	71	83	993.34	0.356803449	10.7
017R-02W 91-93 cm	153.81	35.738	71	84	1012.37	0.362460595	10.6
017R-03W 26-28 cm	154.66	35.740	73	87	1072.60	0.341255351	11.0
017R-03W 118-120 cm	155.58	35.741	74	88	1111.49	0.312388508	11.5

Sample ID	sample top (mbsf)	Age (Ma)	CIA	CIA-K	MAP (mm)	S-Index	MAT (˚C)
017R-04W 36-38 cm	156.26	35.742	77	90	1165.95	0.275464267	12.2

Table A.5. Site U1360 Normalized Major Element Geochemistry in Weight Percent Oxides

Sample ID	SiO2	TiO2	Al2O3	Fe2O3	MnO	MgO	CaO	Na2O	K2O	P2O5	Total
03R-01W 3-4 cm	67.54	0.67	15.12	5.86	0.08	2.43	2.55	2.42	3.14	0.20	100.00
04R-01W 20-24 cm	72.07	0.50	13.73	5.00	0.06	1.83	2.45	1.94	2.32	0.11	100.00
04R-01W 80-84 cm	72.07	0.47	14.20	4.74	0.06	1.81	2.51	1.81	2.21	0.11	100.00
04R-02W 20-24 cm	72.63	0.48	13.43	4.78	0.06	1.80	2.45	1.90	2.36	0.11	100.00
04R-02W 90-94 cm	72.70	0.49	13.43	4.63	0.06	1.84	2.43	1.90	2.40	0.11	100.00
05R-01W 3-6 cm	68.37	0.66	14.25	6.86	0.06	2.06	2.27	2.32	3.04	0.10	100.00
06R-01W 20-24 cm	79.63	0.28	11.18	2.84	0.04	0.86	1.52	1.38	2.22	0.05	100.00
06R-01W 90-94 cm	79.85	0.25	11.35	2.76	0.04	0.81	1.54	1.25	2.09	0.06	100.00
06R-02W 23-29 cm	81.71	0.28	10.00	2.54	0.04	0.72	1.38	1.26	2.01	0.06	100.00

Table A.6. Site U1360 Trace Element data in parts per million. Standards calibrations show that Ni data is unreliable.

Sample ID	Ba	Cr	Ni	Sc	Sr	V	Y	Zr
03R-01W 3-4 cm	440.51	59.34	46.02	21.41	191.55	105.84	28.68	144.16
04R-01W 20-24 cm	399.08	56.27	14.99	14.22	164.41	82.89	21.19	189.82
04R-01W 80-84 cm	420.18	60.56	35.96	13.56	169.12	82.07	20.86	184.35
04R-02W 20-24 cm	437.16	48.51	21.47	17.51	167.99	78.97	20.11	182.74
04R-02W 90-94 cm	456.09	56.03	7.70	14.22	168.02	84.73	22.54	203.09
05R-01W 3-6 cm	455.03	63.35	30.93	18.11	231.98	115.14	24.31	161.66
06R-01W 20-24 cm	379.12	37.16	33.52	7.73	111.65	45.26	13.90	193.33
06R-01W 90-94 cm	393.27	50.91	44.73	11.61	115.97	41.33	15.21	253.85
06R-02W 23-29 cm	384.66	33.74	24.97	7.63	110.32	45.62	16.38	352.83

Table A.7. Paleoclimate data for Site U1360. Gray boxes indicate no CaCO3 correction, Blue boxes account for a 1% CaCO3 correction.

Sample ID	sample top (mbsf)	CIA	CIA-K	MAP (mm)	CIA	CIA-K	MAP (mm)	S-Index	MAT (˚C)
03R-01W 3-4 cm	23.33	56	64	630.02	58	67	673.16	0.487915461	8.3
04R-01W 20-24 cm	32.8	58	64	638.34	60	67	687.77	0.414553229	9.6
04R-01W 80-84 cm	33.4	59	65	653.82	61	68	704.33	0.378333987	10.3
04R-02W 20-24 cm	34.19	57	64	633.19	60	67	682.82	0.422844489	9.5
04R-02W 90-94 cm	34.89	57	64	635.22	60	67	685.28	0.42671502	9.4
05R-01W 3-6 cm	41.93	56	64	637.69	58	67	685.06	0.499078155	8.1

Table A.8. Particle Size data down core with ages for Site 696.

Sample ID	Depth (MBSF)	AGE (Ma)	Clay %	Silt %	Sand %
55R-01W 70-72 cm	568.9	33.631	35.5	60.1	4.4
55R-03W 0-2 cm	571.2	34.127	32.8	58.6	8.6
55R-03W 72-75 cm	571.92	34.162	33.7	61.6	4.8
55R-03W 145-147 cm	572.65	34.197	15.5	69.6	14.9
55R-04W 0-2 cm	572.7	34.199	34.4	53.7	11.9
55R-04W 70-72 cm	573.4	34.233	25.2	48.0	26.8
55R-04W 139-141 cm	574.09	34.266	26.1	59.9	14.1
55R-05W 0-2 cm	574.2	34.271	20.4	49.7	29.9
55R-05W 70-73 cm	574.9	34.304	26.5	51.8	21.7
55R-05W 145-147cm	575.65	34.340	33.9	56.4	9.7
55R-06W 0-2 cm	575.7	34.343	24.5	57.9	17.6
55R-06W 20-23 cm	575.9	34.352	22.8	54.5	22.7
56R-01W 5-7 cm	577.95	34.450	26.3	56.7	17.0
56R-02W 88-90 cm	580.28	34.561	43.1	31.3	25.6

Sample ID	Depth (MBSF)	AGE (Ma)	Clay %	Silt %	Sand %
57R-01W 5-7 cm	587.65	34.914	55.7	23.4	20.9
57R-01W 105-107 cm	588.65	34.962	21.5	15.5	63.0
58R-01W 55-57 cm	597.75	35.397	14.2	27.3	58.5
58R-01W 87-89 cm	598.07	35.412	17.7	33.2	49.1
59R-01W 16-18 cm	607.06	35.842	12.1	41.5	46.4

Table A.9. Particle Size percentages from Ciarletta [2014] with ages and depths for Site 1166.

Sample ID	Depth (MBSF)	AGE (Ma)	Clay%	Silt%	Sand%
15R-02W 64-66 cm	134.69	Unclear	12.4	73.1	14.4
15R-03W 4-6 cm	135.59	35.705	14.5	78.4	7.1
15R-03W 47-49 cm	136.02	35.705	8.1	72.3	19.6
15R-03W 129-131 cm	136.84	35.707	7.4	57.7	34.9
15R-04W 62-64 cm	137.67	35.708	11.0	66.5	22.5
15R-04W 99-101 cm	138.04	35.709	10.1	77.5	12.4
15R-05W 96-98 cm	139.51	35.712	11.6	74.9	13.6
15R-05W 114-116 cm	139.69	35.712	10.1	79.7	10.2
15R-06W 34-36 cm	140.39	35.713	11.3	72.6	16.1
15R-06W 131-133 cm	141.36	35.715	10.4	78.0	11.6
15R-07W 43-45 cm	141.98	35.716	9.3	78.6	12.1
15R-ccw 5-7 cm	142.35	35.717	9.1	81.5	9.4
16R-01W 47-49 cm	142.67	35.718	9.0	70.7	20.3
16R-01W 104-106 cm	143.44	35.719	13.3	80.7	6.0

Sample ID	Depth (MBSF)	AGE (Ma)	Clay%	Silt%	Sand%
16R-02W 37-39 cm	144.07	35.720	12.0	79.7	8.3
16R-02W 98-100 cm	144.68	35.721	8.7	73.9	17.4
16R-03W 58-60 cm	145.78	35.723	11.1	74.0	14.8
16R-03W 127-129 cm	146.47	35.725	12.0	75.3	12.7
16R-04W 42-44 cm	147.12	35.726	9.9	76.6	13.6
16R-04W 114-116 cm	147.84	35.727	10.8	77.4	11.8
17R-01W 44-46 cm	151.84	35.734	6.8	58.1	35.2
17R-01W 131-133 cm	152.71	35.736	16.2	66.4	17.4
17R-02W 10-12 cm	153	35.737	12.3	64.5	23.2
17R-02W 91-93 cm	153.81	35.738	14.2	60.0	25.8
17R-03W 26-28 cm	154.66	35.740	17.1	63.6	19.2
17R-03W 118-120 cm	155.58	35.741	37.2	55.1	7.7
17R-04W 36-38 cm	156.26	35.742	46.2	53.6	0.2

Table A.10. Particle Size percentages from Ciarletta [2014] with depth for Site U1360

Sample ID	Depth (MBSF)	Clay%	Silt%	Sand%
03R-01W 3-4 cm	23.33	11.0	59.4	29.6
04R-01W 20-24 cm	32.8	7.5	63.5	29.1
04R-01W 80-84 cm	33.4	7.7	58.3	34.0
04R-02W 20-24 cm	34.19	10.5	69.0	20.5
04R-02W 90-94 cm	34.89	7.6	64.1	28.3
05R-01W 3-6 cm	41.93	7.3	66.2	26.4
06R-01W 20-24 cm	51.4	6.6	38.4	54.9
06R-01W 90-94 cm	52.1	5.3	38.8	55.9
06R-02W 23-29 cm	52.93	5.9	33.5	60.6